UNIVERSITA' DEGLI STUDI DI NAPOLI "FEDERICO II"

DIPARTIMENTO DI FARMACIA

Dottorato di ricerca in Scienze del Farmaco

XXVI ciclo

"Exploring physical and biological properties of TBA by site specific chemical modifications"

Dott.ssa Maria Scuotto ***Tutor: Prof.ssa Michela Varra***

Coordinatore: Prof.ssa Maria Valeria D'Auria

“The best scientist is open to experience and begins with romance –

the idea that anything is possible.”

Ray Bradbury

Index

Abstract

Coagulation is the process responsible for the transformation of blood into a solid mass formed by fibrin, platelet and blood cell, namely clot. The normal functioning of this process named Homeostasis produces the repair of an injury.

Disorders of coagulation can lead to an increased risk of obstructive clotting (thrombosis), that is, in severe cases, lethal for the organism.

Despite its phenomenal success, current anticoagulation therapy still suffers from the risk toward serious bleeding. A direct correlation exists between the intensity of anticoagulation and severity of bleeding. The need for safer and more effective antithrombotic agents clearly exists. During the last twenty years, aptamer technology is efficiently employed toward the development of therapeutic anticoagulants, by selecting thrombin-binding-oligonucleotides. The term aptamers is generally referred to single-stranded oligonucleotides that bind to a selected protein and specifically inhibits one or more of its functions.

The TBA (Thrombin-Binding-Aptamer), isolated via SELEX , is a 15-nucleotide consensus sequence that binds thrombin and inhibits its coagulant activity. TBA adopts a monomolecular chair-like G-quadruplex structure consisting of two G-tetrads connected by two lateral TT and a central TGT loops. Biological and structural results indicate that TBA exerts its anticoagulant activity competing with fibrinogen at the exosite I on the thrombin. Despite an high number of scientific results concerning the structure and the biological properties of TBA and its analogues were published during the last years, today still, the exact mechanism of action by which TBA exerts its antithrombin activity is an open question.

In the frame of different multidisciplinary studies, I synthesized and I characterized for their tridimensional structures as well as for their biological behavior, different libraries of new TBA analogues, with the aim to acquire new information about the differences in the mechanism of action of TBA and its synthetic analogues.

Furthermore, since TBA is a very promising tool for DNA-functionalized biosensors, I also synthesized new heterochiral TBA mutants with the aim to make stable the phosphodiester bonds of this molecule in biological environment. These new molecules were studied for their ability to fold in stable G-quadruplexes using different spectroscopic techniques.

1.THROMBIN

Thrombin is a serine-protease playing a key role in blood coagulation.[1] In mammalian, the equilibrium between the production and the inhibition of this enzyme, prevents the occurrence of hemorrhagic or thrombotic pathologies. The importance of thrombin is, beside of its unique enzymatic activity towards fibrinogen, the ability to catalyze many other coagulation-related reactions (Figure 1). It is now clear that thrombin, because of allosteric mechanism, is responsible for both procoagulant and anticoagulant stimuli by interaction with several substrates.[2] In presence of procoagulant stimuli[3,4] thrombin activates itself, factor V and factor XIII; the latter is a fibrin-ligase which makes strong the bonds between fibrin molecules. Furthermore, thrombin hydrolyzes the N-terminal extracellular domain of a membrane receptor named PAR-1 (type 1 Protease Activated Receptor, belonging from the G proteins-coupled super family receptors) which promotes platelet activation. All procoagulant stimuli ultimate into the conversion of soluble fibrinogen into insoluble fibrin. However, at the starting point of procoagulant stimuli thrombin and its glycoprotein co-factors must be produced. In the whole process (the coagulative cascade) a series of reactions promote the conversion of the zymogens (inactive enzyme precursors) in to active proteases, which, in turn, catalyze the next reaction in the cascade. The contemporary starting up of fibrinogen and PAR receptors by thrombin, leads to the formation of the platelet plug. Furthermore, thrombin is able to self-generate, through an activation of the feedback type, mediated by zymogen factor XI[5] and cofactors V and VII.[6,7] Thrombin also activates the transglutaminase Factor XIIIa, that, in turn,catalyzes the formation of covalent bonds between the fibrin fibers, stabilizing the clot.[8] Finally, it seems to have an important role in the cleavage of the von

Willebrand factor. This is a large multimeric glycoprotein(2050 aa., 250 kDa) present in blood plasma and is produced constitutively as ultra-large vWF in endothelium (in the Weibel-Palade bodies), megakaryocytes (α-granules of platelets), and subendothelial connective tissue. It recruits and activates platelets and is deficient in an inherited bleeding disorder called von Willebrand disease.[9]

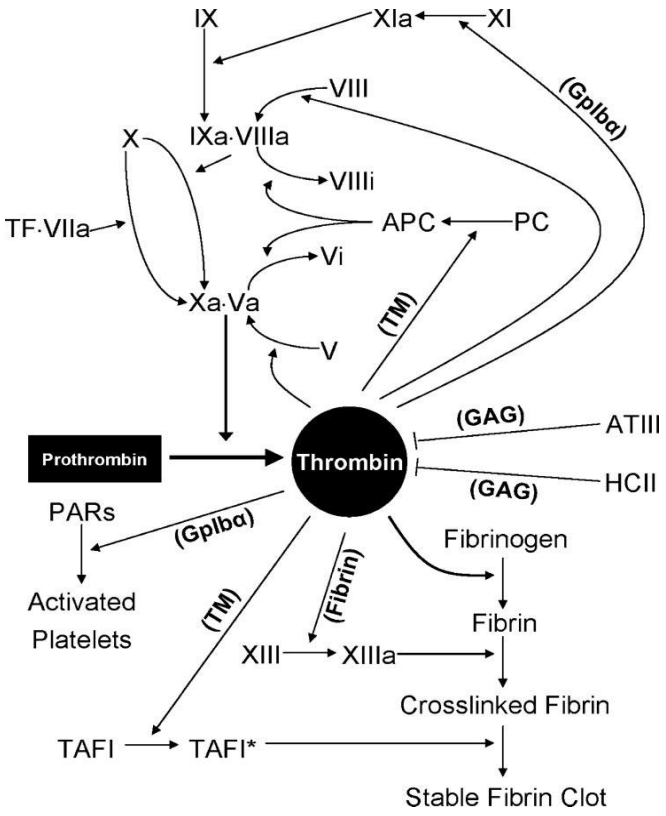

Figure 1.*The network of thrombin.*

In presence of anticoagulant stimuli, thrombin binds to thrombomodulin, a membrane receptor present on endothelial cells and activates protein C.[10] The binding of thrombomodulin suppresses the ability of thrombin to cleave fibrinogen, but enhances 1,000-fold the specificity of the enzyme toward the zymogen protein C. Activated protein C cleaves and inactivates factors Va and VIIIa, two essential cofactors of coagulation, factors Xa and IXa that are required for thrombin generation, thereby down-regulating both the amplification and the progression of the coagulation

cascade. Thrombin is finally inhibited and cleared from the circulation by circulating serpins AT and HCII, in a GAG-dependent fashion.

1.1 Structure of Thrombin

Singular structural features of thrombin determinates the regulation of its multiple functions.[11] In 1989, Bode et al. published the X-ray structure of thrombin. The same group reported a refined crystal in 1992.[12,13] Because of thrombin belongs to the chymotrypsin family, the numbering of its substrates is based on the Schechter and Berger nomenclature, in which substrate residues are numbered from the scissile P1-P1' bond toward the N- and C-termini, respectively.[14]

Thrombin consists of two disulfide-linked polypeptide chains that are folded into a trypsin-like protease. The A chain is composed of 36 residues and is non-essential for proteolytic activities. The B chain is composed of 259 amino acids and is derived from the carboxyl terminal sequence of prothrombin (Figure 2). Thrombin is trypsin-like, since it prefers to cleave its substrates after arginine residues. Like trypsin, the thrombin B chain contains the active site residues Ser195, His57, and Asp102, but also contains insertion loops that extend around the active site cleft, making it deeper and more narrow than that of trypsin. This insertion loops are known as the 60 and γ-insertion loops. The 60-loop is composed of Leu60, Tyr60a, Pro60b, Pro60c, Trp60d, Asp60e,Lys60f, Asn60g, Phe60h, and Thr60i, with Asn60g glycosylated. It is evident from the sequence that the 60-loop is hydrophobic in nature, with the two consecutive prolines serving to rigidify.

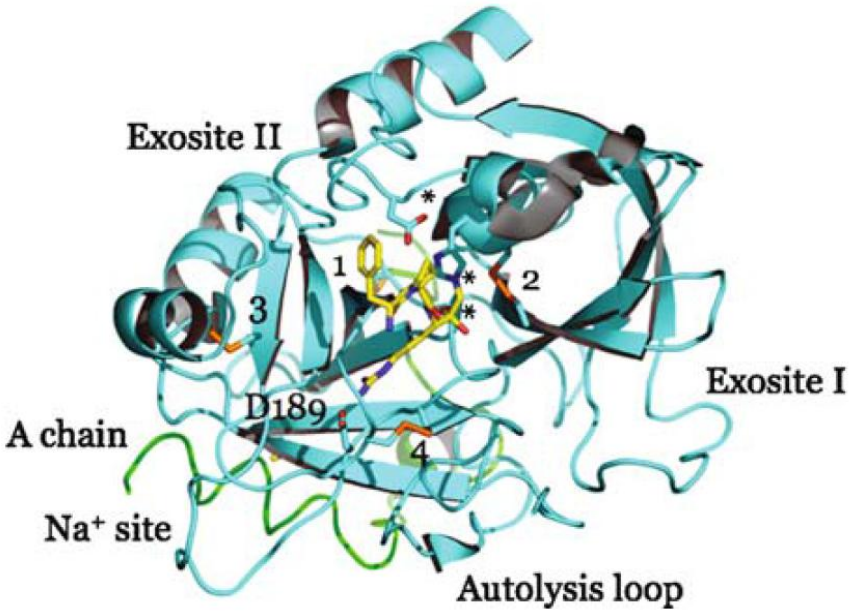

Figure 2. *Structure of thrombin bound to the active site inhibitor PPACK (stick model) and Na^+ (ball). The A chain runs in the back of the B chain. Disulfide bonds are numbered 1 (C1–C122),2 (C48–C52), 3 (C168–C182), 4 (C191–C220). Relevant domains are noted. Catalytic residues (H57, D102, S195) are marked by asterisk, and D189 is labeled. The bound Na + is nestled between the 220-loop and the 186-loop and is within 5 Å from the side chain of D189. Numbering refers to chymotrypsin(ogen) (see Color Plates) [from Thrombin: physiology and disease. 2009. Chapter 1: Thrombin: Structure, Functions and Regulation, pagg 1-18]*

The 60-loop, thus provides a rigid, hydrophobic cap over the active site and mediates contacts with the hydrophobic substrate residues N-terminal to the scissile bond. In contrast, the γ-loop is more hydrophilic and flexible in nature; composed of Thr147, Trp147a, Thr147b,Ala147c, Asn147d, and Val147f. It is often incompletely modeled in crystal structures due to its inherent mobility, but, as it is adjacent to the active site cleft of thrombin, it can contact substrate residues C-terminal to the scissile bond, and can make contacts with the body of substrate proteins. In forming the active site, the loops also serve to restrict access to the catalytic domain of thrombin to proteins with long, flexible substrate loops, or to proteins with complementary surfaces which mediate contact with the loops. In addition to these two insertions, the area also

includes access to the active site residue Glu192, whose negative charge plays an important role in discriminating substrates containing acid residues in the proximity of the scissile peptide bond (i.e. in the case of the binding to protein C orto receptor I of thrombin). In the active site there is another important zone, the Na^+ binding site that was first identified crystallographically in 1995.[15] Na^+ binds 16–20 Å away from residues of the catalytic triad and within 5 Å from D189 in the S1 site, nestled between the 220- and 186-loops and coordinated octahedrally by two carbonyl O atoms from the protein (residues R221a and K224) and four buried water molecules.

Unlike trypsin, thrombin, has extra surface structures that influence the interactions with macromolecular substrates and thus make it a more discriminating protease. One of these subsites is called the anion-binding exosite-1 (ABE-1) that is adjacent to the P' side of active site cleft. It contains residues from the Arg67 to the Glu80, Arg35, Lys149e, Lys81, Lys110, Lys109, and Lys36. Thrombin ABE-1 has been implicated in binding of fibrinogen, hirudin, and heparin cofactor II. Another surface structure of thrombin is called the anion-binding exosite-2 (ABE-2), that is primarily responsible for the ability of thrombin to bind glycosaminoglycan. Furthermore, the region from Leu144 to Gly150 forms an additional surface subsite, that contributes to the interaction of thrombin with hirudin and thrombomodulin.

Thrombin specificity can thus be understood as a competition for three sites: the active site and exosites I and II. Structural biology has revealed important information on how thrombin utilizes both the active site and exosites for interaction with substrates, inhibitors, and effectors.[2,16,17]

1.2Thrombin Substrates

A lot of studies conducted on thrombin mutants highlighted that the binding of natural substrates and cofactors to thrombin require one or both anion binding exosites.

Among the cofactors of thrombin there is glycoprotein Ibα. It is present on the platelet membrane and is important for three actions: platelet aggregation[18], activation of factor XI[19] and cleavage of glycoprotein V.[20,21] The interaction of glycoprotein Ibα with thrombin occurs between a negatively charged region of the glycoprotein and the exosite II of thrombin. There are mainly electrostatic interactions and hydrogen bonds. In particular, there is a contact between Arg 233 from exosite II and several oxygen atoms of Tyr sulfate 276, 278 and 279,[22] which forms the negatively charged region of glycoprotein. The exclusive involvement of exosite II has been demonstrated by mutagenesis studies:[23,24] thrombin variants having mutated residues in the exosite II showed reduced binding affinity for the glycoprotein Ibα respect to wild-type protein, while similar modifications involving exosite I had no effects on the binding affinity.

Fibrinogen, the principal protein of vertebrate blood clotting, is an hexamer, containing two sets of three different chains (α, β, and γ), which are joined each-other in the N-terminal E domain by five symmetrical disulfide bridges[25] (Figure 3). Thrombin converts the soluble fibrinogen into insoluble fibrin strands. These strands are then cross-linked by factor XIIIa to form stable blood clot. Fibrinogen is a substrate whose recognition by thrombin is directly mediated by active site and exosite I interactions to form a Michaelis complex, defined by a K_m in the micromolar range. Thrombin residues seen in direct contact with fibrin were F34, S36a, L65, Y76, R77a, I82, and K110. Although the interface interposes the basic exosite I of thrombin with an acidic surface of fibrin, the majority of the contacts, and presumably the major energetic

contribution, derive from the opposition of hydrophobic surfaces on the two molecules (F34, L65, Y76 andI82 on thrombin and F35 and A68 on the Aα and Bβ chains of fibrin, respectively).[26]

The high binding affinity suggests that thrombin-fibrin interactions also involves thrombin exosite II. In particular the C-terminal of the γ' fibrin chain, which contains negatively charged residues, contributes to the binding of fibrin on thrombin exosite II.

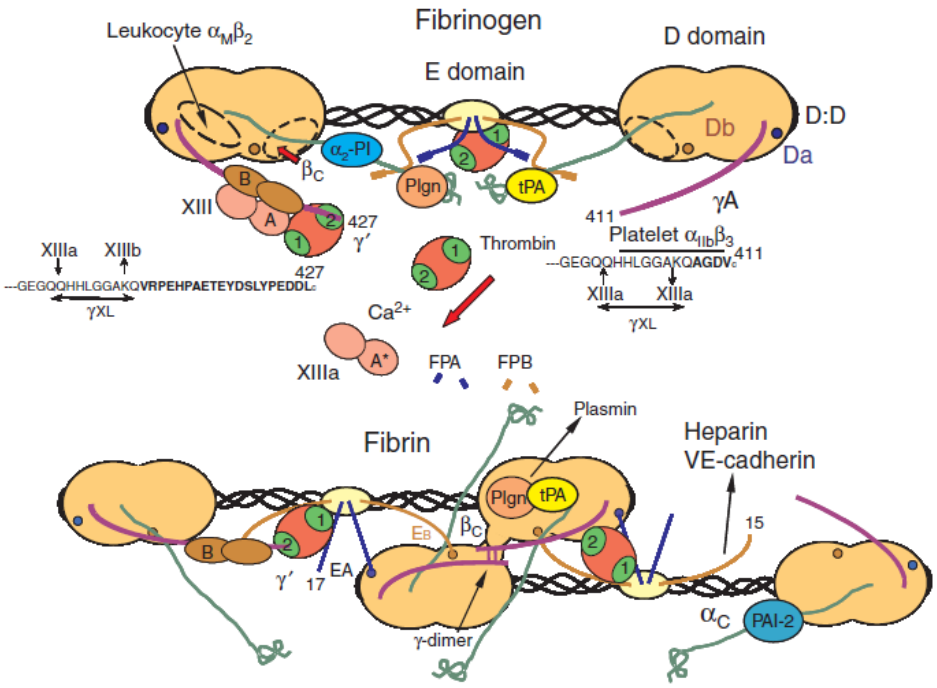

Figure 3. *Schematic diagram of fibrinogen structure, its conversion to fibrin, and the thrombin-mediated conversion of native factor XIII to XIIIa. Binding sites for proteins, enzymes, receptors, and other molecules that participate in fibrin(ogen) functions are illustrated. [from Journal of Thrombosis and Haemostasis, 2005, 3, 1894–1904]*

Another important cofactor is thrombomodulin[27] (TM), that is expressed on the surface of endothelial cells. It is a single chain glycoprotein that participates in the activation of protein C which, in turn , inactivates factors V and VIII. It is composed of

five regions: (1) the N-terminal lectin-like domain; (2) six consecutive EGF-like repeats; (3) a proteoglycan-like Ser-Thr-rich region which is highly O-glycosylated; (4) a single transmembrane helix; and, (5) the C-terminal cytoplasmic tail. The thrombomodulin binds mainly exosite I by hydrophobic contacts between isoleucine 414 and 424 of thrombomodulin and leucine 65 of thrombin. The replacement of isoleucine with alanine 37 reduces the binding efficiency and shows the importance of this hydrophobic contact.[28] However, chondroitinsulfate (CS) moiety, found on about 20% of TM molecules in the vascular endothelium and about 30%–35% of those lining the arteries, improves the affinity of TM for thrombin by an order-of-magnitude.[29]

In the final phase thrombin is inhibited by serpins and cofactor II. Serpins are inhibitors of serine proteases and are activated by heparin-like glycosaminoglycans (GAGs) such as heparan sulfate, chondroitin sulfate and dermatan sulfate, that are long chain polysaccharides able to bind thrombin and to accelerate 1000 folds its inhibition by serpins.[30,31] Heparin and dermatan sulfate also accelerate the thrombin inhibition mediated by heparin cofactor II. Several studies have shown that the heparin-binding site of thrombin was localized in the exosite II. The heparin-thrombin interaction is ionic in nature and involves the negatively charged sulfate groups of heparin and several positively charged residues of thrombin represented by basic amino acids. The Arg 93 is responsible for 3 ionic interactions with the oxygens of the sulphate, the Lys 236 participates in two interactions. The Arg 101 and 233 have only one interaction. The Lys 240 provides probably other three interactions and finally, the His 230 determines the formation of an hydrogen bond. Five heparin residues are sufficient to achieve the right length for the complete occupation of thrombin binding

site.[32]However, to inhibit thrombin heparin must be formed at least by 18 saccharide residues, since single molecule of heparin binds to both thrombin and serpin.[33]

Monovalent cation sodium (Na^+) is an important cofactor able to modulate thrombin activity. It coordinates the carbonyl oxygens of Arg 221a and Lys 224 and 4 water molecules in a octahedral geometry (Figure 4). The presence of Na^+influences the thrombin conformations.[34,35] It has been suggested that the enzyme can exist in two forms named "fast" and "slow". In the form bonded to Na^+, thrombin assumes the "fast" conformation and activates PAR-1 and fibrinogen, there by playing the pro-coagulant action. In contrast, without Na^+, thrombin loses affinity for the pro-coagulant factors but activates protein C.

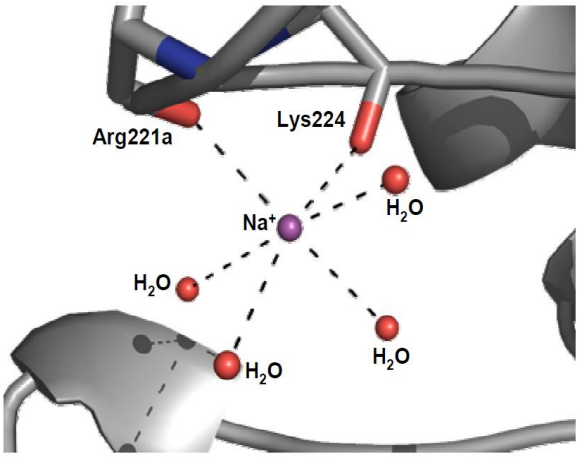

Figure 4.*The Na^+ binding site of thrombin representation.*

It is evident that, during the hemostatic process, thrombin binds a large number of cofactors. Initially thrombin binds species that induce pro-coagulant stimuli promoting the formation of the platelet plug. After its formation, fibrin acts as a cofactor for thrombin-activated, factor XIII and all substrates with anticoagulant activity. This

points out that the efficiency of the coagulation cascade depends on the balance between the procoagulant and anticoagulant pathways, and the thrombin together its ligands are the key arbiter of this balance.

1.3Thrombin allostery

The ability of thrombin to adopt pro-coagulant and anti-coagulant form, known as the "paradox of thrombin", suggests the hypothesis of an allosteric modulation of the protein functions.

Protein allostery[36,37] is based on the existence of equilibria between multiple conformations, each of them linked to distinct functional properties. The allosteric regulation of a protein starts with the formation of a complex protein-effector, in which the enzyme assumes a slightly modified tertiary structure. This new structure can have modified affinity for other substrates, and, consequently, can influences the catalytic activity of the enzyme. Effectors that enhance the protein activity are referred to as allosteric activators, whereas those that decrease the protein activity are called allosteric inhibitors. Generally, the regulatory site of an allosteric protein is physically distinct from its active site. The original studies concerning the molecular allosteric mechanism of multimeric proteins were been performed by Perutz.[38] For such systems, the conformational transitions influence the quaternary structure and allostery features have been detected crystallographically. One of the most popular allosteric protein is Hemoglobin. The binding of O_2 to one hemoglobin subunit induces conformational changes that are relayed to the other subunits, making them more able to bind to O_2 by raising their affinity for this molecule. In particular, after binding

of O_2, the proximal histidine(F8) moving toward heme pocket, triggers structural changes that alter the interaction between the α and β chains, leading to the transition from T to R form. T or "stretched" state, represents the conformation having low oxygen affinity, while the R or "released" state is the high oxygen affinity one. The allostery, however, is not exclusive of multimeric assemblies; in fact, many monomeric proteins, such as thrombin, show a remarkable structural plasticity, attributable to the existence of an allosteric modulation of their functions.[39-41]

As described in the section 1.2 thrombin utilizes exosites I and/or II in the molecular events that modulate its functions. Although X-ray data indicate that some substrates are able to bind both exosites, several different studies support absolute exosite discrimination. Such experimental and theoretical analyses[1] indicate that hydrophobic contacts provide the majority of the binding energy for exosite I interactions, while the electrostatic contacts in this site seem to have the role of orientate the complementary hydrophobic surfaces (so-called electrostatic steering). Exosite II interactions, on the other hand, are primarily ionic in nature, with hydrophobics contributing minimally to the overall binding energy[1]. On these basis it has been proposed to call, most properly,exosite I ”the apolar-binding exosite”, and exosite II “the anion-binding exosite”.

The concept of thrombin allostery is based on the effects produced by interaction of ligand on exosite I or II. These exosites facilitate the binding of substrates or cofactors and align them for optimal interaction with the active site[42].

Currently, there are two different theories to recognize the thrombin allostery. According to Di Cera et al.[41,43]different thrombin conformations are related to the presence of cation sodium. Recently, some studies insert thrombin allostery in a

continuum balancing of different stimuli that convert the enzyme in zymogen-like or protease-like form.[44]

1.3.1 Effects of Thrombin-Na^+ interaction

Di Cera et al. consider two thrombin conformations named "*slow*" and "*fast*" respectively, in reference to rate of proteolysis fibrinogen reaction.[45]The allosteric transition is regulated by interaction with the Na^+ ion, which binds to 15 Å away from the active site residues, stabilizing the pro-coagulant form (fast) (Figure 5). Under physiological conditions, the K_d of thrombin for Na^+ ions has a value (110 mM) very closed to the Na^+ blood concentration (145 mM) .[46-50]Thus, fast and slow thrombin forms are almost equally populated in vivo (ratio 3:2, respectively) and the binding of specific cofactors can shift the equilibrium towards the slow (such as the anticoagulant heparin) or the fast form (such as the pro-coagulant fibrin).[34]The slow form, called E, accounts for 40% of the molecules in vivo, on the contrary the fast form,also called $E:Na^+$, represents approximately 60% of the molecules *in vivo*. However, there seems to be a third conformation named E* (about 1% of the molecules in vivo), that is in equilibrium with E, unable to bind sodium, defined E* or "inactive conformation" of thrombin. Therefore, the Na^+-free thrombin can be divided in two conformations, E and E*, which only E is able to interact with sodium. A large number of spectroscopic and mutagenesis studies support the following transitions between the different forms: the transition from E to $E:Na^+$ induces a global change involving the nine Trp residues of thrombin, located up to 35 Å from sodium binding site; the second, from E* to E, concerns the whole enzyme structure.[51] The X-ray structure of a complex between a thrombin mutant (D102N) and a peptide fragment of the PAR 1 was

published.[52] The thrombin mutant D102N is stabilized in a self-inhibited conformation where the access to the active site is occluded by a collapse of the entire 215–219 -strand. This study proves that, the binding of a fragment of PAR1 to D102N-exosite I, occurring 30-Å away from the active site region, causes a large conformational change that corrects the position of the 215–219 -strand and restores the access to the active site. These conformational changes of the mutant protein, as well as other experimental data, has been understood by Di Cera et al. through the Na^+allosteric regulation of thrombin; in fact:

1. no conformational changes occurred upon the formation of native protein-PAR1 complex;
2. exosite I-PAR3 interaction[53-57] induced relevant conformational changes. This disturbance consists in the moving of the indole ring of Trp 60 and in the upward movement of the loop 60, thus allowing thrombomodulin to fulfill the function of cofactor. In fact, the exosite I -TM binding fully opens the active site by increasing the rate of diffusion of protein C.[58,59] This conformational change can be deleted in the presence of an active site inhibitor;
3. no changing/disruption of thrombin conformation follows the ligand contacts with exosite I, such as the case of the binding of hirugen, a deca-peptide derived from the C-terminal fragment of hirudin. The hirugen-thrombin, as well as thrombomodulin-thrombin complex has just slight differences in the active site,compared to free-thrombin.[60]

According to Di Cera et al., the influences of exosite I ligands on thrombin can be explained taking into account the three forms of enzyme: E* , E and E: Na^+. The binding of PAR 1 fragment to the exosite I of the E:Na^+ form causes only a shift of 60-loop that

opens the active site. On the contrary, the same ligand can generate an extensive conformational transition of the E*form, as in the case of the mutant D102N. The conformational transition results in a long-range communication of exosite I and the opposite site of thrombin, nearly to 30 Å distant.

Finally, the E form can be achieved by the binding of the PAR-3 to the exosite I, that allows to anticoagulant effects.

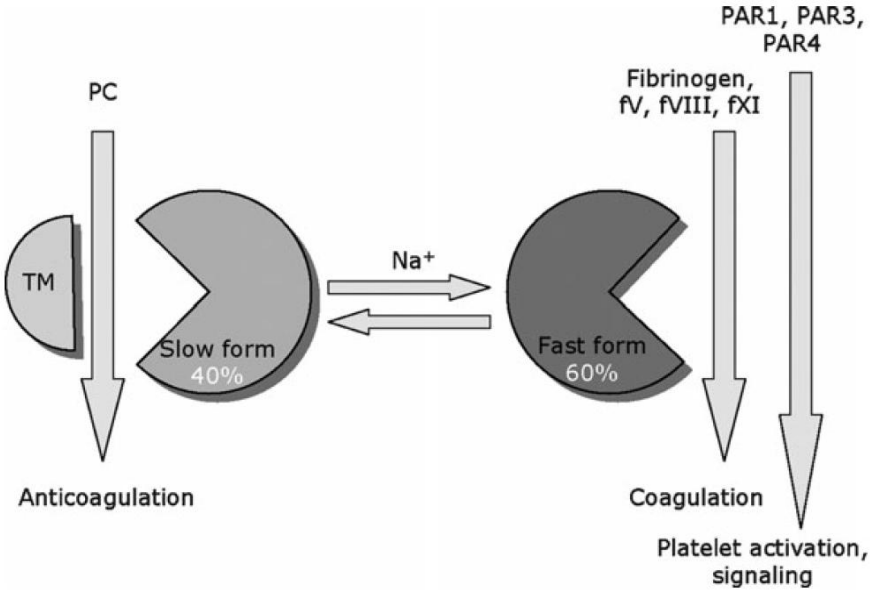

Figure 5. *Schematic representation of the multiple roles of thrombin inthe blood and how Na+ binding influences them.The fast form is responsible for the efficient cleavage offibrinogen leading to clot formation, and activation of factors V, VIIIand XI that promote the progression of the coagulation response tovascular injury. The fast form is also responsible for the activation ofPAR1, PAR3 and PAR4 leading to platelet activation and cellsignaling. The slow form, on the other hand, activates efficiently theanticoagulant protein C with the assistance of the cofactor thrombomodulin. Na+ binding to thrombin is the major driving force behindthe procoagulant, prothrombotic and signaling roles of the enzyme inthe blood, but is not required for its anticoagulant role triggered byprotein C activation. Any effect that destabilizes Na+ binding producesan anticoagulant effect by shifting thrombin to the slow form.*

[from Phys. Chem. Chem. Phys., 2007, 9, 1292–1306]

1.3.2 Zymogen-like and Proteinase-like states of Thrombin

The alternative theory to explain allosteric thrombin phenomena came from other works which consider zymogen-like and proteinase-like species of thrombin.

Thrombin is produced by proteolytic activation of the precursor, prothrombin, in the first step of the coagulation pathway. After proteolysis, the transition of zymogen to proteinase is not obvious, since thrombin can reversibly interconvert between zymogen- and proteinase-like forms, depending on the binding of complementary ligands.

According to supporters of this theory, the understanding of thrombin allostery requires knowledge about the equilibria involved in proteinase generation (thrombin) from its zymogen form (prothrombin), because the thrombin regulation is *in continuum* with thrombin generation.[61]

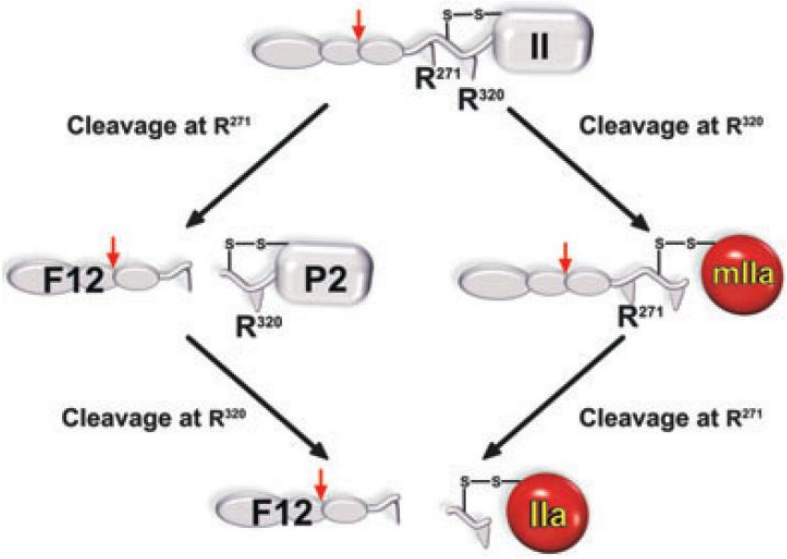

Figure 6. *Pathways for the Proteolytic Conversion of Prothrombin to Thrombin.*

[from Journal of Thrombosis and Haemostasis, 11 (Suppl. 1): 265–276]

There are two pathways for the proteolytic conversion of Prothrombin to Thrombin (Figure 6). The conversion of prothrombin to thrombin results from cleavages following Arg271 and Arg320. Initial cleavage following Arg271 yields the pathway on the left and produces the zymogen, prethrombin 2 (P2) and the propiece, fragment 1.2 (F12) as intermediates. P2 requires further processing at Arg320 to yield thrombin.

The pathway on the right arises from initial cleavage following Arg320, which produces the proteinase meizothrombin (mIIa) as an intermediate. Further cleavage following Arg271 is required to yield thrombin (IIa) and the propiece, F12. The Arg155 site (Red Arrow) is susceptible to thrombin cleavage and separates the fragment 1 region from fragment2 within F12.

Isothermal titration calorimetric experiments highlighted substantial differences in affinity and energetics between the binding of F12 to thrombin and to the P2 zymogen.[62]

Profound differences in ΔH and ΔS with modest changes in ΔG were observed for the binding of F12 to P2, a cleaved but zymogen-like form of thrombin, the catalytically inactive variant of thrombin containing Ser195 substituted with Ala and thrombin covalently stabilized in the most proteinase-like form by covalent modification with FPRck. Large compensating changes in ΔH and ΔS for F12 binding were observed as the species increasingly became proteinase-like and were consistent with the binding of the propiece to structurally related zymogen- and proteinase-like forms expected to be in reversible equilibrium with each other. Accordingly, high concentrations of an active-site-directed ligand could transition the zymogen-like form of thrombin along this thermodynamic trajectory to resemble FPR-thrombin.[63] Conversely, removal of Na^+ at constant ionic strength could transition the thermodynamic constants along the

same trajectory until binding resembled that seen with the cleaved by zymogen like form of thrombin.[63] Finally ligands directed towards anion binding exosite 1 (ABE1) could favor proteinase-like forms.[64] In the extreme, uncleaved P2 could be imbued with catalytic activity in the absence of cleavage by strong ligand binding. These points illustrate that thrombin occupies a continuum of zymogen-like and proteinase-like forms following initial cleavage. The continuum and associated thermodynamic compensation in F12 binding derives from the fact that the series of changes associated with proteinase maturation following cleavage are additive. These ideas are surprising when taken in the context of the irreversibility of peptide bond hydrolysis but are in line with the findings with factor VIIa.[65]

The previously reported data on mutant inactive thrombin (see section 3.1.1) can be reinterpreted considering every mutation that destabilizes the status proteinase-like affects this equilibrium and encourages the zymogen-like form.

Ligand-dependent interconversions of cleaved thrombin between zymogen- and proteinase-like forms can formally be considered by a two-state model although multiple sub-states of thrombin are likely involved (Figure. 7).

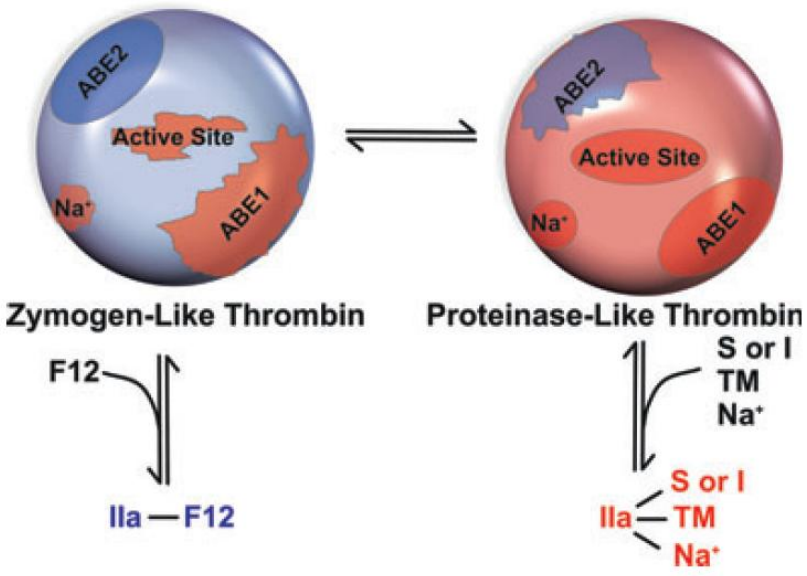

Figure 7. *Ligand-Dependent Interconversions of Thrombin Between Zymogen- and Proteinase-Like Forms*. *[from Journal of Thrombosis and Haemostasis, 11 (Suppl.1):265–276]*

The reasoning behind this model lies in the fact that anion binding exosite 2 (ABE2), to which F12 binds, is properly configured in the zymogen-like form but distorted in the proteinase-like form.

In fact, the thrombomodulin binds ABE1 shifting the balance towards the proteinase-like form and activating protein C.[66-67]The two species were found to be approximately equally populated and the distribution between the two forms could be altered predictably by thrombomodulin or by decreasing Na^+.

The Na^+ enhances the binding of the hirugen or the thrombomodulin to thrombin. These results are in agreement with the fact that both the Na^+, and ABE1 ligands energetically favor the protease-like form as documented by NMR studies.[68]

The binding of F12 to ABE2 favors the zymogen-like form and it is opposed to the binding of thrombomodulin-hirugen toABE1. Consequently, the F12-ABE2 binding has a negative effect on exosite I ligands and *vice versa*.

Other findings with thrombin imply that mIIa would be exceptionally zymogen-like.[69] Indeed, rapid kinetic studies revealed the slow equilibration of mIIa between zymogen-like and proteinase-like forms, only the latter of which could bind active-site ligands with high affinity. Single turnover rapid kinetic studies revealed that initial cleavage at Arg320 by prothrombinase yields a zymogen-like form of mIIa that only slowly equilibrates with the proteinase-like species. [69]

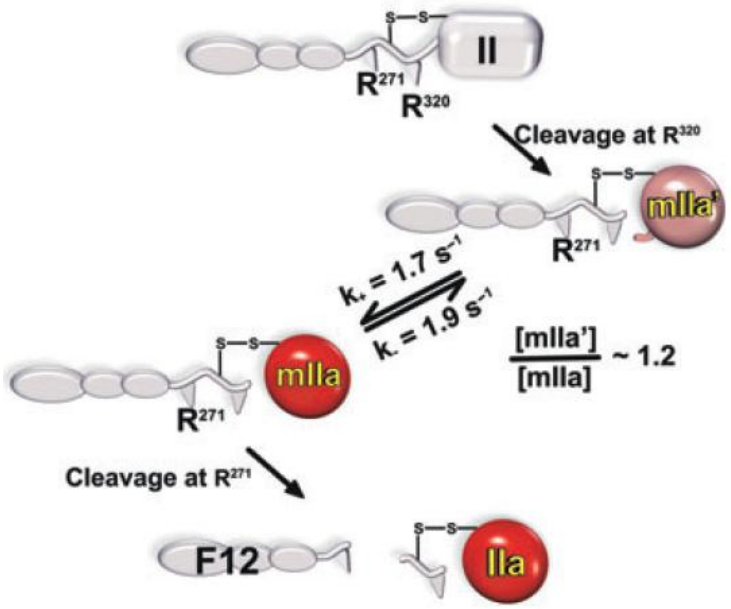

Figure 8. *A New Rate-Limiting Step in the Conversion of Prothrombin to Thrombin. Initial cleavage of prothrombin following Arg320 yields a zymogen-like form (mIIa') that interconverts slowly and reversibly with the proteinase-like form (mIIa). Because the proteinase-like conformation is required for further cleavage at Arg271, it is only mIIa rather than mIIa' that is processed to thrombin. The reversible conversion of mIIa' to mIIa there represents a previously unanticipated rate-limiting step in thrombin formation. [from Journal of Thrombosis and Haemostasis, 11 (Suppl. 1): 265–276]*

Because of the essential role of the zymogen to proteinase transition in facilitating the second cleavage reaction by prothrombinase to yield thrombin, this slow reversible

interconversion of mIIa between the two forms describes the ratcheting step proposed to separate the two half-reactions of prothrombin activation by prothrombinase.

1.3.3. Long range communication between exosite I and II

Although exosites 1 and 2 regulate thrombin activity by binding substrates and cofactors and by allosterically modulating the active site, it is still unclear whether there is direct allosteric linkage between the two exosites.

To address this, a thrombin variant fluorescently labeled at exosite 1 was titrated with exosite 2 ligands, HD22 (a DNA aptamer), γ'-peptide (analog of the COOH terminus of the γ'-chain of fibrinogen) or heparin C oncentration-dependent and saturable changes in fluorescence were elicited, supporting inter-exosite linkage.[70]

To explore the functional consequences of these phenomena, the capacity of exosite 2 ligands to inhibit thrombin binding to γ_A/γ_A-fibrin, an interaction mediated solely by exosite 1 was evaluated. When γ_A/γ_A-fibrinogen was clotted with thrombin in the presence of HD22,γ'-peptide, or prothrombin fragment 2 there was a dose-dependent and saturable decreasing in thrombin binding to the resultant fibrin clots.

Furthermore, HD22 reduced the affinity of thrombin for γ_A/γ_A-fibrin 6-fold and accelerated the dissociation of thrombin from preformed γ_A/γ_A-fibrin clots. Similar responses were obtained when surface plasmon resonance was used to monitor the interaction of thrombin with γ_A/γ_A-fibrinogen or fibrin. There is bi-directional communication between the exosites, because exosite 1 ligands, HD1 (a DNAaptamer) or hirugen (an analog of the COOH terminus of hirudin), inhibited the exosite 2-mediated interaction of thrombin with immobilized γ'-peptide. These findings provide evidence for long range allosteric linkage between exosites 1 and 2 on thrombin,

revealing further complexity of thrombin regulation. However it is also unclear whether the allosteric connection between the exosites has physiological relevance. [70]

1.4 Thrombin and anticoagulant therapy

Currently, in anticoagulant therapy were considered molecules that are able to influence exosite-active site interaction exclusively. There are heparinoids, which assist antithrombin in the inhibition of thrombin and factor Xa.

Nature has engineered two distinct mechanisms for heparin-activated antithrombin inhibition of factor Xa and thrombin. The interaction of high-affinity heparin, or pentasaccharide H5, expels the partially inserted RCL residues thereby significantly changing the conformation of the P1-P10 reactive center and exposing an exosite in antithrombin (Figure 9). [71-74] This phenomenon is called the conformational activation of antithrombin. The altered RCL in heparin-antithrombin co-complex is better recognized by factor Xa resulting in accelerated cleavage of the P1-P10 bond and rapid formation of the covalent inhibited complex (E*-AT*). Thus, conformational activation of antithrombin is necessary and sufficient for accelerated factor Xa inhibition. Thrombin inhibition, in contrast, is accelerated only two fold through the conformational activation mechanism.[30] The predominant effect of heparin in accelerating thrombin inhibition arises from a bridging mechanism. Tight binding of antithrombin to the H5 sequence in full length heparin is followed by the binding of thrombin to the same chain at non-specific sites to form an antithrombin–heparin–thrombin ternary complex. Thrombin then diffuses along the polyanionic chain to encounter the inhibitor resulting in a 2,000-fold acceleration in inhibition under physiological conditions. A saccharide length of 18 residues is needed to

simultaneously hold thrombin and antithrombin for the accelerated inhibition.[75,76] Thus, while sequence-specific H5 is necessary for tight binding of heparin chains, H5 alone cannot potentiate antithrombin inhibition of thrombin.

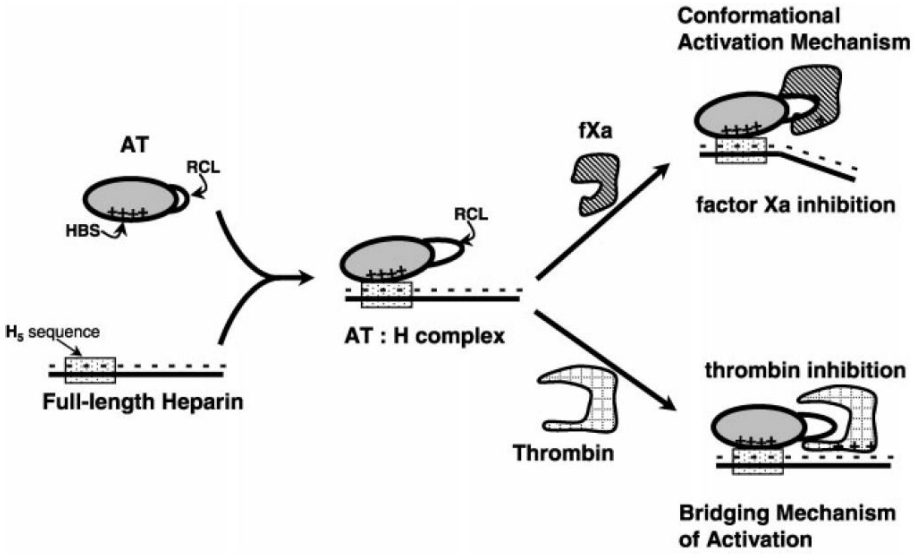

Figure 9. *Mechanism of antithrombin inhibition of factor Xa and thrombin in the presence of full-length heparin. An antithrombin- heparin complex (AT:H) is formed following an interaction of the high-affinity pentasaccharide sequence (H5) in heparin with the pentasaccharide-binding site (PBS).This causes expulsion of the reactive center loop (RCL) that better recognizes factor Xa (fXa). This mechanism is called the conformational activation mechanism. Thrombin inhibition, in addition to conformational activation, requires the bridging of thrombin and antithrombin on a full-length heparin chain. An exosite (shown as'+ + +') in thrombin binds non-specifically to some negative charges available at the extended heparin chain. This mechanism is called the bridging mechanism of activation and is the dominant contributor to inactivation of thrombin.[from Medicinal Research Reviews, 2004,. 24, 151-181]*

Unfractionated heparin and warfarin are characterized by a narrow therapeutic window and by an almost unpredictable dose response profile. Furthermore, unfractionated heparin can trigger heparin-induced thrombocytopenia and is unable to promote inhibition of fibrin-bounded thrombin and platelet-bounded factor Xa. Low molecular-weight heparins feature have a more predictable dose-response relation

compared with the unfractionated forms and are avoided of the former limitation, but not of the latter.[77]

Another class of antithrombotic drugs is represented by direct inhibitors. Among these only hirudin and bivalirudin are able to interact with the exosite I. The mechanism of action for these agents consists in the inhibition of thrombin bound-fibrin, as well as fluid-phase thrombin. However, the current direct thrombin inhibitors do not have a superior therapeutic efficacy and safety compared with low-molecular-weight or even unfractionated heparins.

Despite its phenomenal success, current anticoagulation therapy still suffers from the risk toward serious bleeding. A direct correlation exists between the intensity of anticoagulation and severity of bleeding. Furthermore, each anticoagulant is associated with additional problems specific to its class. The need for safer and more effective antithrombotic agents clearly exists. [78]

The observation that allosteric "long-range communication" can affect thrombin-fibrin interaction provides a novel way through which thrombin activity can be modulated.

Recent experimental evidences reported by Weitz and coll. and previously described in paragraph 3.1.3. seem to indicate the existence of allosteric "long-range communication" produced by different ligands, and in particular, by two aptamers, HD1 and HD22. An aptamer is a folded single-stranded oligonucleotide that binds to a molecular target such as a protein. The advantages of aptamers are manifold, the most prevalent being their chemical synthetic access. [79] This renders aptamers distinct from antibodies, the second class of macromolecular therapeutics. They cannot, at least regarding the current state-of-the-art, be synthesized chemically but their access in large scale can be facilitated by fermentation, like other recombinant protein

therapeutics. Chemical synthetic access to aptamers is: affordable, highly controlled, and allows modifications at a site-specific, hence, in a strategic manner.[79]

The first aptamer that was described to bind to and inhibit a coagulation factor is the thrombin aptamer HD1. This 15-base DNA oligonucleotide named TBA,[80] identified in 1992, inhibits the procoagulant functions of thrombin such as conversion of fibrinogen to fibrin and platelet aggregation. HD1 interacts with one of the two anion-binding sites of thrombin, in particular with exosite I (see chapter II).

HD22 (5'AGTCCGTGGTAGGGCAGGTTGGGGTGACT-'3), is a single-stranded DNA consisting of 26 residues. Several evidences suggest that this aptamer folds into a quadruplex - duplex mixed structure (Figure 10b) through which recognizes and binds specifically the thrombin exosite II.[81]

Recently a bivalent aptamer that simultaneously binds to both exosites of thrombin was synthesized. The corresponding molecule named HD 1-22 joins the distinct thrombin aptamers HD1 and HD22 via a polynucleotidic linkage (Figure 10c). This molecule is the most potent “aptameric” thrombin inhibitor to date. [82,83]Therefore it is clear, that the aptamers may be a good starting point for the search of allosteric inhibitors of thrombin. Indeed, an ideal thrombin inhibitor should bind the exosite I, competing against pro-coagulants stimuli, but at the same time, it should have the ability to induce conformational perturbations to exosite II, increasing the affinity for those species that induce anti-coagulants stimuli.

In other words, if the binding of an inhibitor is also able to induce conformational changes to the thrombin, the allostery may act in a synergistic way to create a more efficient modulation of the clotting process. Inhibitors having these properties are very useful in drug therapy as well as in biotechnological applications.

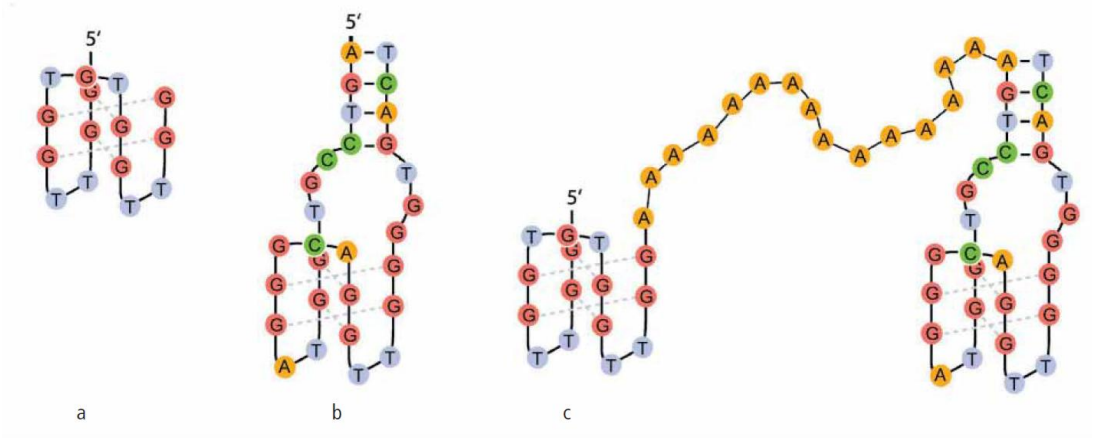

Figure 10. *Aptamers that bind to and inhibit thrombin via recognition of exosite I (a), exosite II (b), or both exosites (c). [from Hämostaseologie 2011, 4, 258-263]*

2. Thrombin Binding Aptamer (TBA)

The first reported consensus sequence able to inhibit thrombin activity was the 15-mer oligonucleotide (ON) GGTTGGTGTGGTTGG, usually known with the acronym TBA (thrombin-binding aptamer).[80] In the presence of thrombin and/or monovalent cations TBA folds into a specific three-dimensional structure that dictates its thrombin-binding affinity. The structures of TBA alone and in complex with thrombin were determined by NMR[84-86] and X-ray[87-89] methods, respectively. In all experimentally determined structures TBA adopted a monomolecular chair-like G-quadruplex folding topology, consisting of two G-tetrads connected by one TGT loop and two TT loops. First,[87,88] different TBA–thrombin X-ray complexes were reported, in which TBA adopted either the same folding as derived by NMR (PDB ID 1HAO; Figure 11A) or a different one (PDB IDs 1HUT and 1HAP; Figure 11B),presenting a diverse positioning of the connecting loops.

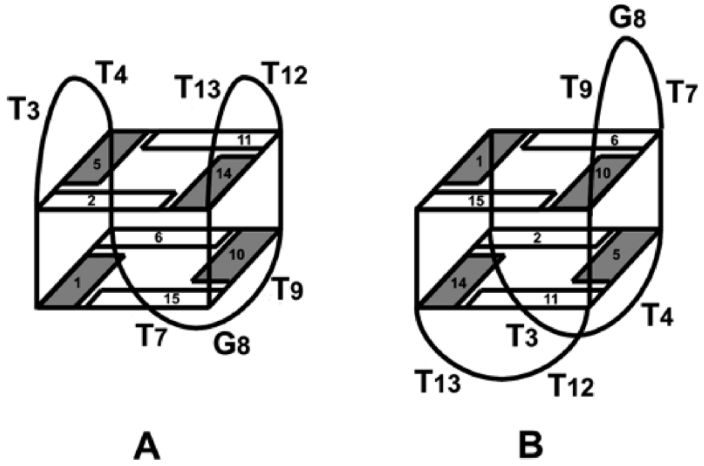

Figure 11. *Schematic drawings of the X-ray derived G-quadruplex structures of TBA as reported in PDB IDs 1HAO (A) and 1HUT and 1HAP (B). In (A) TT loops span narrow grooves and TGT spans wide grooves, vice versa in (B). White and gray squares indicate G bases in anti and syn conformation, respectively.*

In these X-ray complexes, the aptamer interacts with distinct regions of two thrombin molecules, (i) the fibrinogen exosite (namely anion-binding exosite I, ABE I) and (ii) the heparin exosite (namely, ABE II) near the carboxylate terminal helix of a neighboring thrombin. Thus, according to the adopted folding and the relative orientation with respect to thrombin, TBA bound to ABE I by using the TT loops (PDB ID 1HAO; Figure 11A) or the TGT loop (PDB IDs 1HUT and 1HAP;Figure 11B). A subsequent re-evaluation[90] of the diffraction data of TBA−thrombin complexes[87,88] evidenced that the NMR derived folding (Figure 11A) could fit all diffraction data if alternative aptamer orientations with respect to thrombin were considered. Indeed, according to the electron density maps, it was assumed that the oligonucleotide quartet region (including the DNA backbone) was correct as reported in the crystal structures, whereas, due to the D2 symmetry of the aptamer core, there are four distinct possible orientations of the NMR folding that overlap with the core of the X-ray model (Figure 12). The re-evaluation of the X-ray complex gave similar results among orientations I−IV, but orientation III showed the best agreement with the experimental data.[90]

Accordingly, different TBA−thrombin complexes in which the aptamer can bind ABE I through the TGT loop and ABE II through the TT loops (Figure 12, orientations I and II), or the other way around (Figure 12, orientations III and IV), are possible. Supporting this view, the newly released X-ray structures of thrombin−TBA−Na^+ and thrombin−TBA−K^+complexes (PDB IDs 4DIH and 4DII, respectively)[89]showed the aptamer interacting with the enzyme assuming orientation IV (Figure 12). Moreover, the X-ray structure of human thrombin in complex with a modified TBA containing a 5’-5’inversion of the polarity site(3 ’GGT5 ’-5’TGGTGTGGTTGG3’, namely mTBA) has also been reported (PDB ID 3QLP).[91]

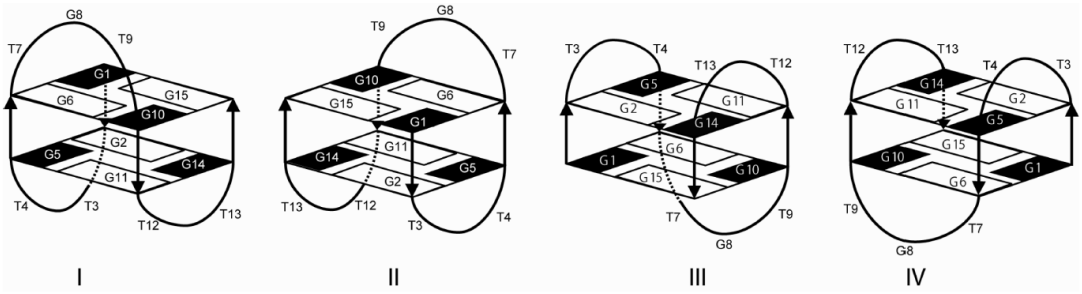

Figure 12. *Representation of the four orientations of the NMR derived folding with respect to thrombin corresponding to the D2 symmetry of the quadruplex core assuming the same strand polarity of the X-ray complex.*

The X-ray complex revealed that the interaction occurs between the TT loops and ABE I (orientation III in Figure 12), whereas the TGT loop, particularly T7, is not involved in any relevant interaction with the protein. Despite the fact that mTBA binds to thrombin with higher affinity with respect to TBA[92] it showed poor anticoagulant activity if compared to TBA in PT assay.[93] On the other hand, Toggle-25t, an RNA aptamer that contains 2'-fluoropyrimidine nucleotides, and a 29-mer single-stranded DNA, designated DNA60-18 or HD22, bind selectively thrombin at ABE II and they also showed limited effect on clotting times.[94,95] Because of their thrombin allostery, ABE I and ABE II aptamers were used in combination to test their mixed effect on thrombin activity.[83,96,97] The obtained results showed that synergistic anticoagulant effects can be achieved by mixing TBA with Toggle-25t or HD22 and by linking TBA to HD22with an appropriate-sized spacer.

The phase I clinical trial for TBA demonstrated its positive pharmacokinetic profile in humans; however, clinical trials were halted after phase I due to suboptimal dosing profiles[98]. To optimize its anticoagulant properties, of particular interest is the enlargement of data gathering about TBA structure–activity relationships (SARs)

through the development of new derivatives. In the nucleic acids research area the introduction of suitable modifications on natural oligonucleotide sequences represents a method widely employed to explore the relevance of single nucleotides both on secondary structure folding topology and on binding with target proteins. The explored modifications involve the nucleobases,[99,100] the sugar–phosphate backbone,[101,102] and the conjugation to flexible non-nucleotide linkers.[103-105]

2.1. Modified TBA

Considering the extremely short *in vivo* half-life (~2 min) of unmodified TBA, a number of different approaches have been adopted to improve the enzymatic degradation resistance of the aptamer as well as its anti-thrombin effect for potential in vivo applications.

In various strategies TBA maintained its natural backbone and was only modified in the sequence: by substituting several bases in the loops[103,106,107] and/or in the G-quartets or by inserting 5'- or 3'-extensions[108,109]. Sugimoto et al. for example synthesized TBA analogs in which thymine residues were substituted by adenine. This study demonstrated that thrombin stabilizes the G-quadruplex via the interaction with residues in the loops but not via direct stabilization of G-quartets.

Some researchers have explored non-natural modifications of the nucleobases[99,110-114] which included: guanines modified with hydrophobic substituents in the N2 and C8 positions; 6-thio-, 8-amino-,iso-, and 8-bromo-guanine modifications; and thymine with 4-thio-uracil substitutions.

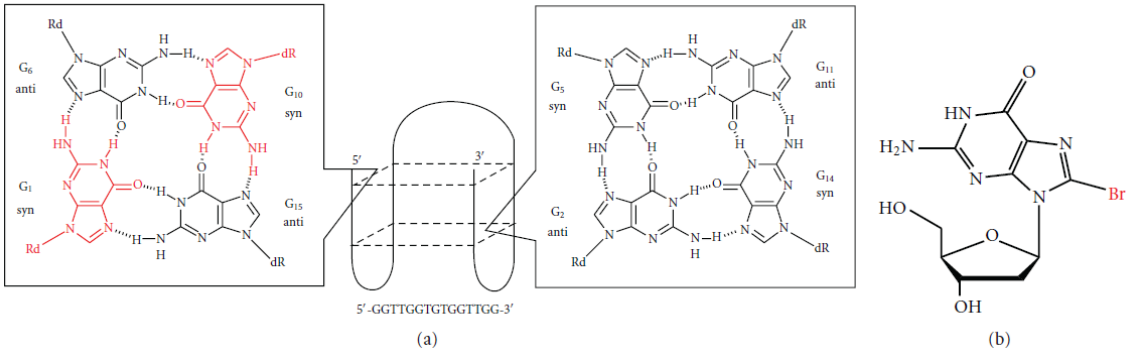

Figure 13. *Structure of (a) G-quadruplex of thrombin binding aptamer and (b) 8-bromodeoxyguanosine. Modification sites, G1 and G10, are indicated in red.*

Other research groups modified the nucleotide backbone of TBA by introducing valuable surrogates replacing the natural phosphodiester linkages, such as: neutral formacetal groups,[101] phosphorothioate linkages,[102,115] 3′-3′ or 5′-5′ phosphodiester bonds[91-93]and methylphosphonate[102] bonds or the nucleoside moieties, with insertion within the backbone of: 2′-deoxy-2′-fluoro-D-arabinonucleotides (2′F-araN) [116] (Figure 14), locked-nucleic acids,[117,118] unlocked nucleic acids (UNA),[119-121] acyclic thymine nucleoside residues.[122]

Most of these chemical modifications do not result into relevant improvements in the anticoagulant properties of TBA, even if in some reports an increase of the overall stability of the G-quadruplex structure and/or of the affinity for thrombin is registered.

In this scenario, due to the symmetry of TBA and the complexity of the regulatory mechanism of thrombin, which includes a long-range allosteric linkage between ABE I and ABEII, the exact binding mode of aptamers to thrombin and its correlation with the observed biological activity is still a matter of debate.

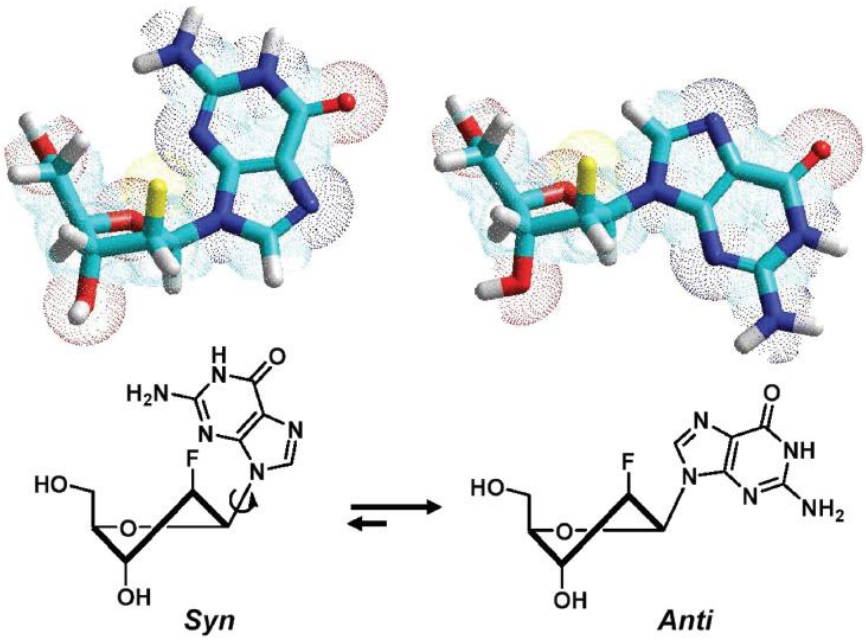

Figure 14. *Glycosic conformation equilibrium of dG and 20F-araG with south furanose sugar ring.*

Herein will describe the results obtained by synthesis and biological characterization of several TBA analogs libraries to clarify the key parts of the sequence for the interaction with the natural substrate, in order to obtain the best analog more stable and active than TBA.

3.Investigating the Role of T7 and T12 Residues on the Biological Properties of Thrombin-Binding Aptamer: Enhancement of Anticoagulant Activity by a Single Nucleobase Modification.

In the understanding of the bases of TBA–thrombin recognition, it was previously developed new single-stranded TBA analogues, in which the acyclic nucleoside **a** (Figure 15) replaced, one at a time, all thymine residues along the aptamer sequence.[122]

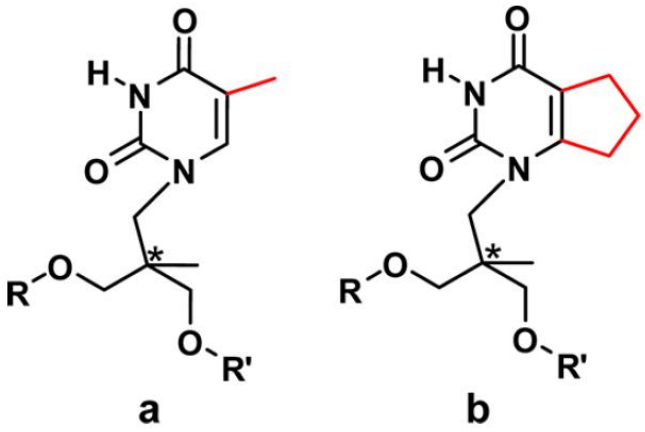

Figure 15. *Acyclic nucleosides mimicking T. The presence of the carbon atom marked with an asterisk causes the formation of two diastereomeric ONs when the nucleoside is inserted in the TBA sequence.*

The modification at position 7 in the $T_7G_8T_9$ loop (herein TBA-T7a) gives rise to an ON that folds into a quadruplex structure that is more stable and active than the quadruplex structure formed by TBA. On the other hand, within the four ONs containing the acyclic nucleoside **a** at one position of TT loops, the ON modified at T12 (herein TBA-T12a) showed the most significant biological properties.[122] In line with data reported from other authors,[121] the results evidenced that modification at T7 and T12 along the TBA sequence can be fruitful to improve the biological activity.

To investigate the role of the modification at T7 and T12 in affecting the structural stability and the biological activity, I synthesized two new modified TBAs, named TBA-T7b andTBA-T12b, which differed from the previously reported analogues only in the thymidine base coupled with the acyclic linker, which was bulked by fusing a hydrophobic five member cycle with the pyrimidine ring (**b**, Figure 15). The abilities of TBA-T7b and TBA-T12b to fold into G-quadruplex structures, as well as their biological properties, were evaluated by CD and ^{1}H NMR experiments and by PT and purified fibrinogen clotting assays, respectively. Finally, a computational study allowed the analysis of the obtained SARs.

3.1 RESULTS AND DISCUSSION

Synthesis of Monomer 6. The synthesis of the modified acyclic nucleoside phosphoramidite building block 6, used for the automated synthesis of TBA-T7b and TBA-T12b, is summarized in Scheme 1.

The synthesis of N1-alkylated intermediate 3 was performed via Mitsunobu reaction[123] between 2, obtained as described under Experimental Section, and 1. The yields of this coupling reaction were strongly dependent on the initial temperature of the system and on the order in which the reagents were added. We found that temperatures lower than 30 °C were always detrimental to the reaction yield, and that higher yields (45−50%) were obtained by mild heating (30 °C) of a dioxane solution containing 2 and triphenylphosphine followed by addition of di-tert-butylazodicarboxylate and finally a dioxane solution of protected linker 1 (100 μL of solvent per 1 mmol).

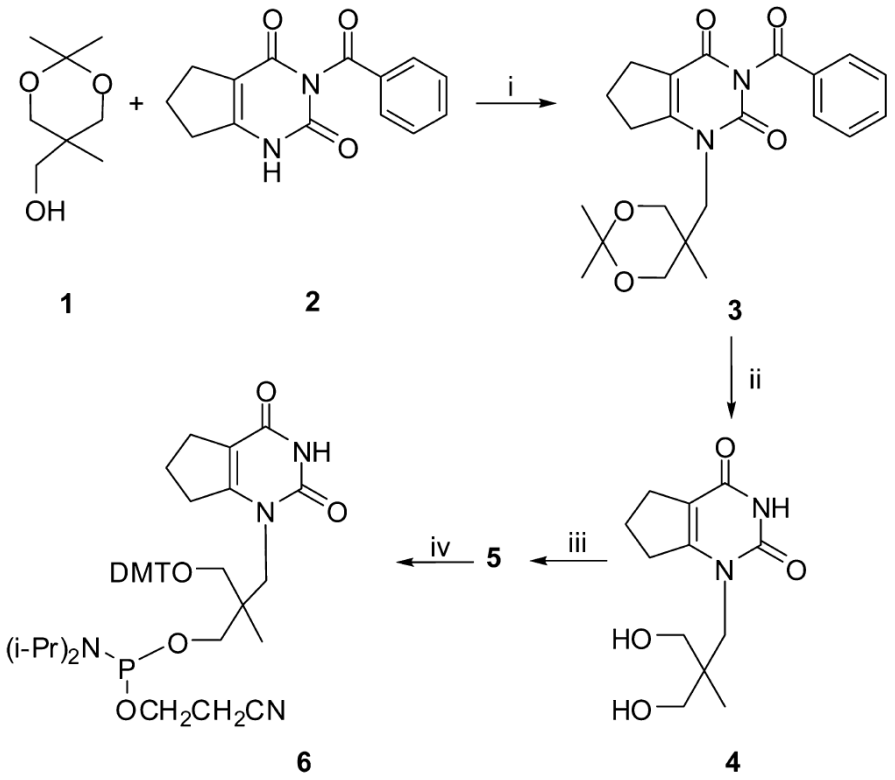

Scheme 1. *Synthesis of Monomer 6. (i) 1 0.94 g (5.9 mmol), 2 1.50 g (5.9 mmol), triphenylphosphine 2.28 g (8.7 mmol), di-tert-butylazodicarboxylate 2.1 g (9.1 mmol), dry dioxane (70 mL), 24 h, 30°C, yields 43%; (ii) (a) 3 1.0 g (2.5 mmol), Dowex H+ 450 mg, MeOH/H2O (9:1 v/v) 100 mL; (b) aqueous NaOH (1.0 M, 5 mL) yields 98%; (iii) 4 640 mg (2.5 mmol), 4,4'-dimethoxytrytylchloride 541 mg (1.6 mmol), 2,4-dimethylaminopyridine 15 mg (0.12 mmol), pyridine (20 mL), acetonitrile (10 mL), 1.5h, rt, yields 45%; (iv) 5 600 mg (1.1 mmol), 2-cyanoethyldiisopropylchlorophosphoramidite 300 µL (1.2 mmol), DIPEA 600 µL (3.6 mmol), DCM (8 mL), 40 min, rt, yields 99%*.

The intermediate 4 was obtained by removing both the linkerand nucleobase protecting groups from 3 using a one-pot procedure (see Experimental Section). Finally, 4 was functionalized to phosphoramidite building-block 6 using standard procedure.

The acyclic nucleoside 6 was inserted as a T mimic at position 7 or 12 along the TBA sequence to obtain TBA-T7band TBA-T12b, respectively.

Structural Characterization TBA-T7b and TBA-T12b were characterized by circular dichroism (CD), CD melting, and ^{1}H NMR for their ability to fold into G-quadruplexes. Circular dichroism is a useful technique to preliminarily study a G-quadruplex structure or to confirm a particular conformation inferred by other more informative techniques. The introduction of the new acyclic nucleoside **b** at position 7 or 12 does not affect the overall G-quadruplex topology formed in solution. CD profiles of TBA-T7b and TBA-T12b are similar to those of TBA in both PBS and K^{+} buffer (left and right panels, respectively, in Figure 16), showing maxima at about 208, 245,and 295 nm and a minimum at 267 nm. As expected, positive CD bands have higher molar ellipticities in K^{+} buffer than in PBS, according to the well-known dependence of G-quadruplex stabilities from the type of cations present in the buffer solution.[124-126]

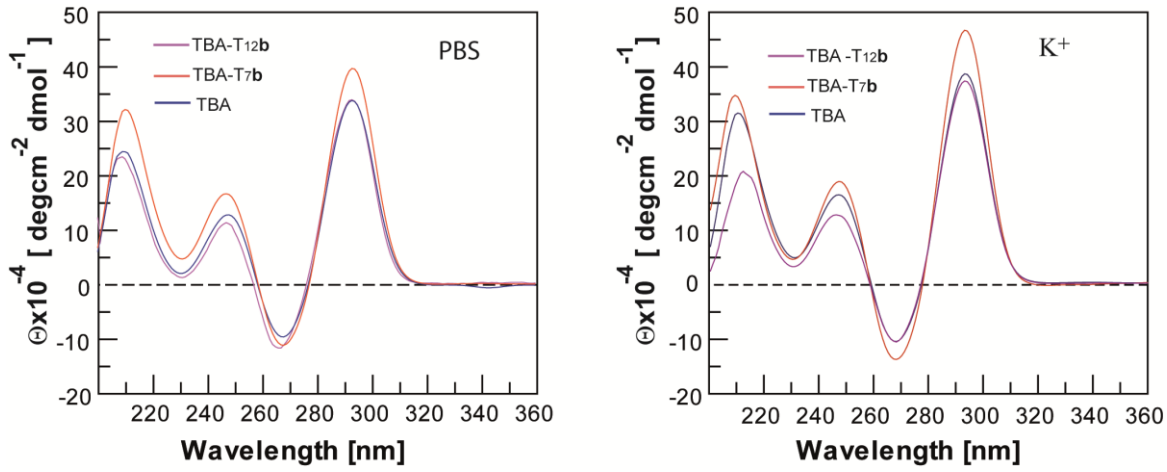

Figure 16.*CD profiles in PBS (left) and in potassium phosphate buffer (right); [ON]=2.0 × 10^{-5} M.*

The ^{1}H NMR analysis, performed at temperatures in the range of 25–50 °C, confirmed that TBA-T7b and TBA-T12b form a stable G-quadruplex structure when annealed in K^{+}buffer. However, ^{1}H NMR spectra appear more crowded than expected for a single quadruplex species, even at 25 °C (Figure 17), where only 14 aromatic signals and 8

imino proton signals are expected. This finding was previously explained by considering that the replacement of a T residue with the acyclic nucleoside a produces two closely related diastereomeric G-quadruplex forming ONs.[122]

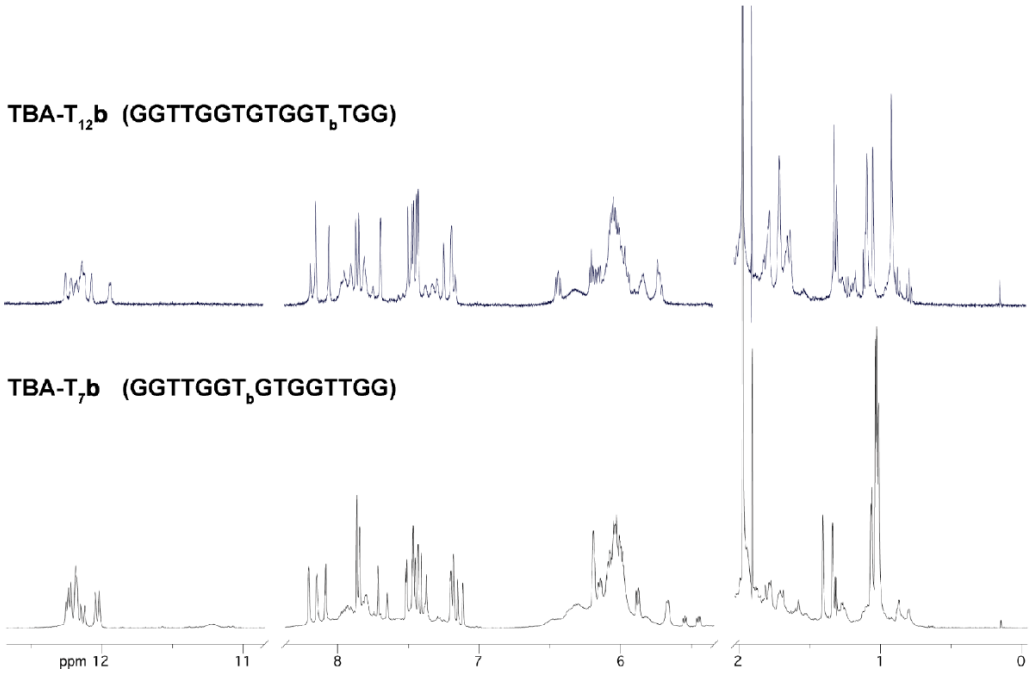

Figure 17. *^{1}H NMR spectra of TBA-T7b and TBA-T12b recorded at 25 °C in K^{+} buffer.*

Although both modified ONs show Tm values higher than that of TBA (Figure 18 and Table 1), the replacement of T7 with the acyclic nucleoside **b** stabilizes the resulting G-quadruplexes more efficiently than replacement of T12.

In fact TBA-T7b and TBA-T7a show the same melting profile, with a Tm higher than that of TBA (Table 1), it can be concluded that the sole presence of the acyclic linker unit at position 7 is responsible for the structural stabilizing effect.

These data account for the nucleobase 7 always positioned outside the G-quadruplex core and not involved in intramolecular interactions, as well as for the reported stabilizing role played by T4 and T13 on TBA structural stability.

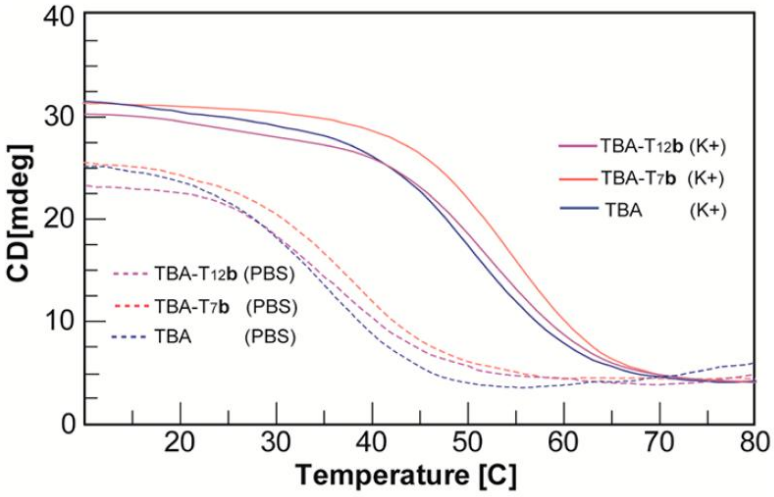

Figure 18. *CD melting curves of TBA and its analogues in potassium phosphate(continuous lines) or PBS (dotted lines) buffer. Concentration of each ON was 2.0 × 10^{-5} M. The curves were obtained by monitoring the variation of absorbance at 295 nm from 10 to 80 °C at 0.5 °C/min.*

	T_m (±0.5 °C)	
ON	PBS	K^+ buffer
TBA	33.0	50.0
TBA-T_{12}**a**	34.0[a]	51.0[a]
TBA-T_{12}**b**	34.5	51.5
TBA-T_7**a**	37.5[a]	54.0[a]
TBA-T_7**b**	37.5	54.0

[a]Data taken from ref.122

Table 1. *Tm Values of TBA and Its Analogues*

In line with these results, a similar increase in Tm value has also been observed by replacing the sugar moiety of T7 with a different acyclic linker.[121]

PT Assay. The anticoagulant activity in the presence of all thrombin substrates and cofactors was evaluated by PT assay.PT analyses were performed at [ON] of 2 and 20 µM after 2min of incubation with human plasma (Figure 19).

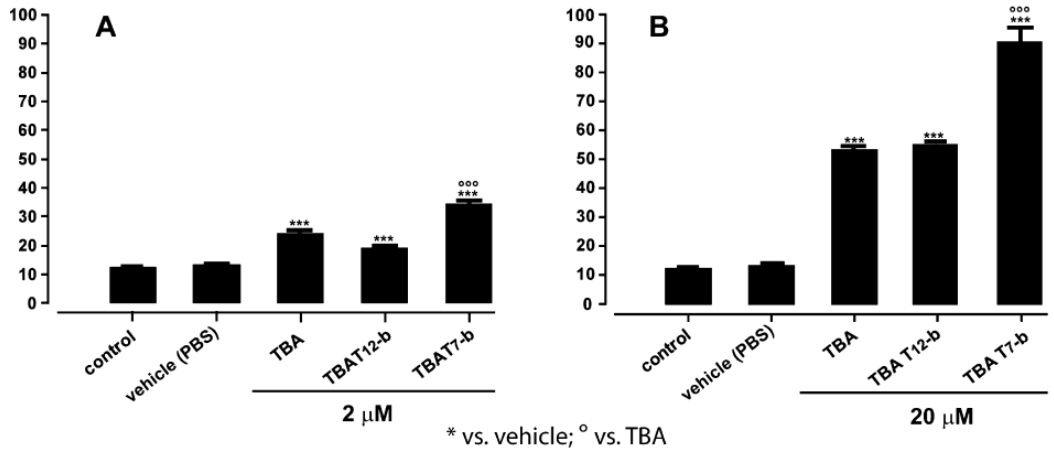

Figure 19. *Concentration-dependent response, following 2 min ON incubation with human plasma at 2 (A) or 20 μM (B) [ON]. PT values are expressed in seconds. Each measurement was performed in triplicate and is shown as the mean ± SEM. The basal PT time is 13.4 ± 0.2 s.*

To better understand the effects induced by the presence of nucleoside **b** on the anticoagulant activity, we compared the prolonging of clotting time caused by TBA-T7b and TBA-T12b with that of TBA and those of the previously reported[122]analogues TBA-T7a and TBA-T12a (Table 2). It is noteworthy that TBA-T7b prolonged the basal PT valueto a significantly larger extent with respect to TBA and TBAT7a (Figure 19). Replacement of nucleoside **a** for **b** was more effective also at position 12 (Table 2).

ON	PT value[a] (20 μM)	fold increase
TBA	53.68 ± 1.48	4.01 ± 0.70
TBA-T_7**a**	60.20 ± 1.38[b]	4.50 ± 0.60
TBA-T_7**b**	90.60 ± 5.26	6.77 ± 0.24
TBA-T_{12}**a**	44.83 ± 1.29[b]	3.35 ± 0.60
TBA-T_{12}**b**	55.20 ± 0.47	4.12 ± 0.20

[a]PT values are expressed in seconds. [b]Data taken from ref.122

Table 2. *PT Values Measured after 2 min of incubation using 20 μM ON concentration and Fold Increases of Basal PT Time (13.4 ± 0.2 s).*

In particular,TBA-T12b is less active than TBA at 2 µM, but showed a greater increase of activity at higher concentration, thus attaining that of TBA at 20 µM (Figure 19).

To exclude that the observed activity of modified aptamers could be due to higher nuclease stability with respect to TBA, the experiments were repeated, changing the incubation time of TBA and analogues with plasma from 30 s to 15 min. PT results were almost unchanged for all sequences (Table 3).

	Prolonged clotting time (s)				
ON	**200 nM**	**300 nM**	**500 nM**	**750 nM**	**1000 nM**
TBA	18±2.7	50±2.3	137±6.3	170±24	170±25
TBA-T_7**b**	10±2.5	26±2.3	120±6.0	120±22	140±27
TBA-T_{12}**b**	NA[a]	16.8±0.71	98.9±0.7	100±30	100±10

[a]Not active.

Table 3*. Prolonged fibrinogen clotting time results in presence of human thrombin. Each value was calculated subtracting the clotting time produced by thrombin alone from that measured in the presence of one of the aptamers. The measurements were performed preincubating for 1 min 200 µL of purified fibrinogen solution (2.0 mg/mL in PBS) with various concentrations of aptamers. The reaction started by the addition of 100 µL of human thrombin solution (10 NIH* per mL) and clotting time *was recorded*. *In absence of any inhibitor, the measured clotting time for human thrombin was 24.9± 0.5 s.*

Fibrinogen Assay Using Human and Bovine Thrombin. The new ONs were subjected to purified fibrinogen clotting assay to evaluate their ability to inhibit the conversion of soluble fibrinogen into insoluble strands of fibrin in the absence of any other thrombin ligands/effectors (Figure 20).

The assay was performed using various concentrations of each aptamer. The purified fibrinogen solution was preincubated with the aptamer and the reactions were initiated by the addition of human thrombin and clotting times were recorded.

The fibrinogen assay results evidenced that at all ON concentrations tested, the most efficient inhibitor is the unmodified TBA sequence (Figure 20A), thus reversing the results gathered from the PT assay.

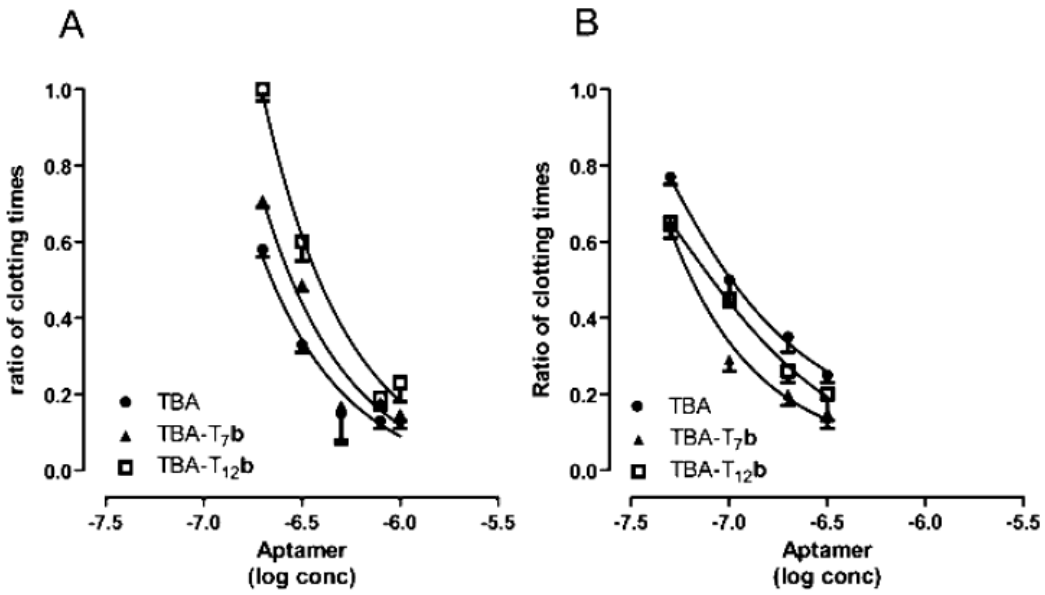

***Figure 20**. Effects of aptamers on human (A) and bovine (B) thrombin clotting time in fibrinogen solution. The results are expressed as the ratio ofclotting times measured in the absence and in the presence of the aptamers. The effects are reported as a function of log [ON]. Each measurementwas performed in triplicate and is shown as the mean ± SD.*

To further investigate this phenomenon, the fibrinogen assay was performed by using bovine thrombin, which differs from human thrombin in some residues of the fibrinogen-binding site (ABE I) that are crucial for TBA−thrombin interaction (see next paragraphs for details). By changing the source of the target enzyme, both modified sequences showed a substantial increase in their ability to inhibit thrombin activity (Figure 20B), whereas the inhibitory activity of TBA was only slightly increased; as a consequence, TBA-T7b became again the best inhibitor.

Conformational Search on TBA and Modified Analogues TBA-T7b and TBA-T12b.

An extensive molecular modeling study, including molecular mechanics (MM) and dynamics (MD) calculations, was undertaken to analyze the SARs of new modified TBAs. In particular, to investigate the conformational properties of TBA and the new modified aptamers, a simulated annealing(SA) procedure followed by MM energy minimization was applied. Following the criteria described under Experimental Section, resulting conformers were analyzed and each nucleotide of loops was classified on the basis of (i) χ torsional angle values, to identify the conformation of the glycosidic bond (i.e., syn, anti, or s/a); and (ii) the interatomic distance between its own centroid and that of the two G-tetrads, to investigate the position of loop nucleotides with respect to the guanine planes (i.e., "stacked" or "not-stacked"). Occurrence rates were calculated and compared to those obtained for TBA. Because the replacement of T7 and T12 residues with nucleoside **b** produced a mixture of diastereoisomers, characterized by S or R configuration at the acyclic linker, the occurrence rates reported in Tables 4 and 5 are the mean of the values obtained for the two diastereoisomers.

	TBA			TBA-T_7**b**			TBA-T_{12}**b**		
	syn	*anti*	s/a	*syn*	*anti*	s/a	*syn*	*anti*	s/a
T_3	28.5	69.5	2.00	37.0	61.5	1.50	47.0	50.5	2.50
T_4	38.5	56.0	5.50	29.0	65.5	5.50	43.0	52.0	5.00
T_7[a]	39.0	59.5	1.50				36.0	62.5	1.50
G_8	39.5	38.0	22.5	35.0	46.5	18.5	34.5	44.0	21.5
T_9	41.5	50.0	8.50	34.0	57.0	9.00	42.0	51.0	7.00
T_{12}[b]	32.0	66.0	2.00	42.0	56.0	2.00			
T_{13}	37.0	59.0	4.00	36.0	60.5	3.50	42.0	54.5	3.50

[a] T_7 residue in TBA-T_7b is replaced by the acyclic nucleoside b. [b] T_{12} residue in TBA-T_{12}b is replaced by the acyclic nucleoside b.

Table 4. *Calculated Occurrence Rates (Percent) of syn, anti, and s/a Conformers of TGT and TT Glycosidic Bonds.*

The structural analysis evidenced that, although inducing some variations, the introduced modifications at T7 and T12 did not cause a reversal of the conformational preference of the glycosidic bonds with respect to TBA (Table 4). Consequently, in agreement with previously reported NMR studies,[86] TBA and modified aptamers TBA-T7b and TBA-T12b conserved an overall preference for the anti conformation of thymines in TGT and TT loops. With regard to the stacking of the TGT loop nucleobases on the G-tetrads, TBA-T7b and TBA-T12b present an increased stacking of T9 and a decreased stacking of G8 (Table 5). Nevertheless, the conformational features of the TGT loop still evidenced the same trend of TBA with the following order of residue stacking on the G-tetrads: G8 > T9 > T7.

The two modified analogues showed a similar conformational behavior at the T3 T4 loop because, either in TBA-T7b or in TBA-T12b, the rate of stacked conformation of T3 and T4 decreased and increased, respectively, with respect to TBA, evidencing a conformational linkage between TGT and T3T4loops. On the contrary, different results were obtained for theT12T13 loop. In fact, as expected, the substitution of T12 with the acyclic nucleoside **b** (TBA-T12b) affected the conformational flexibility of the T12 T13 loop, inducing a decreased stacking rate of both nucleobases, which was not observed in TBA-T7b (Table 5).

	TBA	TBA-T_7**b**	TBA-T_{12}**b**
T_3	62.5	33.0	39.0
T_4	46.0	60.0	65.0
T_7[a]	14.0	12.0	10.0
G_8	78.5	50.0	49.0
T_9	26.0	39.5	42.5
T_{12}[b]	33.5	37.0	29.0
T_{13}	38.0	40.5	29.0

[a] T_7 residue in TBA-T_7**b** is replaced by the acyclic nucleoside **b**. [b] T_{12}

Table 5. *Calculated Occurrence Rates (Percent) of Conformers Presenting TGT and TT Nucleobases "Stacked"on the Guanine Planes.*

NMR studies performed on TBA[84] revealed that the positioning of T4 and T13 plays a key role in quadruplex folding and stability; accordingly, due to the increased stacking of T4 and T13 on the guanine planes, TBA-T7b was structurally more stable than TBA in CD melting experiments (Table 1 and Figure 18).

Molecular Modeling Studies on Aptamer Interaction with Human and Bovine Thrombin. With the aim of identifying the effects of the new structural modifications on aptamer−thrombin interactions, first, all possible aptamer−thrombin binding modes and the corresponding binding interactions were analyzed (PDB IDs 1HAO, 1HAP, 1HUT,4DIH, and 4DII; see Experimental Section). This study revealed that the various binding orientations of TBA with respect to human thrombin (Figures 11 and 12) produced different binding modes in the crystal complexes sharing similar interactions with ABE I but involving different aptamer residues (Figure 21).

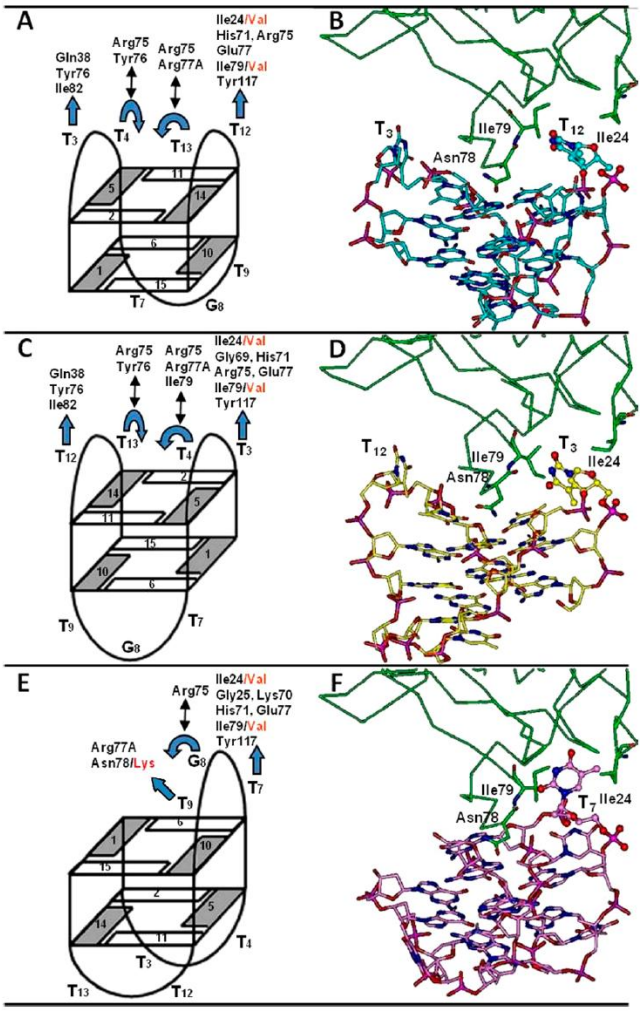

Figure 21. *Cartoon (left) and 3D (right) structure of the different binding orientations of TBA with respect to human thrombin ABE I(green). (A, C, and E) Amino acid residues involved in TBA−thrombin interactions are evidenced in black; where mutated, the corresponding bovine residues are reported in red. The blue curve and straight arrows indicate loop nucleotides "stacked" or "not-stacked" on G-tetrad, respectively. (B) PDB ID 1HAO (TBA carbons = cyan); (D)PDB ID 4DIH (TBA carbons = yellow); (F) PDB ID 1HAP (TBA carbons = magenta). Protein carbons are colored in green, residues within TBA binding site that are mutated in bovine thrombin are shown and labeled. The nucleotides T3, T7, and T12 are evidenced as ball and stick. Heteroatoms are colored as follows: O = red; N = blue; P = magenta. Hydrogens are omitted for the sake of clarity.*

Indeed, a thymine residue of TBA always interacts with ABEI hydrophobic cleft lined by Ile24, His71, Ile79 and Tyr117, but, depending on the binding mode, the interactions involveT3 (Figure 21C,D), or T7 (Figure 21A,B), or T12 (Figure 21E,F).

T_7 interacts penetrating into the hydrophobic cleft more thanT_{12} and T_3 (Figure 21F vs Figure 21B,D); while the positioning ofthese latter resulted identical due to the symmetry of the twoTT loops (Figure 21B vs Figure 21D). By consequence, a second ABE I subsite, including Gln38, Tyr76 and Ile82, interacts withT_{12} or T_3, depending on the binding orientation (Figure 21A–D). When the TGT loop binds to ABE I, the interaction with this second subsite is absent (Figure 21,F).

Second, to identify the structural differences in TBA-binding site, experimentally determined structures of human and bovine thrombin were compared (PDB IDs are listed in the Experimental Section). Only three TBA-binding site residues,Ile24, Asn78, and Ile79, were mutated in bovine thrombin, with no significant variation of the backbone structure (Figure 21). Human thrombin Asn78 residue (replaced by a lysine in bovine thrombin) interacts only with the TGT loop, establishing an H bond interaction with the phosphate group of T9 (PDB IDs1HUT and 1HAP; Figure 21E,F).

On the contrary, the interactions with human ABE I hydrophobic cleft containing Ile24 and Ile79 are conserved in all crystal complexes and involve T3 or T7 orT12 depending on TBA-binding orientation (Figure 12). The replacement of these two isoleucine residues in human thrombin by two valine residues in the bovine homologue determines an enlargement of the employable volume within the ABE I cleft. We then calculated the occurrence rates of TBA, TBA-T7b,and TBA-T12b SA/MM conformers presenting solvent accessible surface areas of residues 3, 7, and 12 equal to or greater

than that of the corresponding residue of TBA binding the ABE I hydrophobic cleft in experimentally determined complexes (Table 6).

ON	T_3	T_7[a]	T_{12}[b]
TBA	16.5	85.0	36.5
TBA-T_7**b**	21.0	88.0	34.5
TBA-T_{12}**b**	22.0	76.0	50.0

[a]T_7 residue in TBA-T_7**b** is replaced by the acyclic nucleoside **b**. [b]T_{12} residue in TBA-T_{12}**b** is replaced by the acyclic nucleoside **b**.

Table 6. *Occurrence Rates (Percent) of TBA, TBA-T7b, andTBA-T12b SA/MM Conformers Presenting a Solvent-Accessible Surface Area (Å2) of Residues 3, 7, and 12 Equal to or Greater than That of the Corresponding Residue ofTBA Assuming the Bioactive Conformation at the ABE I Hydrophobic Cleft.*

Interestingly, the replacement of T7 and T12 with the acyclic nucleoside **b** determined in both cases a greater rate of conformations presenting a solvent-exposed conformation. Moreover, in agreement with the results reported in Tables 4 and 5, T3 is more exposed to the solvent in the new modified aptamers than in TBA. Finally, we calculated the occurrence rates of bioactive conformations of residues at positions 3, 7, and 12 resulting from SA/MM calculations on TBA, TBA-T7b, and TBA-T12b (Figure 22 and Table 7).

With this aim, all obtained conformers were superimposed on the experimentally determined TBA–thrombin complexes by fitting the guanine tetrads to evaluate the overlap with the residue interacting with the ABE I hydrophobic cleft (see Experimental Section for details). Obtained results show that TBA-T7b presents an increased rate of bioactive conformations if compared to TBA; on the contrary, the substitution of T12 with **b** decreases the rate of bioactive conformations of T3 and T7. Interestingly, the replacement of T7 and T12 with the acyclic nucleoside **b** determined in both cases a

greater rate of conformations presenting a solvent-exposed position able to drive the interaction with the ABE I hydrophobic cleft. Nevertheless, likely due to the higher flexibility of the TGT loop with respect to the TT loops, there is a higher occurrence rate of T7b assuming the ABE I bioactive conformation compared to T3 and T12b (Table 7 and Figure 22). In the new TBA derivatives TBA-T7b and TBA-T12b, the introduction of the acyclic linker facilitates the extension of the phosphate backbone toward the solvent and the penetration of the modified nucleobase within the ABE I hydrophobic cleft, thus amplifying the steric hindrance caused by the presence of the five member cycle on modified nucleobase **b** (Table 6 and Figure 22).

Accordingly, the presence of the smaller Val24 andVal79 residues in bovine thrombin could explain the increased activity of the new modified TBA analogues for this enzyme. The observed higher activity of TBA-T7b is indeed correlated to the calculated higher rate of bioactive conformations at the ABE I hydrophobic cleft with respect to TBA and TBA-T12b (Table 7 and Figure 22). This hypothesis is supported by the previously reported activity of TBA-T7a and TBA-T12a,[122]which, lacking the steric bulk at the modified nucleoside, was more active in the fibrinogen assay using human thrombin. On the other hand, the charged group at the lysine side chain allows the establishment of an ionic interaction with the modified TGT phosphate backbone of TBA-T7b, likely contributing to the enhancement of inhibitory ability.

On these bases, the apparent incongruence of PT and fibrinogen assay results, using human thrombin, can be interpreted by taking into account the effects of different aptamer binding modes on thrombin allostery. In the PT assay a number of thrombin ligands/effectors other than fibrinogen that are able to modulate thrombin activity are

present,[1,2,41,68,127-129] thus driving different binding modes; the new modified aptamers could differently affect this ligand/effector binding network.

In this scenario, it is noteworthy that the 65−84 thrombin loop, involved in specific interactions with the modified nucleobase of the new TBA derivatives according to our binding mode hypothesis, has been proved to be responsible for the allosteric long-range communication among ABE I, the catalytic site, and ABE II.[68] Altogether, our results reveal the absence of a direct correlation between the structural stability and the anticoagulant property in our series of modified TBAs, suggesting that the role played by T7 (placed in the TGT loop) and T12(placed in the TT loop close to the 3′ terminus) in the biological activity of TBA and its analogues could involve alternative aptamer binding modes and the complex and not yet fully understood allosteric mechanism of action of thrombin.

ON	T_3	T_7[a]	T_{12}[b]
TBA	9.50	12.0	10.0
TBA-T_7**b**	8.00	14.0	13.5
TBA-T_{12}**b**	6.50	6.50	10.0

[a] T_7 residue in TBA-T_7**b** is replaced by the acyclic nucleoside **b**. [b] T_{12} residue in TBA-T_{12}**b** is replaced by the acyclic nucleoside **b**.

Table 7. *Occurrence Rates (Percent) of Bioactive Conformations at the ABE I Hydrophobic Cleft of Residuesat Positions 3, 7, and 12 Resulting from SA/MMCalculations*

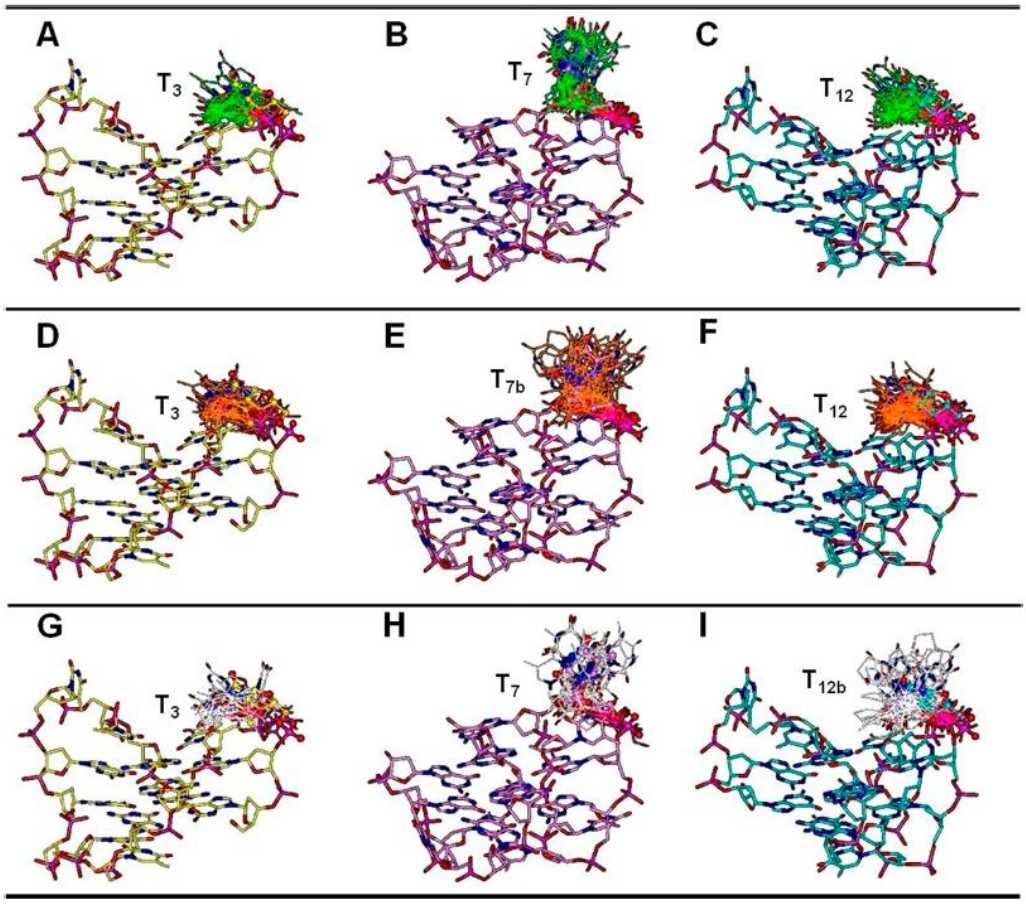

Figure 22. *TBA (green; A–C), TBA-T7b (orange; D–F), and TBA-T12b (white; G–I) SA/MM conformers presenting residue 3, 7, or 12 assuming ABE I hydrophobic cleft binding conformation. Molecular models are superimposed on 4DIH (A, D, G; yellow), 1HAP (B, E, H; pink), or 1HAO(C, F, I; cyan) by fitting the guanine tetrads. All conformers of TBA and the mean of those obtained for the two diastereoisomers of TBA-T7b andTBA-T12b are shown. For the sake of clarity only the residue interacting with the ABE I hydrophobic cleft is displayed and hydrogens are omitted. Heteroatoms are colored as follows: O = red; N = blue; P = magenta.*

3.3 CONCLUSIONS

Bringing together the so far acquired knowledge of the thrombin−TBA interaction and thrombin allosteric regulatory mechanism with reported SAR data, I determined that the G quadruplexes formed by the modified TBAs can bind the thrombin ABE I hydrophobic cleft by using either TGT or one of the two TT loops. Reported results indicate that the incoherency of their behaviors in the two explored biological tests is due to the molecular process through which they exert the anticoagulant activity, which is surely more intricate than a competitive inhibition with the fibrinogen-binding site. Besides their high anticoagulant activity, these molecules represent valuable tools to further explore the complex regulatory mechanism of thrombin during plasma coagulation that is, as yet, not completely clarified.

3.4 EXPERIMENTAL SECTION

General Procedure. Chemicals and anhydrous solvents were purchased from Fluka-Sigma-Aldrich. TLCs were run on Merck silica gel 60 F254 plates. Silica gel chromatography was performed by using Merck silica gel 60 (0.063−0.200 mm). An API 2000 (Applied Biosystem) mass spectrometer was used to perform the analyses of the intermediates and monomer 6. NMR experiments were recorded using Varian Mercury Plus 400 MHz and Varian UNITYINOVA 500 and 700MHz spectrometers and processed using the Varian VNMR software package. Reagents and phosphoramidites for DNA synthesis were purchased from Glenn Research. ON syntheses were performed on a PerSeptive Biosystem Expedite DNA synthesizer. HPLC purifications and analyses were carried out using a JASCO PU-2089 Plus HPLC pump equipped with a JASCO BS-997-01 UV detector. The purity of the final products was determined as >95% by using a C-18 RP analytical column (C-18 Purospher STAR, Merck) eluted by a gradient of CH3OH in H2O (from 0 to 100% in 30 min). CD experiments were performed on a JASCO 715 spectropolarimeter equipped with a PTC-348 temperature controller.

Synthesis of Monomer 6. (a) 3-Benzoyl-6,7-dihydro-1Hcyclopenta[d]pyrimidine-2,4(3H,5H)-dione (2). Nucleobase 6,7-dihydro-1H-cyclopenta[d]pyrimidine-2,4(3H,5H)-dione was obtained as previously reported by Renault et al.[130] and converted in its N3 benzoyl derivative 2.[122]

^{1}H NMR (400 MHz; mixture of CD_3OD and $CDCl_3$),δ 7.75 (d, J = 8.0 Hz, 2H), 7.60 (t, J = 8.0 Hz, 1H), 7.43 (t, J = 8.0 Hz,2H), 3.03 (t, J = 7.3 Hz, 2H), 2.67 (t, J = 7.3 Hz, 2H), 2.10 (q, J = 7.3Hz, 2H);

^{13}C NMR (100 MHz; mixture of CD3OD and CDCl3), δ169.3, 166.3, 155.2, 147.3, 134.2, 132.2, 128.9, 128.3, 127.5, 127.0,113.4, 34.8, 30.5, 18.0.

ESI mass (positive mode), calculated 256.1;found 257.1 [M + H]+, 279.1 [M + Na]+.

(b)3-Benzoyl-1-[(2,2,5-trimethyl-1,3-dioxan-5-yl)methyl]-6,7-dihydro-1H-cyclopenta[d]pyrimidine-2,4(3H,5H)-dione (3).

Compound 2 (1.5 g, 5.9 mmol) was suspended in 70 mL of dry dioxane at 30° C in the presence of triphenylphosphine (2.28 g, 8.7 mmol) before the addition of di-tert-butyl azodicarboxylate (2.1 g, 9.1 mmol).To the resultant mixture, after 10 min of stirring at room temperature, was added 5.9 mmol of 1 dissolved in dry dioxane (300 μL). The reaction mixture was stirred at room temperature for 18 h under argon. The solution was concentrated under reduced pressure and the residue purified by column chromatography on silica gel eluted with 95:5 Et2O/CH2Cl2 to give 3 as a white solid (yield 43%, Rf 0.70).

^{1}H NMR (400 MHz; CDCl3), δ 7.98 (d, J = 8.0 Hz, 2H), 7.60 (t, J = 8.0Hz, 1H), 7.43 (t, J = 8.0 Hz, 2H), 4.0 (bs, 2H), 3.62 (m, 4H), 3.03 (t, J= 7.3 Hz, 2H), 2.66 (t, J = 7.3 Hz, 2H), 2.09 (q, J = 7.3 Hz, 2H), 1.38(s, 3H), 1.42 (s, 3H), 0.87 (s, 3H).

ESI mass (**positive mode),**calculated 398.2; found 399.2 [M + H]+, 421.2 [M + Na]+.

(c) 1-(3-Hydroxy-2-(hydroxymethyl)-2-methylpropyl)-6,7-dihydro-1H-cyclopenta[d]pyrimidine-2,4(3H,5H)-dione (4).

Compound 3 (1.0 g, 2.5 mmol) was suspended in 9:1 MeOH/H2O (100 mL)containing 450 mg of Dowex 50WX8 (H^+). After 8 h at room temperature, a NaOH 0.5 M aqueous solution was slowly added to neutralization. The solution was filtered and, in turn,

basified with NaOH 1.0 M (5 mL) to remove the N-3 benzoyl group from the nucleobase. After 12 h at room temperature, the pH of the reaction was neutralized, the solvent was evaporated under vacuum, and the residue was dissolved in MeOH and purified by HPLC (C-18 reverse phase column, Grace Davison Discovery Sciences, eluted with ACN inH2O from 0 to 50% in 30 min) to give 4 as a white solid (yield 98%, elution time 15 min).

^{1}H NMR (700 MHz; CD3OD), δ 3.80 (bs, 2H),3.41 (d, J = 11.4 Hz, 2H), 3.38 (d, J = 11.4 Hz, 2H), 3.03 (t, J = 7.3Hz, 2H), 2.66 (t, J = 7.3 Hz, 2H), 2.09 (q, J = 7.3 Hz, 2H), 0.87 (s,3H);

^{13}C NMR (175 MHz; CD3OD), δ 163.8, 161.4, 155.7, 113.6,66.6, 49.5, 44.0, 34.2, 28.2, 22.6, 17.8;

NOESY (700 MHz; CD3OD),fundamental NOE signal between 3.80 and 3.03 ppm that confirms the linker at the N1 position.

ESI mass (positive mode), calculated 254.1;found, 255.3 $[M + H]^+$, 277.3 $[M + Na]^+$, 293.2 $[M + K]^+$.

(d) 3-(Bis(4-methoxyphenyl)(phenyl)methoxy)-2-((2,4-dioxo-3,4,6,7-tetrahydrohydro-1H-cyclopenta[d]pyrimidin-1-yl)methyl)-2-methylpropyl-2-cyanoethylDiisopropylphosphoramidite (6).

Compound 4 (640 mg, 2.5 mmol), 4,4’-dimethoxytrytyl chloride (541 mg, 1.6 mmol), and 4-dimethylaminopyridine (15.0 mg, 0.12 mmol) were dissolved in dry pyridine (20 mL) and dry ACN (10 mL). The resulting solution was stirred at room temperature under argon for 1.5h. Dry methanol (200 µL) was then added to quench the reaction.

After 30 min under stirring, the solution was concentrated under reduced pressure and the residue purified by column chromatography on silica gel (eluted with 50:50:1 EtOAc/hexane/Et_3N) to give monodimethoxytritylated 5 as a clear yellow solid (44% yield from 4;Rf 0.51 in EtOAc/hexane 1:1 v/v). The solid (600 mg, 1.1 mmol) was dried in vacuo overnight before being dissolved in anhydrous DCM (8mL) and diisopropylethylamine (600 µL, 3.6 mmol) under argon. Three hundred microliters of β-cyanoethyldiisopropylchlorophosphoramidite was then added (1.2 mmol). After 40 min, the reaction was quenched by the addition of dry methanol (100 µL), diluted with ethyl acetate (15 mL), and finally washed with 10% sodium carbonate solution (15 mL) and brine (15 mL). The organic layer was dried on magnesium sulfate and concentrated in vacuo. The residue was purified by silica gel chromatography eluted with DCM, ethyl acetate, and triethylamine (80:10:10). The fractions containing the product were collected and concentrated under vacuum, yielding 6 as a white foam (99% yield; Rf 0.65 in $CHCl_3$/MeOH/TEA 97:3:0.05 v/v/v).

^{1}H NMR (700 MHz; CDCl3), δ 7.90 (2H), 7.38 (2H), 7.35 (4H), 7.12(1H), 6.85 (4H), 3.90 (2H), 3.70 (6H), 3.65 (2H), 3.60 (2H), 3.45(2H), 3.39−3.02 (4H), 2.60−2.45 (4H), 2.16 (2H), 1.45 (3H), 1.09(6H), 1.04 (6H);

^{13}C NMR (175 MHz; CDCl3), δ 158.6, 151.6, 147.3,139.4, 135.1, 130.3, 129.1, 127.8, 127.7, 127.1, 113.1, 64.4, 60.4, 55.2,47.3, 33.6, 29.7, 27.6, 20.9, 19.3, 17.3;

^{31}P NMR (202 MHz, CDCl3), δ146.1 and 145.9.

ESI mass (positive mode), calculated 756.3; found757.9 [M + H]+, 779.9 [M + Na]+.

Synthesis of Oligomers. TBA and analogues were synthesized by using standard solid phase DNA chemistry on controlled pore glass (CPG) support following the β-

cyanoethylphosphoramidite method. The oligomers were detached from the support and deprotected by treatment with an aqueous ammonia solution (33%) at 55° C overnight. The combined filtrates and washings were concentrated under reduced pressure, dissolved in H_2O, and purified by HPLC using an anionic exchange column eluted with a linear gradient (from 0 to 100% B in 30 min) of phosphate buffer at pH 7.0 (A, 20 mM NaH2PO4 aqueous solution containing 20% CH3CN; B, 1.0 M NaCl, 20 mM NaH_2PO_4 aqueous solution containing 20% CH_3CN). The oligomers were successively desalted by molecular exclusion chromatography on Biogel P-2 fine. The purity was checked on HPLC by using reverse phase column. The concentrations of the samples used in CD and UV experiments were determined by measuring the absorbance at 260 nm at 80 °C and using the open access program available onhttp://basic.northwestern.edu/biotools/OligoCalc.html.[131]

NMR Experiments. 1D NMR spectra were acquired as 16384 data points with a recycle delay of 1.0 s at temperatures in the range of 2−50 °C. Data sets were zero filled to 32768 points prior to Fourier transformation and apodized with a shifted sine bell squared window function. The pulsed-field gradient DPFGSE[132,133]sequence was used for H_2O suppression. NMR samples of TBA-T7b and TBA-T12b (0.5 mM single-strand concentration) were prepared in 100 mM K^+ buffer(H2O/D2O 9:1 v/v containing 90 mM KCl, 10 mM KH2PO4, and 0.2mM EDTA).

CD Experiments. To perform CD experiments, each ON was dissolved in the potassium (90 mMKCl, 10 mM KH_2PO_4, pH 7.0) or PBS (Sigma-Aldrich; 10 mM phosphate buffer, 2.7 mMKCl, 137 mMNaCl, pH 7.4) phosphate buffer at the final ON concentration of

2.0 ×10^{-5} M and submitted to the annealing procedure (heating at 90°C and slowly cooling at room temperature). Before each experiment, the samples were equilibrated at 10°C for 30 min. CD spectra were recorded from 200 to 360 at 100 nm/min scanning rate, 16 s response, and 1.0 nm bandwidth. Each CD profile was obtained by taking the average of three scans from which the spectrum of background buffer was subtracted. CD melting curves were obtained by monitoring the variation of absorbance at 295 nm from 10 to 80°C. Two melting experiments for each ON were recorded at 0.5°C/min heating rate.

Prothrombin (PT) Time. PT time was measured by using a Koagulab MJ Coagulation System with a specific kit RecombiPlas TinHemosIL (Instrumentation Laboratories, Lexington, MA, USA). The procedure was performed according to the manufacturer's instructions. In our experimental protocol a time course of each ON or vehicle incubated with 100 µL of plasma at 37 °C has been performed. For three valuation of PT at 20.0 µM, in the apposite microtube, 2.0 µL of the corresponding ON solution (1.0 × 10^{-3} M in PBS) or vehicle was added. The PT at final ON concentration of 2.0 µM was determined by using 2.0 µL of a diluted ON solution (the initial ON solution 1.0 ×10^{-3} M in PBS was diluted at a final concentration of 1.0 × 10^{-4} M).Using six different incubation times from 30 s to 15 min (i.e., 30 s and 1, 2, 5, 10, and 15 min) 200 µL of the kit solution containing Recombiplastin was added with consequent activation of extrinsic pathway. The PT measurement, for each incubation time, was produced in triplicate, and the average and its standard error values were calculated. The basal clotting time was determined by measuring the clotting time in the absence of any ON.

The fold increase of basal PT time was calculated as the ratio between the measured PT time in the presence of each ON and the basal PT value (13.4 ± 0.2 s).

Purified Fibrinogen Clotting Assay. ONs were incubated for 1min at 37 °C in 200 µL of buffer (20 mM tris acetate, 140 mM NaCl,2.7 mM KCl, 1.0 mM $MgCl_2$, 1.0 mM $CaCl_2$, pH 7.4) containing 2.0mg/mL of fibrinogen (fibrinogen from human plasma, F 3879, Sigma-Aldrich). One hundred microliters of human (Sigma-Aldrich, T8885,human thrombin suitable for thrombin time test) or bovine(HemosIL, Thrombin Time Kit, Instrumentation Laboratories)thrombin (10 NIH per mL) was then added to the solution containing the fibrinogen and the ON. The time required to clot was measured using a Koagulab MJ Coagulation System. The clotting time of each ON was determined in triplicate at different concentrations. The basal clotting time was determined by measuring the clotting time in the absence of any ONs. Prolonged clotting time was obtained by subtracting the basal clotting value from each ON clotting time. The ratio of basal and prolonged clotting time versus log [ON] was reported.

Molecular Modeling. Molecular modeling calculations were performed on SGI Origin 200 8XR12000 and E4 Server Twin 2 xDual Xeon 5520, equipped with two nodes. Each node was 2 x Intel Xeon QuadCore E5520, 2.26 GHz, 36 GB RAM. The molecular modeling graphics were carried out on SGI Octane 2 work stations.

(a) Conformational Analysis. Experimentally determined structure sof TBA alone (PDB ID 148D) and in complex with thrombin(PDB IDs 1HAO, 1HAP, and 1HUT) were downloaded from Protein Data Bank (PDB, http://www.rcsb.org/pdb/) and analyzed using the Homology module of Insight 2005 (Accelrys Software Inc., San Diego,CA,

USA). Hydrogens were added to all of these structures considering a pH value of 7.4 (Biopolymer Module, Insight 2005).Because the replacement of T7 and T12 residues with nucleoside **b** produced a mixture of diastereoisomers characterized by S or R configuration at the acyclic linker, for each new TBA analogue TBAT7band TBA-T12b, the two diastereoisomers were built by modifying the experimentally determined structure of TBA in complex with thrombin (PDB ID 1HAO; Insight 2005 Builder module). Atomic potentials and charges were assigned using the CVFF force field.[134]

The conformational space of TBA (PDB ID 1HAO) and the new modified analogues was sampled through 200 cycles of simulated annealing (SA) followed by molecular mechanics (MM) energy minimization. During the SA procedure, the temperature is altered in time increments from an initial temperature to a final temperature by adjusting the kinetic energy of the structure (by rescaling the velocities of the atoms). The following protocol was applied: the system was heated to 1000 K over 2000 fs (time step of 1.0 fs); a temperature of1000 K was applied to the system for 2000 fs (time step of 1.0 fs) to surmount torsional barriers; successively, the temperature was linearly reduced to 300 K in 1000 fs (time step of 1.0 fs). Resulting conformations were then subjected to MM energy minimization within Insight 2005 Discover_3 module (CVFF force field) until the maximum rms derivative was <0.001 kcal/Å, using a conjugate gradient[135] as the minimization algorithm. To reproduce the physiological environment where these molecules act and, to evaluate the effects of the implicit solvent, we sampled the conformational space through the combined procedure of SA/MM calculations, using the dielectric constant of the water (ε = 80r).

Moreover, to allow a complete relaxation of the structures preserving the monomolecular chair-like G-quadruplex folding topology, during the entire course of

SA/MM calculations, we applied a tether force of100 kcal/Å2 to the guanine bases of two quartets .All resulting conformers were subsequently analyzed and loopnucleotides were classified on the bases of (i) glycosidic bond χ values, that is, 0° < χ < 90° = syn; −60° < χ < −180°= anti;[136,137] 90°< χ <180°and −60° < χ < 0° = s/a); (ii) the interatomic distance between the centroid of the ring atoms of the nucleobase of each loop nucleotide and the centroid of the ring atoms of the nucleobases of the two G-tetrads (Pseudo_Atom Define command, Biopolymer Module, Insight2005). According to the latter parameter, the loop nucleotide was classified as “stacked” when the distance was <8 Å or as “not-stacked” when the distance was >12 Å, whereas a 3D visual inspection was needed to classify the nucleotide as “stacked” or “not-stacked” when the distance was between 8 and 12 Å. A nucleotide termed “stacked” presented at least one nucleobase atom shielded by the G-tetrads; anucleotide termed “not-stacked” presented no atoms shielded by the G-tetrads. Occurrence rates were calculated for TBA and for each diastereoisomer of the new analogues TBA-T7b and TBA-T12b.Because all experimental data refer to the mixture of the two diastereoisomers, the mean of the values obtained for the two diastereoisomers was also calculated.

(b) Structural and Bioinformatics Analysis. To analyze the binding modes of TBAs and the corresponding aptamer−thrombin interactions, all of the experimentally determined structures of aptamers in complex with human thrombin were downloaded from Protein DataBank: 1HAO, 1HAP, 1HUT, 3DD2, 3QLP, 4DIH, and 4DII. On the other hand, to identify the structural differences in TBA binding site between human and bovine thrombin, additional structures of human (PDB IDs 1HXF, 1TB6,

1TMT, 1TMU, 1XMN, 3HTC, and 4HTC)and bovine (PDB IDs 1HRT, 1VIT, and 3PMA) thrombin, sharing similar ABE I and ABE II ligands, were selected and analyzed.

Hydrogens were added to all of the PDB structures considering a pH value of 7.4 (Biopolymer Module, Insight 2005). All structures were superimposed by Cα atoms, and their sequences were extracted using the Homology module of Insight 2005 (Accelrys). On the other hand the human (entry P00734) and bovine (entry P00735) prothrombin sequences were downloaded from the UniProt Knowledgebase(http://www.uniprot.org), and the sequence alignments were performed using Multiple_Sequence Alignment pulldown in theInsight 2005 Homology module. Moreover, for each ligand/enzyme complex, a subset around the ligands that consisted of all residues and water molecules having at least one atom within a 6 Å radius from any given ligand atom was defined. The created subsets were displayed and analyzed through a 3D visual inspection. The results of this analysis were compared with those obtained through the sequence alignments. Starting from the results obtained from this structural and bioinformatics analysis, to evaluate in detail the possibility of the residues at positions 3, 7, and 12 to interact with thrombin ABE I hydrophobic cleft, the solvent-accessible surface area of these nucleotides was evaluated by calculating the Connolly surface with a probe radius of 1.4 Å, which approximates the radius of a water molecule (Viewer Module, Insight 2005, Accelrys Software Inc.). In particular, the Connolly surface of the considered nucleotides was calculated for the TBA experimentally determined structures (PDBIDs 1HAO, 1HAP, 4DIH, and 4DII) and for all conformers of TBA and new modified analogues, resulting from SA/MM calculations.

The TBA, TBA-T7b, and TBA-T12b SA/MM conformers presenting solvent-accessible surface areas of residues 3, 7, and 12 equal to or greater than that of the corresponding residue of TBA when interacting with the ABE I hydrophobic cleft in experimentally determined complexes (i.e., T3, 191.01 Å2; T7, 159.35 Å2; and T12,180.59 Å2) were selected, and their occurrence rates were calculated. Because all experimental data refer to the mixture of the two diastereoisomers, the mean of the values obtained for the two diastereoisomers was also calculated. Finally, with the aim to calculate the occurrence rates of bioactive conformations of residues at position 3, 7, and 12 of TBA and new modified analogues TBA-T7b and TBA-T12b, all conformers, resulting from SA/MM calculations, were superimposed on the experimentally determined structures of TBA in complex with thrombin (PDB IDs1HAO, 1HAP, 1HUT, 4DIH, and 4DII) by fitting heavy atoms of the guanine bases of two quartets, and the overlap with the residue interacting with the ABE I hydrophobic cleft (I1e24, His71, I1e79, and Tyr117) was evaluated. To assess the bioactive conformation of the residue at position 7, the orientation that allows residue 7 to be located in the same position of T7 of 1HAP or 1HUT crystal structure was considered (orientation II in Figure 12).

The conformation of residues at positions 3, 7, and 12 was considered bioactive when the correspondent nucleobase was positioned within the ABE I hydrophobic cleft and presented at least one atom superimposed on T3 (PDB IDs 4DIH and 4DII) or onT7 (PDB IDs 1HAP and 1HUT) or on T12 (PDB ID 1HAO), respectively. Occurrence rates of bioactive conformations of residues at positions 3, 7, and 12 were then calculated. Because all experimental data refer to the mixture of the two diastereoisomers, the mean of the values obtained for the two diastereoisomers was also calculated.

Finally, with the aim to calculate the occurrence rates of bioactive conformations of residues at position 3, 7, and 12 of TBA and new modified analogues TBA-T7b and TBA-T12b, all conformers, resulting from SA/MM calculations, were superimposed on the experimentally determined structures of TBA in complex with thrombin (PDB IDs1HAO, 1HAP, 1HUT, 4DIH, and 4DII) by fitting heavy atoms of the guanine bases of two quartets, and the overlap with the residue interacting with the ABE I hydrophobic cleft (I1e24, His71, I1e79, andTyr117) was evaluated. To assess the bioactive conformation of the residue at position 7, the orientation that allows residue 7 to be located in the same position of T7 of 1HAP or 1HUT crystal structure was considered (orientation II in Figure 12). The conformation of residues at positions 3, 7, and 12 was considered bioactive when the correspondent nucleobase was positioned within the ABE I hydrophobic cleft and presented at least one atom superimposed on T3 (PDB IDs 4DIH and 4DII) or onT7 (PDB IDs 1HAP and 1HUT) or on T12 (PDB ID 1HAO),respectively. Occurrence rates of bioactive conformations of residues atpositions 3, 7, and 12 were then calculated. Because all experimental data refer to the mixture of the two diastereoisomers, the mean of the values obtained for the two diastereoisomers was also calculated.

4. Outstanding effects on antithrombin activity of modified TBA diastereomers containing an optically pure acyclic nucleotide analogue.

Disadvantageously, since the introduced residues **a** or **b** presented a pro-chiral carbon (Figure 23), each obtained modified sequence existed as a mixture of two diastereomers.

On these bases, the substitution of the identified key residues with a rationally designed and optically pure acyclic nucleoside analogue, would allow the investigation of the molecular bases of TBA-thrombin interaction. Here, I successful approach this issue by the substitution of T3 or T7 or T12 with each pure stereoisomer of the acyclic nucleoside **c** (Figure 23).

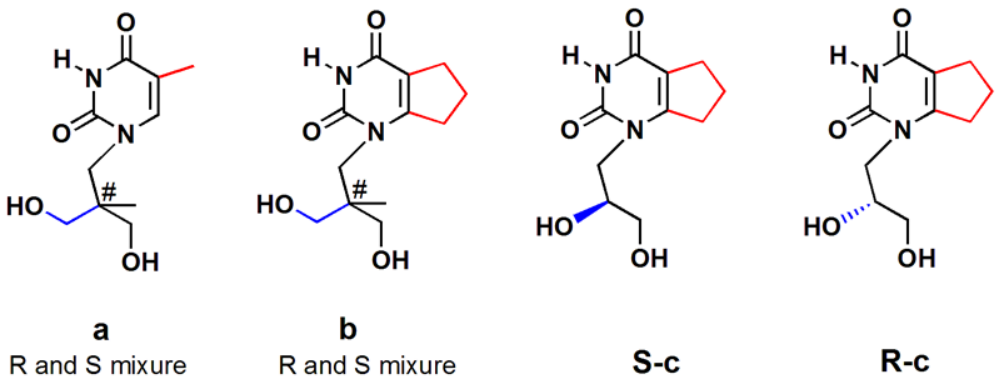

Figure 23. *Acyclic nucleosides mimicking thymine residue. The pro-chiral carbon of* ***a*** *and* ***b*** *is labelled with #.*

4.1 Results and Discussion

Synthesis

The Horhota method[138] was adopted to obtain the stereoselective synthesis of R and S enantiomers of the acyclic nucleoside c (R-c and S-c in Scheme 2 and Figure24). The R or S stereochemistry was attained by ring opening of the enantiomerically pure chiral epoxides 2 by reaction with the modified nucleobase 1 (Scheme 2). Each achieved molecule was converted into the corresponding phosphoramidite building block (5a,b) and incorporated into the TBA sequence to obtain a pool of six ONs (Table 8).

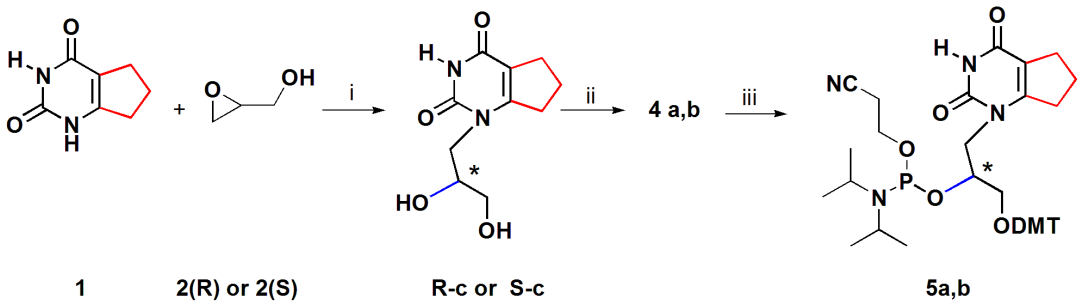

Scheme 2. *Synthesis of monomers 5a,b. i) 1 1.0 g (6.6 mmol), 2 (pure enantiomer R or S) 0.490 g (6.6 mmol), potassium carbonate 0.152 g (1.1 mmol), dry DMF (24 mL), 12-18 h, 80 °C, yields R-c 60% and S-c 45%; ii) R-c or S-c 560 mg (2.5 mmol), 4,4'-dimethoxytrytylchloride 850 mg (2.5 mmol), 4-dimethylaminopyridine 15 mg (0.12 mmol), pyridine (20 mL), 2.0 h, r.t., yields 85%; iii) 4a,b 859 mg, (1.6 mmol), 2-cyanoethyldiisopropylchlorophosphoramidite 536 µL (2.4 mmol), DIPEA 1,7 mL (10 mmol), DCM (9 mL), 40 min, r.t., yields 99%.*

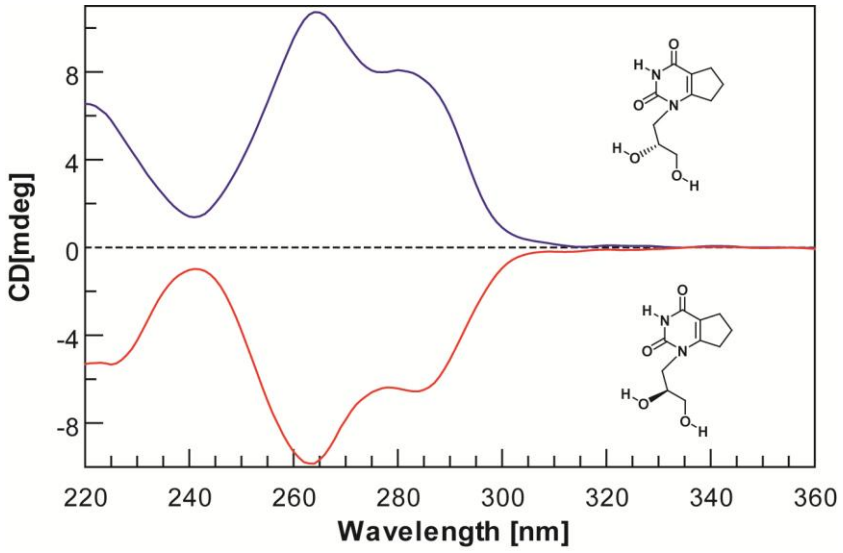

Figure 24. *CD spectra of modified acyclic nucleosides (3.6 × 10^{-4} M in CH_3OH)* ***R-c*** *(positive spectrum) and* ***S-c*** *(negative spectrum).*

ON	SEQUENCE
TBA	GGTTGGTGTGGTTGG
TBA-R_{12}	GGTTGGTGTGG**R**$_{12}$TGG
TBA-R_3	GG**R**$_3$TGGTGTGGTTGG
TBA-R_7	GGTTGG**R**$_7$GTGGTTGG
TBA-S_7	GGTTGG**S**$_7$GTGGTTGG
TBA-S_{12}	GGTTGGTGTGG**S**$_{12}$TGG
TBA-S_3	GG**S**$_3$TGGTGTGGTTGG

Table 8. *Modified sequences containing the* ***c*** *derivatives instead of a T residue. The incorporation of* ***R-c*** *or* ***S-c*** *stereoisomer was specified substituting, at each position, the letter T of the unmodified sequence for the letter* ***R*** *or* ***S****, respectively.*

Structural characterization

To probe if the introduction of R or S acyclic nucleoside **c** at TBA position 3, 12 or 7 affected the overall G-quadruplex topology formed in solution, all modified TBAs were characterized by circular dichroism (CD) and CD melting experiments.

As expected, in PBS and K^+ (90 mMKCl, 10 mM K2HPO4, pH = 7.3) buffers, the modified sequences fold into G-quadruplexes having CD profiles (Figure25) and apparent melting temperatures (Table 9) comparable to that of TBA. Particularly, a stabilizing effect on the G-quadruplex structure (ΔT = 4-5 °C) was attained by replacing T residue at position 3 and 12 with the R stereoisomer of **c**, or at position 7 with both the R and S stereoisomers.

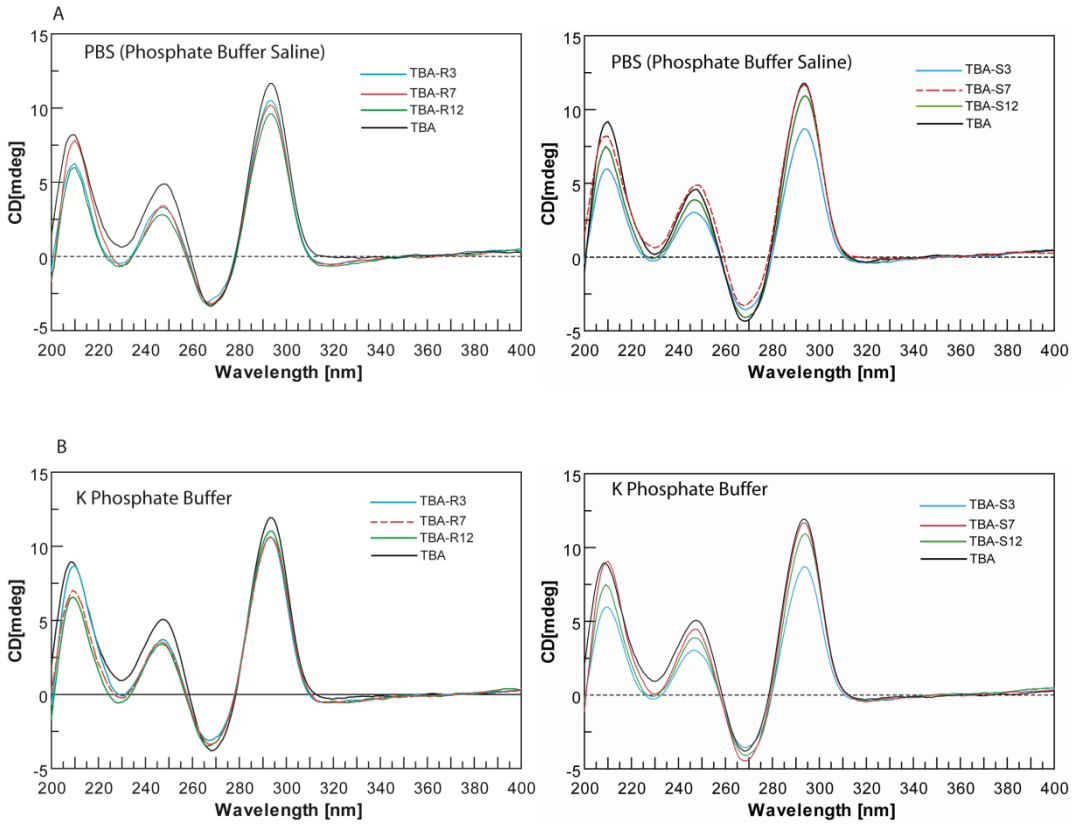

Figure 25.*CD spectra of TBA and modified ONs in PBS (A) and K^+ phosphate buffer (B).*

ON	T_m °C (± 1.0 °C)	
	K^+	PBS
TBA	50	34
TBA-R_{12}	55	39
TBA-R_3	55	39
TBA-R_7	54	38
TBA-S_7	56	39
TBA-S_{12}	51	35
TBA-S_3	51	35

Table 9. *Tm values of TBA and modified ONs.*

Fibrinogen assay

The new ONs were then evaluated for their ability to inhibit fibrinogen hydrolysis by fibrinogen clotting assay. The clotting of fibrinogen induced by human α-thrombin was measured spectrophotometrically at different aptamer concentrations, following the increase in absorbance at 380 nm as a function of the time (Figure 26, Table 10, and Experimental Section).

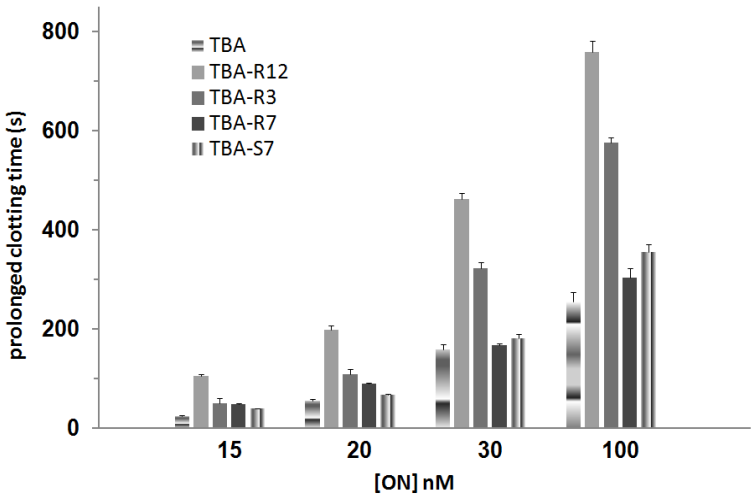

Figure 26.*Prolonged fibrinogen clotting time (s) in presence of TBA or each active aptamer at different concentrations (15-100 nM). The graphics were drew from scattering curves data.*

At 20 nM concentration, TBA and TBA-R12 prolonged the basal clotting time of 56 and 199 s, respectively (Figure26 and Table 10).

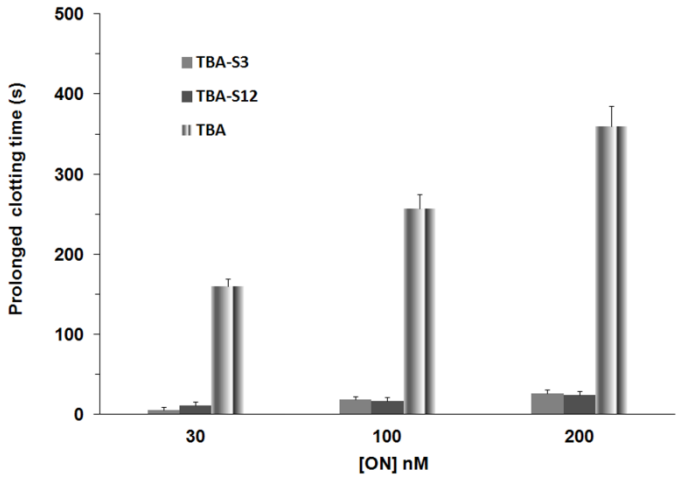

figure 27. *Prolonged fibrinogen clotting time (s) in presence of TBA, TBA-S_3, or TBA-S_{12} at different concentrations (30-200 nM). The graphics were drew from scattering curves data.*

Thus, TBA-R12 resulted 3.5 folds more active than TBA. At the same concentration TBA-S12 resulted completely inactive (Figure 27, and Table 10). A similar activity trend was also observed between TBA-R3 and TBA-S3, being the former 1.9 folds more active than TBA, and the latter completely inactive (Figure26-27 and Table 10). These activity trends were maintained at all tested concentrations, thus evidencing a stereoselective interaction with the target, involving the modified T12 or T3 residues, which is crucial for thrombin inhibition.

	Prolonged clotting time (s)				
ON	15 nM	20 nM	30 nM	100 nM	200nM
TBA	24.6±2.7	56.4±5.0	159.4±11.3	256.4±19.7	N.T.[a]
TBA-R_{12}	105.4±5.7	198.9±10.1	463.4±13.6	759.6±23.8	N.T.
TBA-R_3	50.4±4.0	108.4±5.1	323.4±12.5	576.4±22.8	N.T.
TBA-R_7	49.4±3.0	89.4±3.8	167.4±6.0	304.4±19.9	N.T.
TBA-S_7	39.5±3.0	67.4±4.0	181.4±9.7	355.4±18.0	N.T.
TBA-S_{12}	N.A.[b]	N.A.	10.9±5.7	16.4±2.8	24.4±3.7
TBA-S_3	N.A.	N.A	4.9±3.0	18.4±5.1	26.4±4.6

a Not tested. b Not active.

Table 10. *Prolonged fibrinogen clotting times of TBA and modified ONs. Each value was calculated subtracting the clotting time produced by thrombin in absence of any inhibitor (i.e., 25.6 ± 1.5 s) from that measured in the presence of the aptamer.*

Molecular modelling studies

The resulting SARs of the new modified ONs were rationalized by aid of molecular modelling studies (see Experimental Section for details). As observed by Feigon et al. and confirmed by X-ray data,[88,89] due to the TBA symmetry, residues T3 and T12 occupy equivalent positions with respect to the G quartets, and, by consequence, their binding clefts at thrombin Exosite I (ABE I) can be "exchanged" by rotating the structure 180° around the Y-axis (binding modes III and IV in Figure 12 and 28).

Conversely, the TBA symmetry is lost when either T3 or T12 is modified and, in particular, TT loops are no more equivalent. In our case, monomer **c** is characterized by i) higher conformational flexibility and ii) greater steric hindrance with respect to thymidine. Our computational results indicated that TBA-R3 and TBA-R12, which preserved the stereochemistry of the thymidine residue, could easily adopt bioactive conformation of the TT loops (Figure29a).

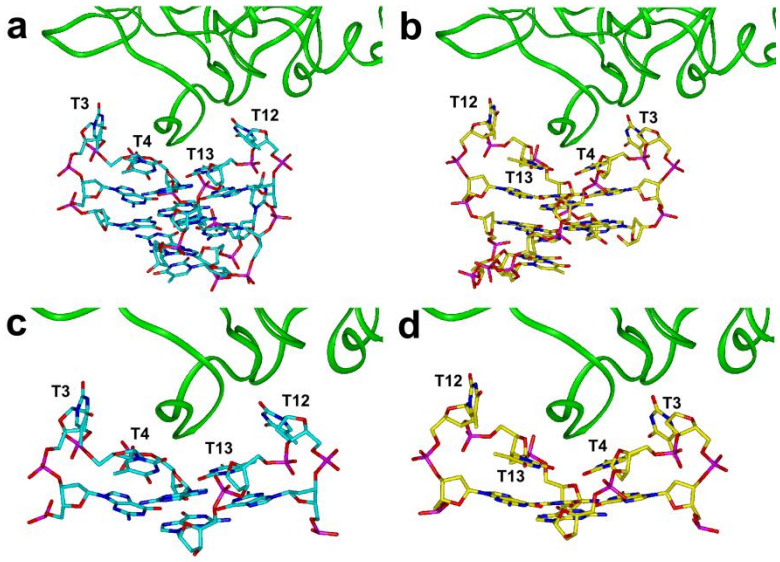

Figure 28. *X-ray structures of the complex between TBA and human α-thrombin presenting aptamer TT loops interacting with thrombin ABE I. (a) and (c): binding mode III; PDB structure 1HAO (TBA carbons = cyan). (b) and (d): binding mode IV; PDB structure 4DIH (TBA carbons = yellow). Heteroatoms are coloured as follows: O = red; N = blue; P = magenta. Thrombin ABE I is shown as green ribbon.*

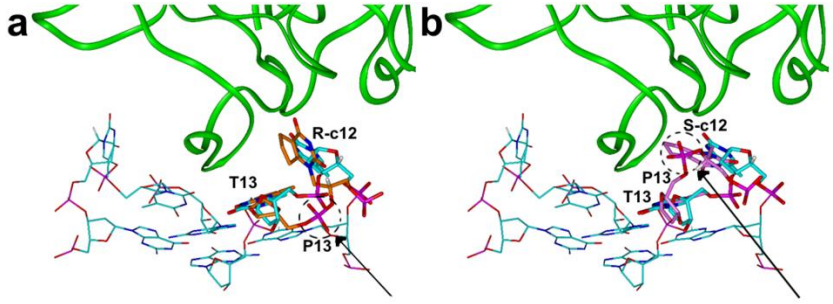

Figure 29*. (a) TBA-R12 (carbons = orange) and (b) TBA-S12 (carbons = pink) superimposed on the bioactive conformation of TBA in complex with thrombin (carbons = cyan; PDB ID: 1HAO). Heteroatoms are coloured as follows: O = red; N = blue; P = magenta. Thrombin ABE I is shown as green ribbon. Hydrogens are omitted with the exception of those present on the modified residue chiral carbon (R-c12 and S-c12) and on TBA T12 C4'. The position of P13 is highlighted by a dashed circle and an arrow.*

The significant increase in inhibitory activity of TBA-R3 and TBA-R12 with respect to TBA indicates the presence of additional favourable hydrophobic contacts with the protein in, at least, one of the TT loops binding clefts. On the contrary, when the stereochemistry of **c** is inverted with respect to the C-4' carbon atom of the natural counterpart (i.e., TBA-S3 and TBA-S12), it is not possible for both binding sites, TT loops to properly place at their thrombin whatever binding mode is assumed. Indeed, although monomers **c** are characterized by higher structural flexibility with respect to thymine, TT loops conformation is highly limited by the stacking of T4 and T13 on the G-quartet. Therefore, when the nucleobase analogue moiety of **c** in TBA-S3 and TBA-S12 projects in the same direction as the nucleobase of T3 and T12 in the bioactive conformation of TBA[87-89]the succeeding phosphate group (i.e., P4 or P13) is forced to distance itself from the G-quartet plane, likely causing steric clashes with the protein backbone (Figure 29b).

Another important outcome which emerged from our results is the higher inhibitory activity of TBA-R12 compared to TBA- R3.

In this case, the lack of structural symmetry does not explain the difference in the activities of TBA-R12 and TBA-R3, since the same TT loops binding mode at thrombin ABE I could be achieved for both analogues by rotating the structure by 180° (Figure28). This indicates that, although TT loops-ABE I interaction is necessary for biological activity, it is not the only factor able to modulate the inhibition of thrombin. Further considerations can be done taking into account the results obtained with aptamers modified at position 7 of the TGT loop. The substitution of T7 with the R or S enantiomer of **c** produced almost equally active aptamers (Figure 23 and Table 10). On one hand, the lack of significant stereo selectivity of action between the two

diastereomers would suggest that the TGT loop is not directly involved in thrombin binding. On the other hand, TBA-R7 and TBA-S7 showed increased inhibitory activity (either with respect to TBA, and to previously developed analogues bearing the monomer **b**)[139] which cannot be ascribed to the increased stability of the quadruplex structure (Tm (PBS) TBA = TBA-T7b[139] = 37.5 °C; TBA-R7 = 38 °C; TBA-S7 = 39 °C), thus supporting the possible direct involvement of the TGT loop in thrombin inhibition.[87,88,139,121] Our molecular modelling studies showed that, contrarily to what observed for the more rigid TT loops, the higher conformational flexibility of the TGT loop allows both **c** enantiomers to adopt the bioactive conformation[87,88]of the residue at position 7, without affecting the height of P7-P9 phosphate groups from the underlying G tetrad plane (Figure 30). In particular, most TBA-R7 conformers presented, similarly to TBA bioactive conformation, G8 stacked on the G1-G6-G10-G15 quartet and T9 pointing outside (Figure 30a).

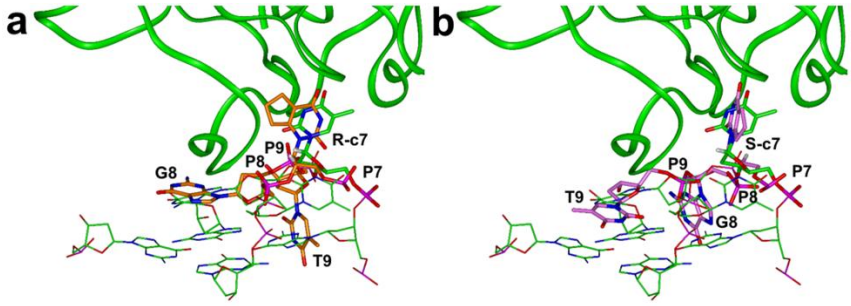

Figure 30. *(a) TBA-R7 (carbons = orange) and (b) TBA-S7 (carbons = pink) superimposed on the bioactive conformation of TBA in complex with thrombin (carbons = green; PDB ID: 1HAP). Heteroatoms are coloured as follows: O = red; N = blue; P = magenta. Thrombin ABE I is shown as green ribbon. Hydrogens are omitted with the exception of those present on the modified residue chiral carbon (R-c12 and S-c12) and on TBA T7 C4'.*

The opposite trend was observed for TBA-S7 (Figure. 30b). Analyzing these results at the light of reported TBA-thrombin binding modes and X-ray structures,[87-89] it resulted that the two different TGT loop conformations can assume the binding modes I and II represented in Figure12.

Taken together, results indicate that either TT loops and TGT loop are involved in thrombin inhibition, but playing different roles. The TT loops are necessary for high affinity thrombin inhibition by establishing a stereoselective interaction with the protein through residues at position 3 and 12. On the contrary, the TGT loop seems to be involved in less specific interactions with thrombin. Indeed, the TGT loop is not sufficient for significant thrombin binding when the binding ability of the TT loops is impaired (TBA-S3 and TBA-S12). Moreover, no significant stereoselectivity of action was observed between TBA-R7 and TBA-S7. The results of our molecular modelling studies suggest that the flexibility of the TGT loop, together with the availability of multiple aptamer-protein binding modes, likely contribute to the observed lack of stereoselectivity between TBA-S7 and TBA-R7. Anyway, a single modification of the TGT loop at position 7 can enhance thrombin inhibition, through a still undefined molecular mechanism. A fascinating hypothesis, supported by some available X-ray data,[87,88] is that the high affinity binding of the TT loops could drive the interaction of the TGT loop with a second unit of thrombin, and this, in turn, due to thrombin allostery, somehow favors the binding of another TBA monomer in a cooperative mechanism.

4.2 CONCLUSIONS

The results presented herein, clearly establish the role of loop conformational preferences on the overall TBA-thrombin complexes and illustrate how a stereochemical modification can impact on aptamer-protein recognition.

Furthermore, since T residues are often loop components of aptamers, our analyses can be widely reproduced in other cases, using the R/S nucleoside derivatives **c** as two simple alternatives for T residue, to acquire and/or refine structure-activity relationship between aptamers and their targets.

4.3 EXPERIMENTAL SECTION

Materials and methods

Chemicals and anhydrous solvents were purchased from Fluka-Sigma-Aldrich. TLCs were run on Merck silica gel 60 F254 plates. Silica gel chromatography was performed by using Merck silica gel 60 (0.063–0.200 mm). The API 2000 (Applied Biosystem) mass spectrometer was used to perform the analyses of the intermediates and the monomer. Melting points of intermediates R-c and S-c were measured using Buchi Melting Point B-540. NMR experiments were recorded using Varian Mercury Plus 400 MHz spectrometer and processed using the Varian VNMR software package. Reagents and phosphorammidites for DNA syntheses were purchased from Glenn Research. ONs syntheses were performed on a PerSeptiveBiosystem Expedite DNA synthesizer. HPLC analyses and purifications were carried out using a JASCO PU-2089 Plus HPLC pump equipped with a JASCO BS-997-01 UV detector. CD experiments were performed on a JASCO 715 spectropolarimeter equipped with a PTC-348 temperature controller. The fibrinogen assay was performed using a JASCO 530 UV spectrophotometer equipped with the PTC-348 temperature controller. $[\alpha]D^{138}$ value for R-c and S-c were determined using JASCO P-2000 Polarimeter. Molecular modelling calculations were performed on SGI Origin 200 8XR12000 and E4 Server Twin 2 x Dual Xeon 5520, equipped with two nodes. Each node was 2 x Intel Xeon QuadCore E5520, 2.26 GHz, 36 GB RAM. The molecular modelling graphics were carried out on SGI Octane 2 workstations.

Synthesis procedure

Synthesis of monomers 4a and 4b. 6,7-dihydro-1H-cyclopenta[d]pyrimidine-2,4(3H,5H)-dione (1). 1 was obtained as previously reported by Takaya et al.[140] Briefly, a solution of ethyl-2-oxocyclopentanecarboxylate (10 g, 64.0 mmol), urea (5.76 g, 96 mmol) and HCl (37% w/w, 0.096 mL) in EtOH (20 mL) was refluxed for 3h. After filtration, the collected white solid was suspended in 5% NaOH (24 mL) and refluxed for 1h. The reaction was cooled to room temperature and the solid 1 collected by filtration and dried (yields 60%; Rf 0.42 in 9:1 CH_2Cl_2:CH3OH, v/v).

^{1}H NMR (400 MHz, mixture of CD_3OD and $CDCl_3$): δ 4.00 (bs, 2H), 3.62 (m, 4H), 3.03 (t, J = 7.3 Hz, 2H), 2.67 (t, J = 7.3 Hz, 2H), 2.10 (q, J = 7.3 Hz, 2H).

^{13}C NMR (400 MHz, mixture of CD_3OD and CDC_{l3}): δ 166.3, 155.2, 147.3, 113.4, 34.8, 30.5, 18.0.

ESI Mass (positive mode): calculated 152.1; found 153.1 $[M+H]^+$, 175.1 $[M+Na]^+$.

1-(2,3-dihydroxypropyl)-6,7-dihydro-1H-cyclopenta[d]pyrimidine-2,4(3H,5H)-dione [S-c or R-c][138]. A mixture of compound 1 (1 g, 6.6 mmol) and anhydrous potassium carbonate (0.152 g, 1.1 mmol) in dry DMF (24 mL) were heated at 80 °C for 5 min. Compound 2 (pure enantiomer R or S) (0,490 g, 6,6 mmol) was than added. The reaction mixture was stirred at 80 °C for 18 h under argon. The solution was concentrated under reduced pressure and the residue purified by column chromatography on silica gel eluted with 95:5 CH_2Cl_2/CH_3OH, to give S-c or R-c as white solids (yields S-c 45%, R-c 60%). Figure 24 reports the CD profiles of each pure enantiomer S-c or R-c.

S-c ^{1}H NMR (400 MHz, pyridine-d6): δ 4.66 (m, 1H, CHOH), 4.45 (dd, 1H, J1 = 14.0 Hz, J2 = 3.6 Hz, CHaHbOH), 4.08 (d, 2H, J = 5.2 Hz, CH2N), 3.93 (dd, 1H, J1 = 14.0 Hz, J2 = 8.6 Hz CHaHbOH), 3.17 (m, 1H, CHaHb), 2.83 (m, 1H, CHaHb), 2.69 (m, 2H, CH2), 1.82 (m, 2H).

S-c ^{13}C NMR (100 MHz, CD_3OD): δ 163.0, 160.4, 153.2, 111.6, 69.4, 63.9, 32.6, 27.0, 21.0.

ESI Mass (positive mode): calculated 226.1; found 227.1 $[M+H]^+$, 249.1 $[M+Na]^+$. $[\alpha]D^{138}$= –51.4.

S-c in crystalline state was obtained from CH_3COCH_3: CH_3OH (99:1, v:v). Measured melting point was in the range 141-143 °C.

R-c ^{1}H NMR (400 MHz, pyridine-d6): δ 4.66 (m, 1H, CHOH), 4.45 (dd, 1H, J1 = 14.0 Hz, J2 = 3.6 Hz, CHaHbOH), 4.08 (d, 2H, J = 5.2 Hz, CH2N), 3.93 (dd, 1H, J1 = 14.0 Hz, J2 = 8.6 Hz CHaHbOH), 3.17 (m, 1H, CHaHb), 2.83 (m, 1H, CHaHb), 2.69 (m, 2H, CH2), 1.82 (m, 2H).

R-c ^{13}C NMR (100 MHz, CD_3OD) 163.0, 160.4, 153.2, 111.6, 69.4, 63.9, 32.6, 27.0, 21.0.

ESI Mass (positive mode): calculated 226.1; found 227.1 $[M+H]^+$, 249.1 $[M+Na]^+$. $[\alpha]D^{138}$ = + 54.3.

R-c in crystalline state was obtained from CH3COCH3: CH3OH (99:1, v:v). Measured melting point was in the range 141-143 °C.

1-(2,4-dioxo-3,4,6,7-tetrahydro-2H-cyclopenta[d]pyrimidin-1(5H)-yl)-3-((3-methoxyphenyl)(4-methoxyphenyl)(phenyl)methoxy)propan-2-yl-P-2-cyanoethyl-N,N-cianopropylphosphonamidate 5a and 5b. Compound R-c or S-c (560 mg, 2.5 mmol), 4,4'-dimethoxytrytyl chloride (850 mg, 2.5 mmol) and 4-dimethylaminopyridine (15.0 mg, 0.12 mmol) were dissolved in dry pyridine (20 mL). The resulting solution

was stirred at room temperature under argon for 1.5 h. Dry methanol (200 μL) was then added to quench the reaction. After 30 min under stirring the solution was concentrated under reduced pressure and the residue purified by column chromatography on silica gel (eluted with 50:50:1 CH_2Cl_2/CH_3OH/Et_3N) to give monodimethoxytritylated derivative 4a or 4b as a white foam (1.16 g, 85% yield from each c stereoisomer; Rf 0.7 eluted with CH_2Cl_2/CH_3OH 1:1 v/v). The solid (859 mg, 1.6 mmol) was dried in vacuum overnight before being dissolved in anhydrous DCM (9 mL) and diisopropylethylamine (1.7 mL, 10 mmol) under argon. 536 μL of β-cyanoethyldiisopropylchlorophosphoramidite was then added (2.4 mmol). After 40 min the reaction was quenched by addition of dry methanol (100 μL), diluted with ethyl acetate (15 mL) and finally washed with 10% sodium carbonate solution (15 mL) and brine (15 mL). The organic layer was dried on magnesium sulphate and concentrated in vacuum. The residue was purified by silica gel chromatography eluted with DCM, ethyl acetate, triethylamine (80:10:10). The fractions containing the product were collected and concentrated under vacuum yielding phosphoramidite building block 5a [from R-c] or 5b [from S-c] as a white foam (1.15 g, 99% yield; Rf 0.75 in $CHCl_3$/MeOH/TEA 97:3:0.05 v/v).

^{1}H NMR (400 MHz, $CDCl_3$): δ 7.42-7.17 (9H), 6.90 (4H), 4.18 (m, 1H), 4.03 (m, 1H), 3.78 (s, 6H), 3.90-3.60 (m, 3H), 3.22 (m, 1H), 3.19 (m, 1H), 3.06 (m, 1H), 2.90 (m, 1H), 2.80–2.60 (m, 2H), 2.48 (m, 2H), 2.38 (m, 2H), 2.12 (m, 2H), 1.2-1.0 (m, 12H).

^{13}C-NMR (100 MHz, $CDCl_3$): δ 161.4, 158.6, 153.2, 147.3, 139.4, 135.1, 130.3, 129.1, 127.8, 127.7, 127.1, 113.1, 64.4, 60.4, 55.2, 47.3, 33.6, 29.7, 27.6, 20.9, 19.3, 17.3.

ESI Mass (positive mode): calculated 728.3; found 729.3 [M+H]+, 751.3 [M+Na]+.

Synthesis of oligomers.

See section 3.4

CD experiments

To perform the CD experiments on modified nucleosides R-c and S-c, each compound was dissolved in CH_3OH at the final concentration of 3.6×10^{-4} M, the two solutions were equilibrated for 10 min at r.t. and then the CD spectra were registered.

To perform the CD experiments on modified TBA sequences, each ON was dissolved in the potassium (90 mMKCl, 10 mM KH_2PO_4, pH 7.4) or PBS (90 mMKCl, 10 mM KH_2PO_4, pH 7.4) phosphate buffer at the final ON concentration of 2.0×10^{-5} M and submitted to the annealing procedure (heating at 90 °C and slowly cooling at r.t.). Before each experiment, the samples were equilibrated at 10 °C for 30 min. CD spectra were recorded from 200 to 400 nm at 100 nm/min scanning rate, 16 s response, 1.0 nm bandwidth. Each CD profile was obtained by taking the average of three scans from which the spectrum of background buffer was subtracted.

CD melting-folding curves were obtained by monitoring the variation of absorbance at 295 nm from 10 to 90 °C and *vice versa* in K^+ phosphate buffer (80 mMKCl, 20 mM KH_2PO_4 pH= 7.4) and PBS (147 mMNaCl, 20 mM NaH_2PO_4, 23 mM KCl, pH = 7.4) at [ON] = 2.0×10^{-5} M using a 1.0 cm cuvette. Two melting-folding experiments for each ON were recorded at 0.5 °C/min and 1.0 °C/min heating-cooling rate. No substantial differences between melting and cooling curves were detected. Both types of curves resulted independent from temperature scanning rate (0.5 °C/min or 1.0 °C/min).

Fibrinogen clotting assay

The fibrinogen clotting times were measured spectrophotometrically.[141] ONs were incubated for 1 min at 37 °C in 1.0 mL of PBS containing 2.0 mg/mL of fibrinogen (Fibrinogen from human plasma, F 3879, Sigma-Aldrich) in a PMMA cuvette (vol. 1.5 mL, c.o. 1 cm, Brand). 100 µL of human thrombin (10 NIH per mL; Sigma-Aldrich, T8885, human thrombin suitable for thrombin time test) was then added to the solution containing the fibrinogen and the ON. The time required to fibrin polymerization was determined from UV scattering curve, registered as a function of the time (wavelength fixed at 380 nm) in the presence of each ON. Each curve was determined in triplicate at different concentrations. The clotting time value reported as M ± SE, was derived as the maximum of the second derivative of each scattering curve. The basal clotting time was determined by measuring the UV scattering as a function of the time produced in the absence of any ONs. The 15-mer GTGTGTGTGTTGTGT was used as negative control. In the absence of any inhibitor, the clotting time value was 25.6 ± 1.5 s. The prolonged fibrinogen clotting times of TBA and modified ONs were calculated by subtracting the clotting time produced by thrombin in the absence of any inhibitor from that measured in the presence of the aptamer.

Molecular modeling.

Experimentally determined structures of TBA alone (PDB ID: 148D) and in complex with thrombin (PDB IDs: 1HAO, 1HAP, 1HUT, 4DIH, and 4DII) were downloaded from Protein Data Bank (PDB, http://www.rcsb.org/pdb/) and analyzed using the Homology module of Insight 2005 (Accelrys Software Inc., San Diego, CA). Hydrogens were added to all these structures considering a pH value of 7.4 (Biopolymer Module, Insight 2005).

Since the replacement of T3, T7 and T12 residues with nucleoside c produced diastereomers characterized by S or R configuration at the acyclic linker, for each new TBA analogue, the two diastereomers were built by modifying the experimentally determined structure of TBA in complex with thrombin (PDB ID: 1HAO; Insight2005 Builder module). Atomic potentials and charges were assigned using the CVFF force field.[134]

The conformational space of the new modified analogues was sampled through 200 cycles of simulated annealing (SA) followed by molecular mechanics (MM) energy minimization. During the SA procedure, the temperature is altered in time increments from an initial temperature to a final temperature by adjusting the kinetic energy of the structure (by rescaling the velocities of the atoms). The following protocol was applied: the system was heated to 1000 K over 2000 fs (time step of 1.0 fs); a temperature of 1000 K was applied to the system for 2000 fs (time step of 1.0 fs) to surmount torsional barriers; successively, temperature was linearly reduced to 300 K in1000 fs (time step of 1.0 fs). Resulting conformations were thensubjected to MM energy minimization within Insight 2005 Discover_3 module (CVFF force field) until the maximum rms derivative was less than 0.001 kcal/Å, using conjugate gradient[135] as the minimization algorithm. In order to reproduce the physiological environment where these molecules act and, to evaluate the effects of the implicit solvent, we sampled the conformational space through the combined procedure of SA/MM calculations, using the dielectric constant of water (ε = 80*r). Moreover, in order to allow a complete relaxation of the structures preserving the monomolecular chair-like G-quadruplex folding topology, during the entire course of SA/MM calculations, we applied a tether force of 100 kcal/Å2 to the guanine bases of the two quartets.

Resulting conformers were analyzed and loop nucleotides were classified on the bases of: (i) glycosidic bond χ values, i.e., 0° < χ < 90° = syn; -60° < χ < -180°= anti;[136,137] 90°< χ <180° and -60° < χ < 0° = s/a); (ii) the interatomic distance between the centroid of the ring atoms of the nucleobase of each loop nucleotide and the centroid of the ring atoms of the nucleobases of the two G-tetrads (Pseudo_Atom Define command, Biopolymer Module, Insight 2005). When the distance was <8 Å, the loop nucleotide was classified as "stacked", when the distance was >12 Å it was classified as "not-stacked". A 3D visual inspection was used to classify the nucleotide when the distance was included between 8 Å and 12 Å. In any case, a "stacked" nucleotide presented at least one nucleobase atom under the G-tetrads.

New modified TBA conformers, resulting from SA/MM calculations, were superimposed on the experimentally determined structures of TBA in complex with thrombin (PDB IDs: 1HAO, 1HAP, 1HUT, 4DIH and 4DII) by fitting heavy atoms of the guanine bases of two quartets, and the overlap with the residues interacting with thrombin ABE I was evaluated. All possible TBA binding modes (Figure 12) were considered. For each aptamer/enzyme complex a subset around the ligand including all protein and water molecules having at least one atom within a 6 Å radius from any given aptamer atom was defined. The created subsets were displayed and analyzed using Insight 2005 Biopolymer and Homology modules (Accelrys Software Inc., San Diego, CA).

5. 5-HYDROXYMETHYL-2'-DEOXYURIDINE RESIDUES IN TBA: IMPROVING THE BIOLOGICAL ACTIVITY BY A TINY CHEMICAL MODIFICATION.

In order to acquire new data about the importance of each residue of the TBA loop region (and, in case, by the single chemical groups) in both thermal stability and TBA-thrombin recognition and, particularly, to discriminate the contributions of the ionic and hydrophobic components in the interaction, I have undertaken a systematic investigation using the single-base substitution approach by thymine analogues containing tiny chemical modifications. Particularly, here I describe structural and biological properties of new TBA derivatives (Table 11) in which single thymines have been replaced by a natural occurring unusual base (5-hydroxymethyl-2'-deoxyuridine, hmU, Figure31)[142] that differs from the canonical thymine only in the presence of an hydroxyl group on the exocyclic carbon. This small modification has been selected in order to significantly decrease the base hydrophobicity avoiding, at the same time, severe changes of the positions of the phosphate groups, that are responsible for the ionic interactions with the thrombin.

Name	Sequence (5'-3')	T_m (°C)	ΔT_m
TBA	GGTTGGTGTGGTTGG	50	**n.a.**
H3	GGH_3TGGTGTGGTTGG	51	**+1**
H4	GGTH_4GGTGTGGTTGG	50	**0**
H7	GGTTGGH_7GTGGTTGG	52	**+2**
H9	GGTTGGTGH_9GGTTGG	54	**+4**
H12	GGTTGGTGTGGH_{12}TGG	50	**0**
H13	GGTTGGTGTGGTH_{13}GG	49	**-1**

Table 11. *Aptamers investigated and their melting temperatures (Tm). H = 5-hydroxymethyl-2'-deoxyuridine. ΔTm = Tm (mod. aptamer) - Tm (TBA). N.a. = not applicable*

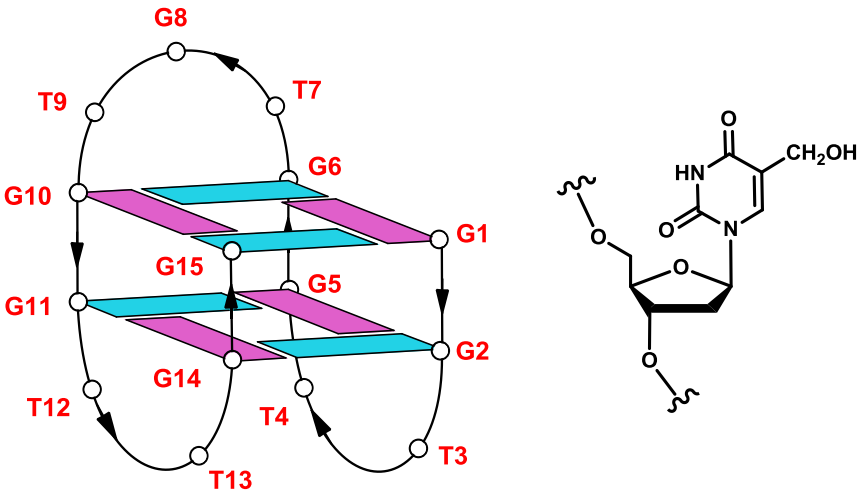

Figure 31. *Schematic representation of the TBA G-quadruplex (left) and chemical structure of hmU (right)*

Collected CD, CD melting, NMR and biological data allowed us to obtain further information about the relevance of some TBA-thrombin contacts for the anticoagulant activity.

5.1 RESULTS AND DISCUSSION

CD and CD melting

Circular dichroism has been utilized to compare the general conformation assumed by natural TBA and the modified oligonucleotides containing a hmU residue. The CD spectrum of TBA shows two positive bands at 247 and 295 nm and a negative band at 266 nm. This CD profile is typical of a G-quadruplex structure in which anti and syn guanosines alternate along the strands.

The CD spectra obtained for the modified analogues could conveniently be divided in two groups. The first one includes ODNs H3, H7, H9 and H12, showing profiles strictly

similar to that of TBA with only a slight intensity decreasing (Figure32, Panel A). In contrast, the second group (ODNs H4 and H13), shows CD profiles quite different in the region 230-280 nm and a remarkable decreasing of the intensity of the band at 292 nm, compared to the TBA (Figure 32, Panel B).

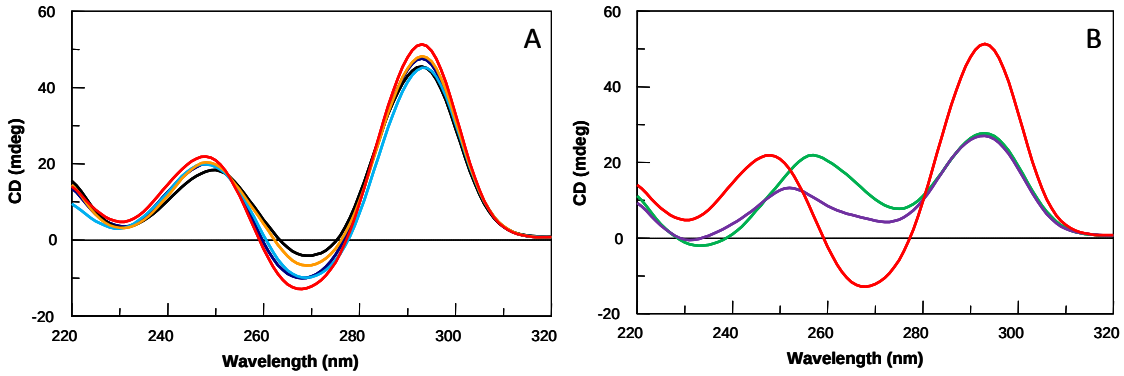

Figure 32. *CD spectra at 5°C of (A)* ***H3*** *(blue), H7 (black),* ***H9*** *(light blue),* ***H12*** *(orange); (B)* ***H4*** *(green),* ***H13*** *(purple) in comparison to TBA (red) at 100 µM ODN strand concentration in a buffer solution 10 mM KH_2PO_4/K_2HPO_4, 70 mM KCl (pH 7.0).*

Notably, CD spectra of H4 and H13 are also characterized by the absence of the negative peak at 266 nm. These data would suggest that H4 and H13 are able to form additional conformations beside that distinctive of TBA. In order to get further data about this point, in different experiments, CD spectra of all the modified ODNs have been recorded after heating at 90°C, followed by rapid cooling. While no significant differences between the two CD profiles could be detected for ODNs H3, H7, H9 and H12, noteworthy changes in the CD profiles of the other modified ODNs are clearly observable (figure 33). Particularly, the CD profile of H13 obtained in these conditions is similar to that of the TBA, but it significantly changes when the sample is left to

equilibrate (Figure 32, Panel B), thus confirming the presence of minor alternative conformations at the equilibrium.

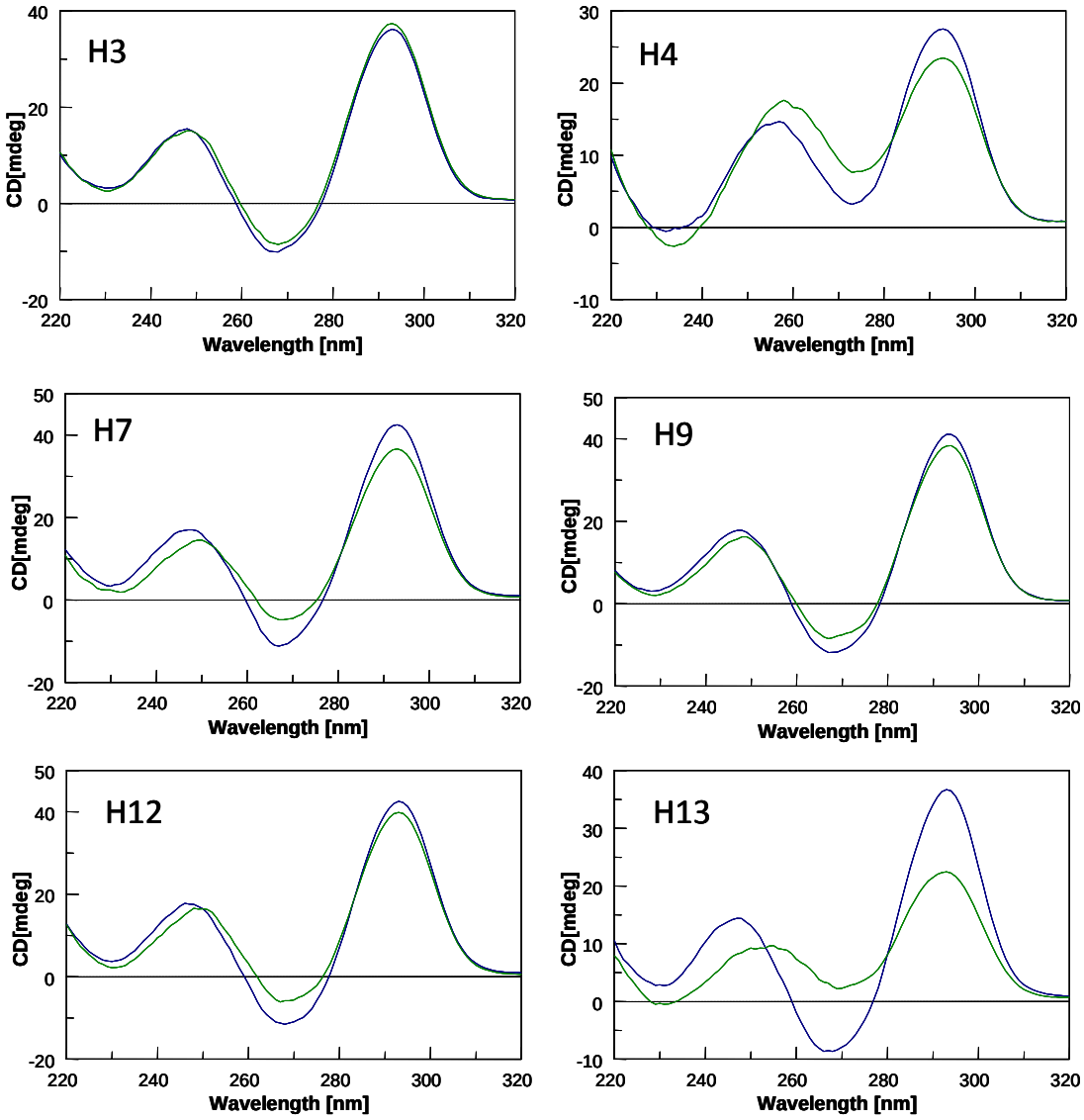

Figure 33. CD spectra at 5°C of modified TBA at 100 µM ODN strand concentration in a buffer solution 10 mM KH_2PO_4/K_2HPO_4, 70 mM KCl (pH 7.0) submitted to different annealing procedure (heating at 90°C and slowly cooling at room temperature: green lines; heating at 90°C and quickly cooling at 5°C: blue lines).

Interesting data have been acquired also from estimation of the thermal stabilities obtained by CD melting measurements, in comparison to TBA. While none or only

modest improvements in the Tm could be observed for ODNs H3, H4, H7, H12 and H13, a noteworthy increment (+4°C) of the Tm has been detected for H9 (Table 11), despite the small structural difference between the canonical thymine present in TBA and the modified base hmU incorporated in H9. Based on previously reported NMR[143,144] and crystallographic data,[88,89,91] these results were expected to some extent. In fact, residues T3, T7 and T12 point out of the G-quadruplex core and toward the solvent. The substitution of a T with hmU residue at any of these positions might explain such positive effects, since the hydroxyl group of hmU is able to form favourable polar interactions with the surrounding water molecules. On the other hand the negative effect produced by the introduction of hmU at 4 and 13 positions might be explained by considering the potential interference of the hydroxyl group on the T4:T13 hydrogen bonding interaction, thus reducing its contribution to the thermal stability of the original structure and then, inducing the formation of alternative conformations. Concerning H9, its higher thermal stability compared to TBA, represents a noteworthy exception, particularly taking into account previous single-base substitution investigations involving T9 residue, in which only G-quadruplex structures strongly less stable than TBA have been obtained.[107,121,122,145]

NMR

The one-dimensional ^{1}H-NMR spectra (700 MHz, T = 25°C) of all the modified thrombin aptamers (Figure 34) in the buffer conditions used here (see experimental section for details) show the presence of eight well-defined signals in the region 11.5–12.3 p.p.m., attributable to imino protons involved in Hoogsteen hydrogen bonds of at least two G-

quartets and, moreover, fifteen main signals in the aromatic region, due to the presence of nine guanine H8 and six thymine H6 protons.

With the exclusion of some weak resonances observable in the aromatic region, due to very minor conformations also present in solution (probably attributable to the unfolded species, since their relative intensities turned out to be sensitive to temperature changes), the simple appearance of 1D spectra of all the samples indicates that the modified oligomers form mainly a single well-defined hydrogen-bonded conformation.

In the cases of H4 and H13, however, it is to report the presence of significant amounts of unfolded species in solution at 25°C and/or alternative conformations that, together with the lowest affinity for thrombin (*vide infra*), deterred us from further NMR investigations. On the contrary, the proton spectra of the modified aptamers H3, H7, H9, H12 were assigned on the basis of NOESY and TOCSY data obtained at 700 MHz, 25°C. The intensities of NOESY crosspeaks between the aromatic base proton and sugar H1' resonances of the modified thrombin aptamers indicate that four Gs (G1, G5, G10 and G14) adopt syn glycosidic conformations while five Gs (G2, G6, G8, G11 and G15) adopt anti conformations, where the H8 resonances of the syn G residues are upfield shifted with respect to those of the anti ones.[85,86] On the other hand, all of the thymines show anti glycosidic conformations.

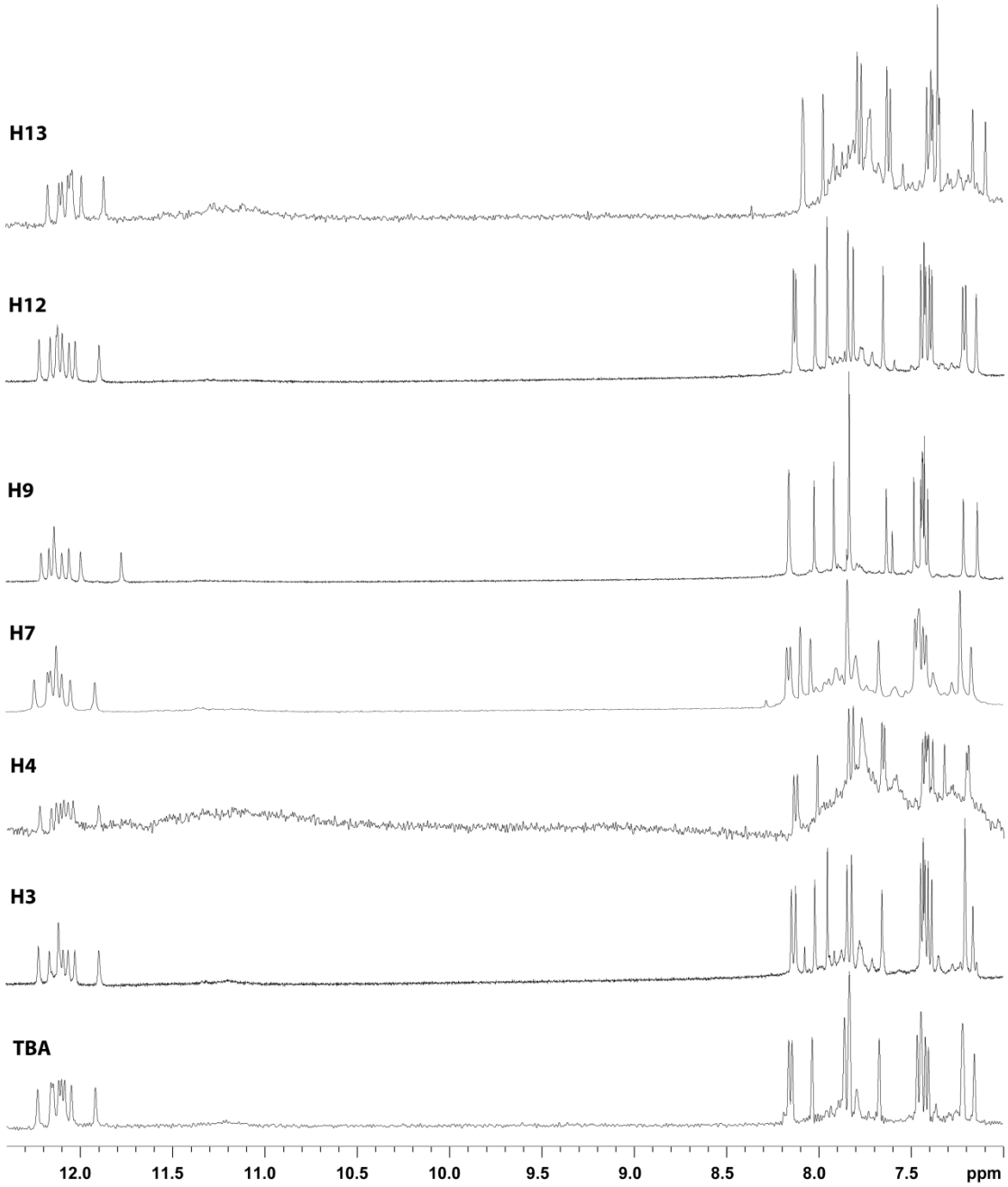

Figure 34. *Aromatic and imino protons regions of the ^{1}H-NMR spectra (700 MHz, T=25°C) of the hmU containing modified TBA and their natural counterpart in 10 mM KH_2PO_4/K_2HPO_4, 70 mM KCl and 0.2 mM EDTA (pH 7.0).*

The crosspeak patterns indicate that four anti-Gs (G2, G6, G11 and G15) have classical H8/H2'–H2'' sequential connectivities to 5' neighboring syn-Gs (G1, G5, G10 and G14, respectively), indicating that the subunits 5'-G1G2-3', 5'-G5G6-3', 5'-G10G11-3' and 5'-

G14G15-3' are involved in the formation of a four-stranded helical structure. In summary, as observed for the unmodified TBA, there are 5'-GsynGanti-3' steps along each strand of the two quartets[86] and moreover, the entire pattern of NOEs observed for all cited Gs indicates that the backbone conformations of these tracts resemble those of the unmodified TBA possessing a right-handed helix structure. The alternation of syn and anti G residues within each strand suggests that, as TBA, all the modified oligomers fold into a monomolecular foldback quadruplex, characterized by two G tetrads.

Since interresidue NOEs are typically weak for 5'-anti-syn-3' steps, there are two strings of 5'-GGTT-3' connectivities, namely 5'-G1G2T3T4-3' and 5'-G10G11T12T13-3' (where syn G residues are designated by G). Further additional connectivities are present for the segments 5'-G5G6T7G8T9-3' and 5'-G14G15-3' and the corresponding stretches, identified on the basis of anti-anti connectivities. There are no sequential connectivities between the 3'-side thymines in each loop (T4, T9, and T13) and the following syn-G.

These two- to four-residue stretches of sequential connectivities were arranged taking into account the primary sequence and the information in long-range NOE connectivities.

As in the case of the parent TBA, for all the modified aptamers studied, there is a number of NOE connectivities observed between residues not adjacent in sequence. In particular, NOEs are present between H8 of G2 and methyl, H2' and H2'' of T4 and between H8 of G11 and methyl, H2' and H2'' of T13. Complementary information is provided by the NOEs from the methyl of T4 with Hl', H2' and H2'' of G2 and from the methyl of T13 with Hl', H2' and H2'' of G11. This collection of NOEs places T4 and T13

residues close to the G2-G5-G11-G14 tetrad. There are also NOE connectivities between H8 of G8 and Hl', H2' and H2'' of G6 and between H1' of T9 and H8 of G15, thus indicating that G8 and T9 residues in the TGT loop are near to the G1-G6-G10-G15 tetrad. This collection of NOEs showed that, as strongly suggested by the CD data, all the modified aptamers investigated by NMR adopt quadruplex structures strictly resembling the parent one.

However, as far as H9 is concerned, it is noteworthy the presence of two further unusual features, in comparison with the parent TBA and the other modified aptamers: 1) a considerable downfield shift of H6 proton of the H9 residue and, 2) an additional NOE between this proton and H2' of G10 (Figure 35). These data could be tentatively explained by considering that the substitution of a methyl group with a hydroxymethyl one in H9 would make possible the occurrence of an H-bond between the $–CH_2OH$ on C-5 of T9 and the N3 of G8. The validity of this consideration is corroborated by the molecular model of H9 (Figure 36) in which, beside the formation of the H-bond, a more effective stacking of the residues H9 and G8 with the underlying tetrad is also observed, in comparison with the unmodified aptamer.The presence of a hydrogen bond involving H9 and G8 facilitating the stacking of these residues with the underlying tetrad G1-G6-G10-G15, positively contributes to the thermal stability.

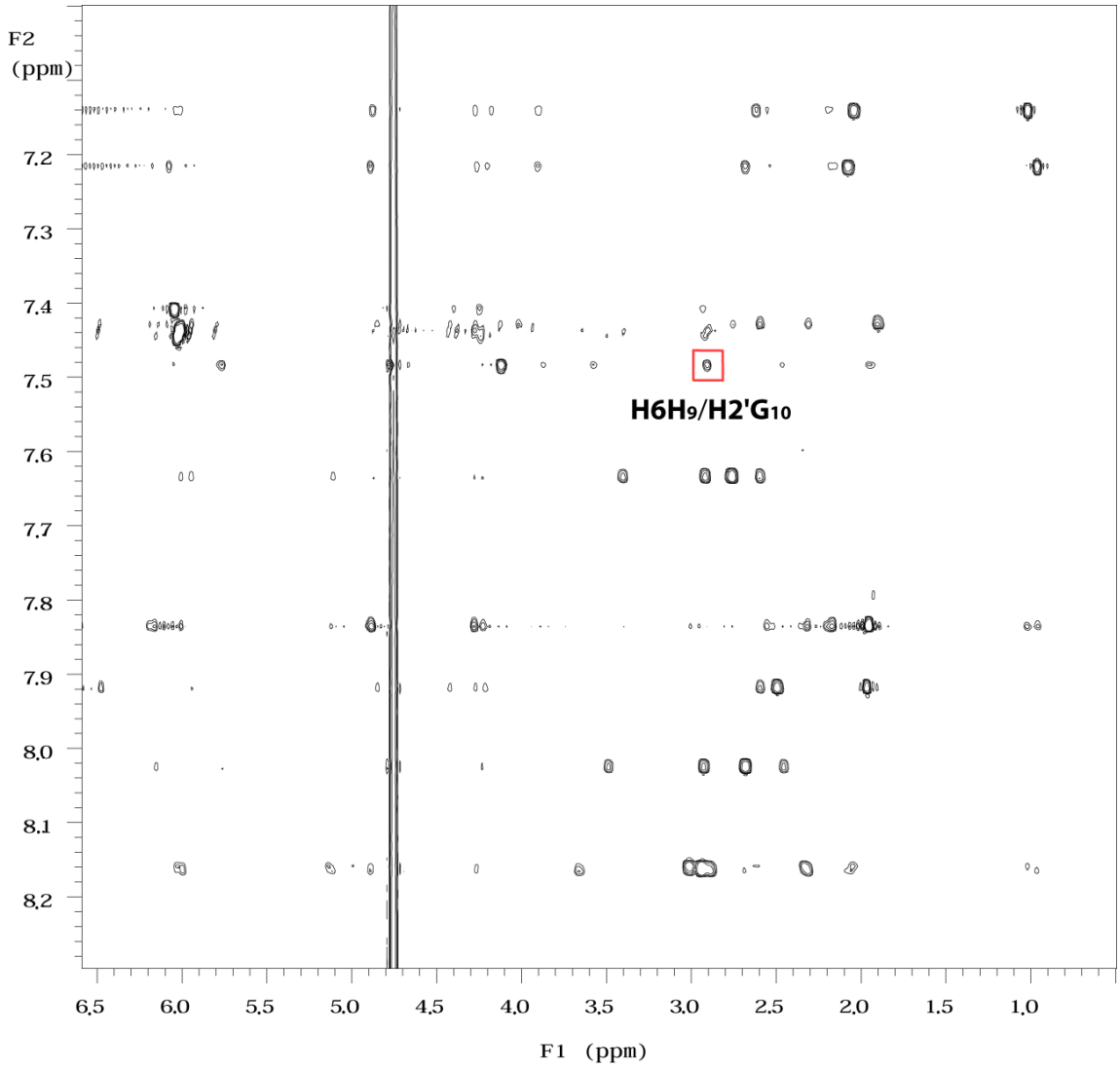

Figure 35. *Expanded 2D NOESY spectrum of* ***H9*** *(700 MHz; 25°C; strand concentration 3 mM; 10 mM KH_2PO_4/K_2HPO_4, 70 mM KCl and 0.2 mM EDTA, pH 7.0 in H_2O/D_2O 9:1; total volume 0.6 mL; mixing time 180 ms) correlating bases H8/H6 and sugar protons. The red box highlights the NOE $H_6H_9/H2'G_{10}$ (see text for details).*

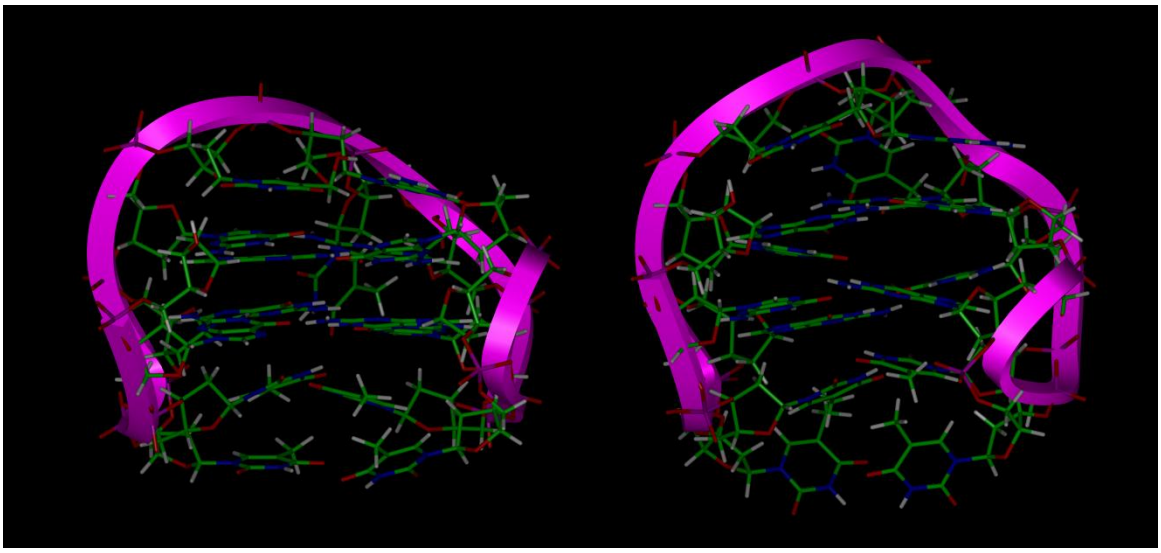

Figure 36. *Molecular models of the quadruplexes formed by H9 (left) and the unmodified TBA (right). The structures are oriented with the 5'- and 3'-ends upward (carbons, green; nitrogens, blue; oxygens, red; hydrogens, white; phosphorus, pink). The ODNs backbone was rendered as colored ribbon.*

Fibrinogen Assay

In order to evaluate their ability to compete with fibrinogen for thrombin anion binding exosite 1 (ABE I) the modified aptamers were subjected to purified fibrinogen clotting assay. The thrombin-induced clotting of fibrinogen was measured spectrophotometrically,[141] following the increase in absorbance at 380 nm as a function of time (Figure 37).

All modified sequences showed an inhibitory efficiency lower than the parent TBA at the explored concentration range. Particularly, the ODNs H4 and H13 resulted unable to significantly prolong the basal clotting time. Indeed, also when present in the test at the highest explored concentration (60 nM), the derived clotting time value was roughly that obtained in absence of any inhibitor. Concerning the other four modified aptamers the loss of affinity compared to TBA, has been of a lesser extent for the two aptamers containing the modified residue at TGT loop, namely H7 and H9, with respect to those modified at one of the TT loops, namely H3 and H12 (Figure 36). These results

have revealed important structure-activity relationships. Differently from other clotting tests performed using plasma samples, in fibrinogen assay, only thrombin and fibrinogen or thrombin, fibrinogen and an inhibitor are present.

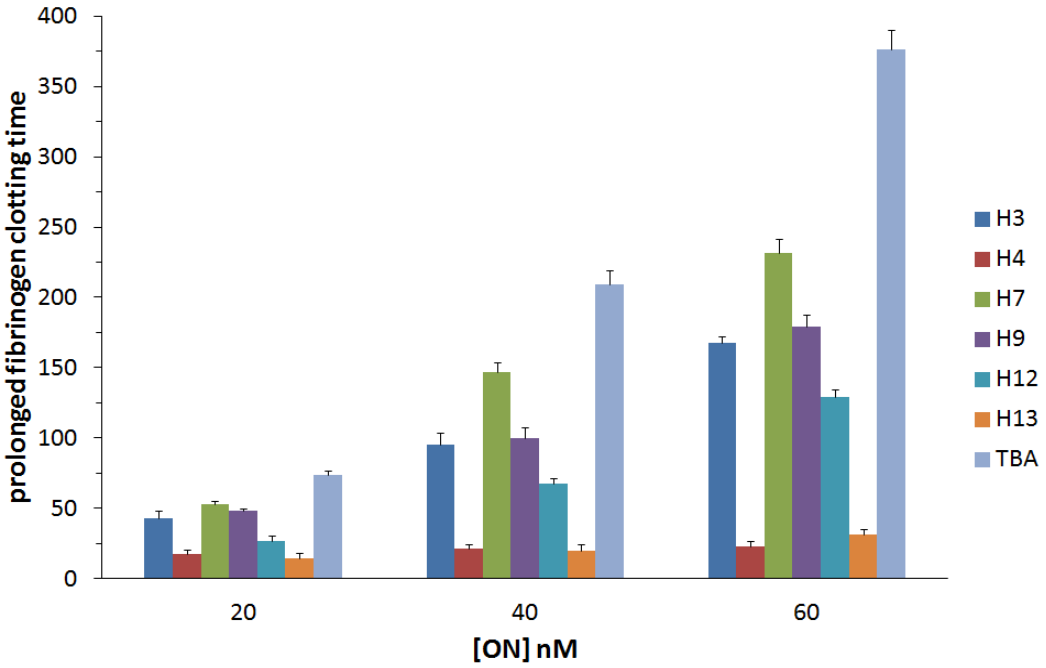

***Figure 37**. Prolonged fibrinogen clotting times measured in PBS buffer in presence of fibrinogen (2mg/mL), thrombin (1,0 NIH) and TBA or each modified ODN at different concentrations.*

Consequently, the interferences produced by other plasma components (such as other thrombin substrates or thrombin precursors) can be excluded and the possible prolongation of the clotting time value can be directly attributed to the competition of the aptamer with fibrinogen for the binding to the thrombin. Data shown in Figure 37 evidence that the loss of the original G-quadruplex conformation causes to become H4 and H13 unable to inhibit fibrin clot formation, at any concentration in the explored range 20-60 nM. This result is in agreement with other previously reported studies,[122]thus confirming the relevant role of T4 and T13 both for G-quadruplex

stability and thrombin inhibitory activity of TBA. However, despite the resemblance of their quadruplex structures to TBA, also the other four aptamers H3, H7, H9 and H12 have shown a general loss of the inhibitory efficiency (Figure 37) respect to TBA, more marked in the cases of H3 and H12. Recently reported crystal structures of TBA-thrombin complexes showed that the TT loops of the G-quadruplex bind the thrombin ABE 1, through residues T3 and T12 interacting with two hydrophobic clefts of the protein, whereas the TGT would be excluded from any interactions with thrombin.[89,91] Taking into account this datum, the introduction of a hmU residue at T3 or T12 positions could produce a steric clash with at least one of the hydrophobic cleft, thus causing the partial loss of the inhibitory activity. Importantly, the fibrinogen assay has shown a negative effect on clotting inhibition also in the cases of H7 and H9, although in a lesser extent. These data are in agreement with results obtained in previous studies,[121,122,139,143] and support the hypothesis that, beside the TT loops, also the TGT loop would be involved in the binding of TBA to thrombin.

PT assay

Finally, using the PT test, we have also valued the ability of each modified aptamer to inhibit the fibrin clot formation in plasma samples (Figure 38). As expected, at all explored concentrations H4 and H13 are unable to prolong the basal PT value significantly. Nevertheless, despite the negative results of the fibrinogen assay, we observed that, at all tested concentrations of aptamer, H12 showed a basal PT value comparable to TBA, whereas, three modified aptamers, namely H3, H7 and H9, increased the basal PT value more efficiently than TBA (Figure 38). In the case of H3 this result is more evident at the aptamer concentration of 10 μM. The observed

trends in PT data suggests that, used in the plasma, H12 is as potent and efficient inhibitor as TBA, H3 is a more potent thrombin inhibitor than TBA, despite its efficiency is similar to that of TBA, whereas H7 and particularly H9, are both more potent and more efficient thrombin inhibitors.

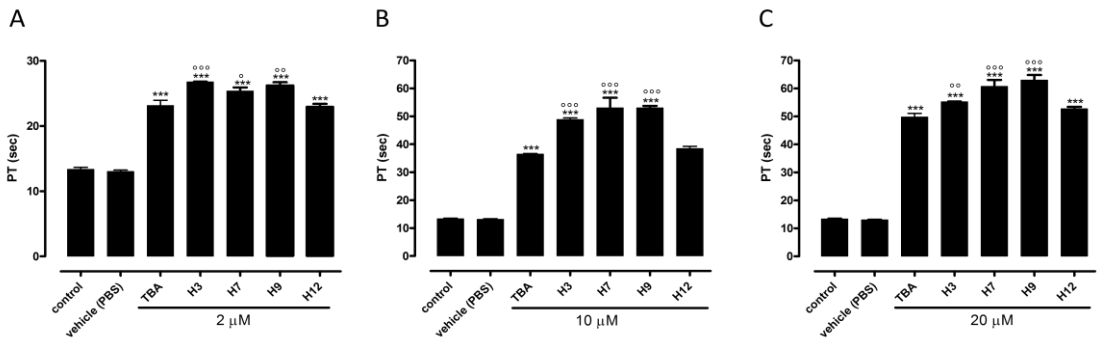

***Figure 38**. PT values of TBA and its modified analogues. ***= p<0.001 vs. vehicle, °=p<0.05, °°=p<0.01, °°°=p<0.001 vs. TBA (n=3).*

The apparent incoherence between fibrinogen and PT assays observed for some of our modified aptamers, was also previously reported for differently modified TBAs.[121,139] These data support the hypothesis that, in presence of other thrombin effectors and/or precursors, such as in the case of plasma tests, the clotting inhibitory activity of some modified TBAs couldn't be explained exclusively on the base of the competition between aptamer and fibrinogen for thrombin ABE 1. Taking into consideration also previous literature data,[121,139] several factors could affect the aptamer anticoagulant activity in the plasma assay: 1) the intrinsic affinity of the aptamer to the thrombin ABE 1 (as judged by the ability of the aptamer to compete with fibrinogen in the fibrinogen assay); 2) the recruitment of the aptamer by other plasma components that could decrease the concentration available to interact with the thrombin; 3) the presence in

plasma of other ligands and effectors able to bind thrombin, thus modifying its affinity for TBA. Then, although aptamers H3, H7, H9 and H12 have shown lower affinities to thrombin compared to TBA, their anticoagulant activities have come out similar (H12) or significantly improved (H3, H7, H9) probably as a result of the interference produced by other plasma components.

5.2 CONCLUSIONS

In conclusion, in this study the structural features of the hmU containing modified TBA were correlate with their ability to inhibit fibrin clot formation in two different tests, providing a better understanding on the biological properties of TBA. All modified TBA preserve the ability to fold in the antiparallel intramolecular quadruplex topology characteristic of the parent TBA. At the explored concentrations, aptamers H4 and H13 have shown no antithrombin activities in the fibrinogen test, or strongly reduced anticoagulant activity in the PT test. On the other hand, the effect of the presence of the hmU residue in four modified aptamers, namely H3, H12, H7 and H9, have consisted in a partial loss of antithrombin activity in fibrinogen assay, thus confirming the crucial role of residues T3 and T12 and suggesting an active role also for the TGT loop of the quadruplex in thrombin interaction, in line with other investigations.[121,122,139,142] Interestingly, despite their sub-optimal affinities to thrombin, three modified aptamers (H3, H7 and H9) showed improved anticoagulant properties in PT test, thus reinforcing the hypothesis that other plasma components could play a role in the anticoagulant activity of TBA and its derivatives.

5.3 EXPERIMENTAL SECTION

Oligonucleotides synthesis and purification

The modified oligonucleotides reported in Table 1 were synthesized on a Millipore Cyclone Plus DNA synthesizer using solid phase β-cyanoethyl phosphoramidite chemistry at 15 μmol scale. The synthesis of the suitably protected 5-hydroxymethyl-2'-deoxyuridine-3'-phosphoramidite was performed following the synthetic strategy proposed by Conte et al.[146] The oligomers were detached from the support and deprotected by treatment with concentrated aqueous ammonia at 55°C overnight.

The combined filtrates and washings were concentrated under reduced pressure, dissolved in H_2O, analyzed and purified by high-performance liquid chromatography on a Nucleogel SAX column (Macherey–Nagel, 1000-8/46), using buffer A: 20 mM NaH_2PO_4/Na_2HPO_4 aqueous solution (pH 7.0) containing 20% (v/v) CH_3CN and buffer B: 1 M NaCl, 20 mM NaH_2PO_4/Na_2HPO_4 aqueous solution (pH 7.0) containing 20% (v/v) CH_3CN; a linear gradient from 0 to 100% B for 45 min and flow rate 1 ml/min were used. The fractions of the oligomers were collected and successively desalted by Sep-pak cartridges (C-18). The isolated oligomers proved to be >98% pure by NMR.

CD spectroscopy

CD samples of modified oligonucleotides and their natural counterpart were prepared at a ODN concentration of 100 μM by using a potassium phosphate buffer (10 mM KH_2PO_4/K_2HPO_4, 70 mM KCl, pH 7.0) and submitted to the annealing procedure (heating at 90°C and slowly cooling at room temperature). CD spectra of all quadruplexes and CD melting curves were registered on a Jasco 715 CD

spectrophotometer. For the CD spectra, the wavelength was varied from 220 to 320 nm at 100 nm min-1 scan rate, and the spectra recorded with a response of 16 s, at 2.0 nm bandwidth and normalized by subtraction of the background scan with buffer. The temperature was kept constant at 5°C with a thermoelectrically-controlled cell holder (Jasco PTC-348). CD melting curves were registered as a function of temperature from 5°C to 80°C for all quadruplexes at their maximum Cotton effect wavelengths. The CD data were recorded in a 0.1 cm pathlength cuvette with a scan rate of 0.5°C/min.

NMR spectroscopy

NMR samples were prepared at a concentration of about 3 mM, in 0.6 mL (H_2O/D_2O 9:1 v/v), buffer solution having 10 mM KH2PO4/K2HPO4, 70 mM KCl and 0.2 mM EDTA (pH 7.0). All the samples were heated for 5-10 min at 80 °C and slowly cooled (10-12 h) to room temperature. The solutions were equilibrated for several weeks at 4 °C. The annealing process was assumed to be complete when ^{1}H NMR spectra were superimposeable on changing time. NMR spectra were recorded with Varian Unity INOVA 700 MHz and Varian Unity INOVA 500 MHz spectrometers. 1D proton spectra of the sample in H2O were recorded using pulsed-field gradient DPFGSE for H_2O suppression.[133] ^{1}H-chemical shifts were referenced relative to external sodium 2,2-dimethyl-2-silapentane-5-sulfonate (DSS). Pulsed-field gradient DPFGSE sequence was used for NOESY[147] (180 ms and 80 ms mixing times) and TOCSY[148] (120 ms mixing time) experiments in H_2O. All experiments were recorded using STATES-TPPI procedure for quadrature detection.[149] In all 2D experiments, the time domain data consisted of 2048 complex points in t2 and 400-512 fids in t1 dimension. A relaxation delay of 1.2 s was used for all experiments

Molecular modelling

The main conformational features of quadruplex adopted by H9 were explored by means of a molecular modelling study. The AMBER force field using AMBER 99 parameter set was used.[150] The initial coordinates for the starting model of H9 were taken from the NMR solution structure of the quadruplex d(GGTTGGTGTGGTTGG) (Protein Data Bank entry number 148D), with the first and best representative conformer of the twelve available ones submitted by Feigon et al.[84]

The initial d(GGTTGGTGHGGTTGG) G-quadruplex model was built by replacing one hydrogen of the 5-methyl group of the thymine in the ninth position with a hydroxyl one, using the Biopolymer building tool of Discover. The calculations were performed using a distance-dependent macroscopic dielectric constant of 4r and an infinite cut-off for non-bonded interactions to partially compensate for the lack of solvent used.[151] Using the steepest descent followed by quasi-Newton-Raphson method (VA09A), the conformational energy of the complex was minimized until convergence to an RMS gradient of 0.1 kcal/mol Å was reached. Illustrations of the structure were generated using the INSIGHT II program, version 2005 (Accelrys, San Diego, CA, USA). All the calculations were performed on a PC running Linux ES 2.6.9.

Fibrinogen Assay

The fibrinogen clotting times were measured spectrophotometrically. ODNs were incubated for 1 min at 37 °C in 1.0 mL of PBS containing 2.0 mg/mL of fibrinogen (Fibrinogen from human plasma, F 3879, Sigma-Aldrich) in a PMMA cuvette (vol. 1.5 mL, c.o. 1 cm, Brand). 100 µL of human thrombin (10 NIH per mL; Sigma-Aldrich, T8885, human thrombin suitable for thrombin time test) was then added to the

solution containing the fibrinogen and the ODN. The time required to fibrin polymerization was determined from UV scattering curve, registered as a function of the time (wavelength fixed at 380 nm) in the presence of each ODN. Each curve was determined in triplicate at different concentrations. The clotting time value reported as M ± SE, was derived as the maximum of the second derivative of each scattering curve. The basal clotting time was determined by measuring the UV scattering as a function of the time produced in the absence of any ODN. In the absence of any inhibitor, the clotting time value was 25.6 ± 1.5 s. The prolonged fibrinogen clotting times of TBA and modified ODNs were calculated by subtracting the basal clotting time produced by thrombin from that measured in the presence of the aptamer.

PT assay

PT assay on human plasma samples was measured by using Koagulab MJ Coagulation System with a specific kit HemosIL RecombinPlasTin 2G (Instrumentation Laboratory, Milan, Italy). Briefly, this method relies on the high sensitivity of thromboplastin reagent based on recombinant human tissue factors. The addiction of recombiplastin to the plasma, in presence of calcium ions, initiates the activation of extrinsic pathway converting the fibrinogen into fibrin, with a formation of solid gel. The procedure was according to the manufacturer's instructions. In our experimental conditions, each ODN or vehicle was incubated with 100 µL of plasma at 37°C for 15 minutes, after that 200 µL of the kit solution containing recombiplastin was added with consequent activation of extrinsic pathway. For the evaluation of PT at 20 µM, in the apposite microtube, 2 µL of the corresponding ODN solution (1 mM in PBS) or vehicle was added. The PT at final ODN concentration of 10 µM and 2 µM was determined using 2

µL of a diluted solution (0.5 mM and 0.1 mM ODN solution in PBS, respectively). The PT measurement was produced in triplicate and the average and its standard error values were calculated and expressed as seconds. The basal clotting time was determined by measuring the clotting time in absence of any ODN.

6. Expanding the Potential of G-Quadruplex Structures: Formation of a Heterochiral TBA Analogue

Oligonucleotides containing L residues (both homo- and heterochirals equences) are endowed with interesting properties and have been exploited for the development of various tools and devices such as aptamers,[152]molecular beacons[153]and microarrays.[154]

Although the capacity of oligonucleotides containing L-residues to form duplex structures has been investigated since 1991,[154]the prospect that this type of oligonucleotide is able to fold also into stable G-quadruplexes (as well as theproperties of these structures and their potential application) has been explored only in recent years. For example, L-homochiral and -heterochiral tetramolecular G-quadruplex structures based on the sequence TGGGGT have been prepared, and their structural properties have been investigated.[155,156]Recently, new dynamic properties of G-quadruplex structures have come to light through the investigation of a heterochiral TGGGGT analogue that contains a 5'–5' polarity inversion site in the G-run centre.[157]

As the most important property of oligonucleotides containing L-residues is their resistance to nucleases, biologically significant L-homochiral monomolecular G-quadruplexes have also been studied. For example, Urata et al. described the anti-HIV-1 activity of a G-quadruplex forming a L-17-mer aptamer that targets the viral gp120 envelope protein.[158]Interestingly, the peroxidase DNAzyme properties of a G-quadruplex that forms another L-17-mer have also been reported. Although TBA was first discovered as an anticoagulant agent, its potential applications have been expanded by the design and preparation of molecular sensors for thrombin, K^+ions[159] and, recently, for the detection of Pb^{++} and Hg^{++} in human serum.[160]As it is evident that

the applications of this sequence would benefit from increased stability in biological environments, we addressed the question of whether heterochiral analogues of TBA are able to form stable G-quadruplex structures. The investigated analogues of TBA are listed in Table 12.

NAME	SEQUENCE 5'→3'[a]	Tm[C°]
D12	ggTTggTGTggttgg	**36**
D23	ggttggTGTggTTgg	**36**
D13	ggTTggtgtggTTgg	**52**
D123	ggTTggTGTggTTgg	**37**
L-TBA	GGTTGGTGTGGTTGG	**50**
TBA	ggttggtgtggttgg	**50**

[a] L residues are in lower case.

Table 12. *Sequences investigated and melting temperatures*

A common feature in all the sequences is the use of only L residues for the guanosines in G-tetrads. The reasons for this preference are: 1) to maintain the same type of chirality for the scaffold, that is, the part of the molecule mostly responsible for both G-quadruplex structural stability and ion binding, and 2) to place L-residues at the ends of the sequences to make the random coil (in equilibrium with the folded structure) resistant to exonucleases, which are ubiquitous in biological systems.

6.1 RESULTS AND DISCUSSION

Heterochiral oligodeoxynucleotides (ODNs) were first investigated by CD to test their ability to fold into G-quadruplexes and, in particular, to adopt a conformation similar to that of TBA. ODNs D12, D123 and D23 showed comparable CD profiles (Figure39): characterized by two positive bands (~236 and 280 nm) and two negative bands (~260 and 298 nm).

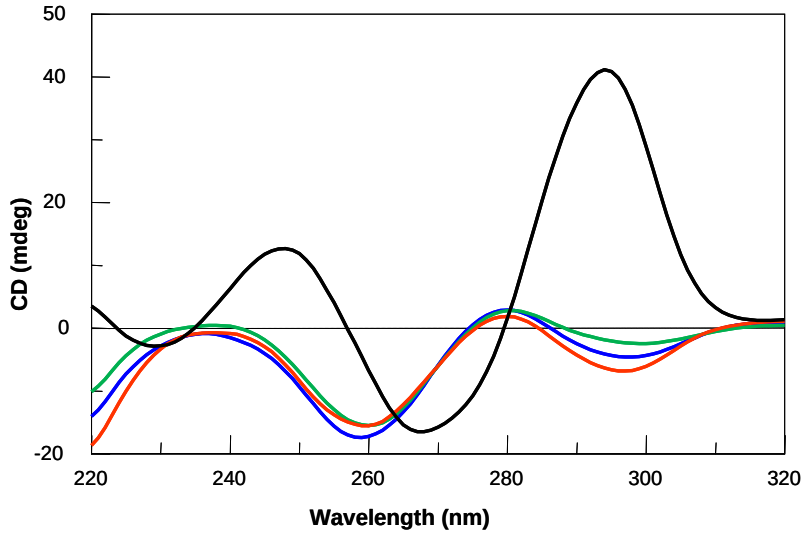

Figure 39.*CD spectra at 20°C of TBA (black), D12 (red), D23 (green), D123 (blue) recorded in a 0.1 cm pathlength cuvette at 100 µM ODN strand concentration in a buffer 10 mM KH_2PO_4/K_2HPO_4, 70 mM KCl (pH 7.0).*

Although their CD spectra suggest the presence of G-quadruplex structures, a comparison of their profiles with those of L-TBA and TBA does not support formation of the antiparallel structure typical of the aptamer. In contrast, the CD profile of D13 showed positive bands at ~230and 268 nm and negative bands at ~247 and 294 nm (Figure40 A). Straightforward comparison of the CD spectra of D13,l-TBA and TBA strongly suggested that D13 folds similarly tol-TBA (the mirror image of natural TBA) and, apart from handedness, to TBA itself. Useful information was also obtained from CD melting/annealing profiles (estimated melting temperatures in Table 12). ODNs

D12, D123 and D23showed values around 36–37°C, whereas D13 exhibited the highest thermal stability (52 °C; slightly higher than that of the natural TBA; Figure 40B). Most importantly, the melting/annealing profiles of D13 do not show a noticeable hysteresis, a feature common to the other heterochiral ODNs investigated here. Taken together, the data suggest the presence of a monomolecular structure only in the case of D13.

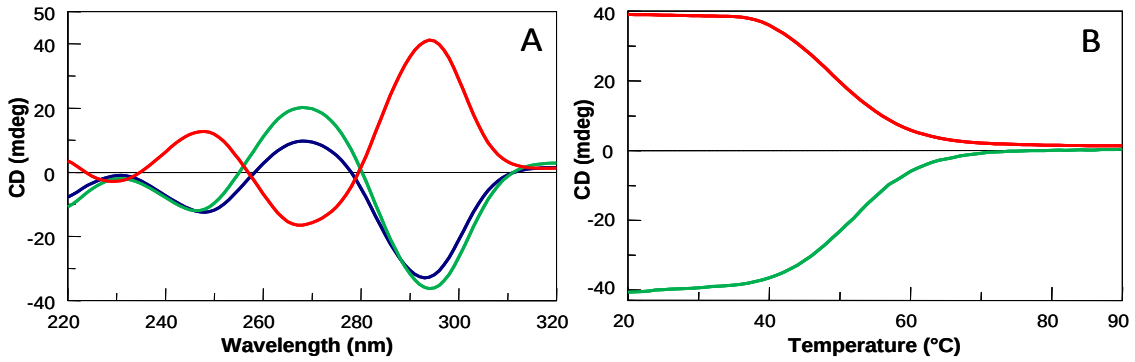

Figure 40. *A) CD spectra at 20°C of TBA (red line), L-TBA (blue line) and D13 (green line); B) CD melting curves of TBA (red line) and D13 (green line). See experimental section for details.*

In order to confirm this, PAGE was performed (Figure 41). The electrophoretic motility of D13 was the same as that of TBA and its mirror-image (L-TBA), thus corroborating the CD melting data that suggested a monomolecular G-quadruplex structure.

In contrast, the bands corresponding to D12, D123 and D23 showed lower motility than those for D13, TBA and L-TBA and appeared quite smeared, thus confirming the presence of multimolecular structures. Close behavior al similarities between D12, D123 and D23 on the one hand, and between D13, TBA and L-TBA on the other were also evident in the ^{1}H NMR spectra (Figure 42).

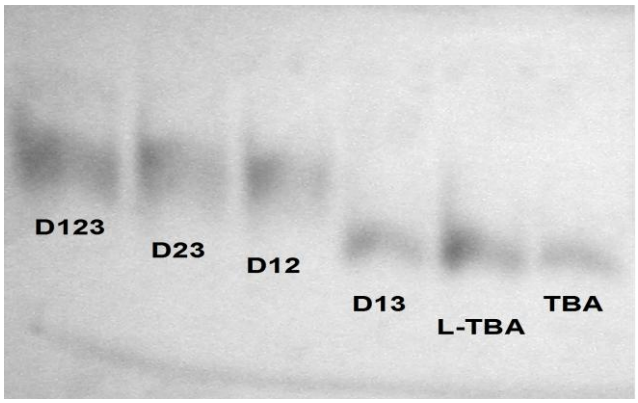

Figure 41. *Non-denaturing PAGE. Samples were loaded on a non-denaturing gel, run at 15°C. Oligonucleotides were revealed by UV shadowing. See text and the experimental section for details.*

In fact, D13, TBA and L-TBA showed imino proton signals (diagnostic for G-tetrads formation) ranging from 11.8 to 12.3 ppm, whereas in the case of D12, D123 and D23, the same signals were spread over a broader spectral region (10.4–12.3 ppm) and, in some cases, appeared larger and with more than the expected eight signals. As the data from the different techniques clearly indicated that only D13 folds similarly to TBA, thus the attention was focused on this ODN for in-depth NMR investigations.

The simple 1D spectrum for this ODN indicates that, under the conditions used, it forms mainly a single well-defined hydrogen-bonded conformation. In fact, the ^{1}H NMR spectrum(700 MHz, T=258C) shows the presence of eight well-defined signals in the region 11.8–12.3 ppm, attributable to imino protons involved in Hoogsteen hydrogen bonds of at least two G-quartets, and 15 signals in the aromatic region from nine guanine H8 and six thymine H6 protons.

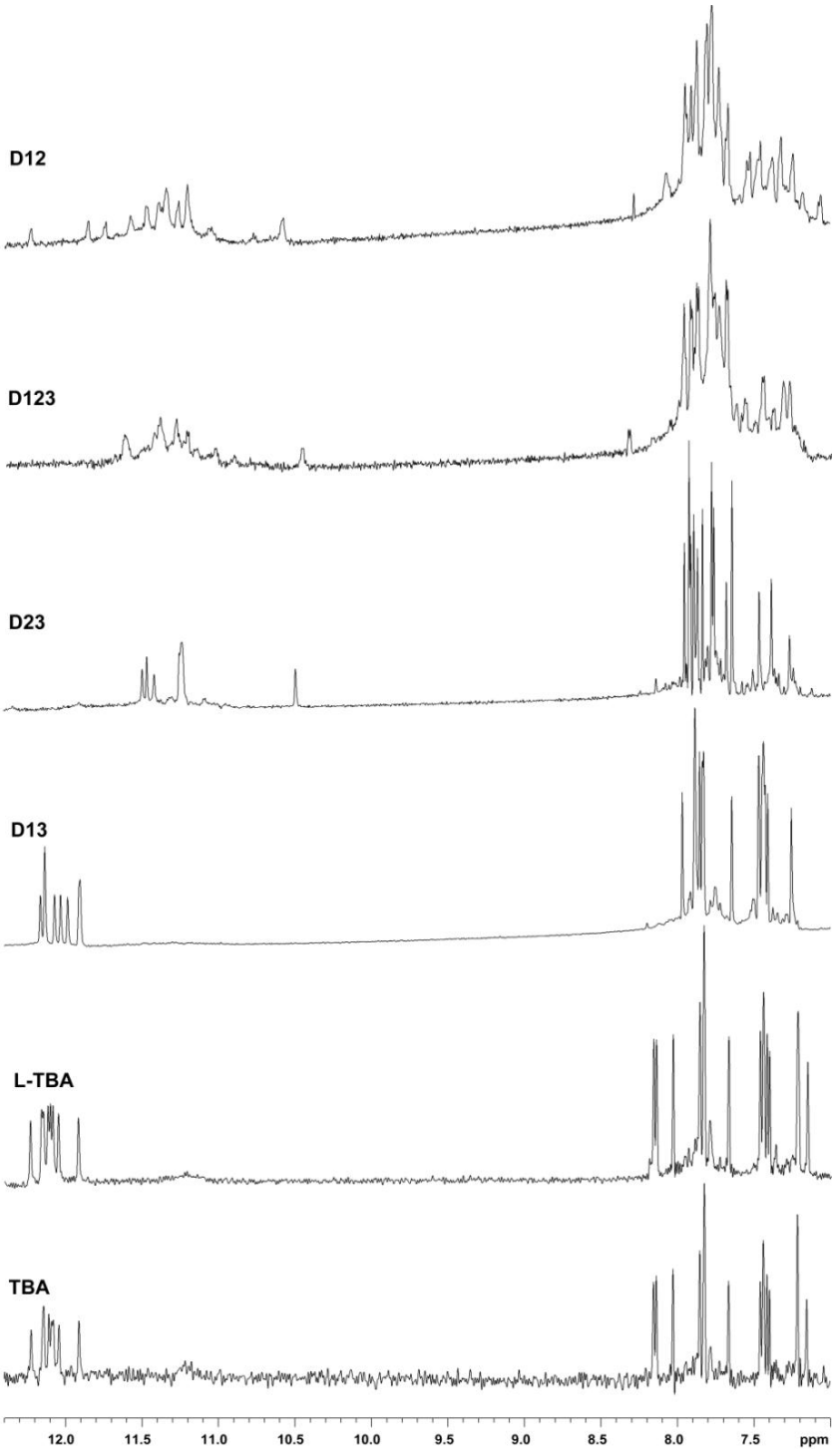

Figure 42. *^{1}H NMR spectra (aromatic and imino proton regions, 700 MHz, T=258°C) of the ODNs (see Table 12).*

Combined analysis of 2D NOESY (Figures 43) and TOCSY spectra (data notshown) allowed us to determine almost completely the assignment of the nonexchangeable protons (Table 13). The intensities of NOESY crosspeaks between the H8 proton bases and sugar H1' resonances indicate that four (G1, G5, G10, G14) out of nine G residues of D13 adopt a syn glycosidic conformation, for which the H8 resonances of syn G residues. The stability of D13 in a biological environment was tested by a degradation assay in foetal bovine serum (Figure 44) and gel electrophoresis. The results clearly indicate that, underthese conditions, D13 is resistant to nucleases up to 24 h,whereas its natural counterpart (TBA) is mostly degraded by 1h.[116]

D13 5'-$G_{L1}G_{L2}T_{D3}T_{D4}G_{L5}G_{L6}T_{L7}G_{L8}T_{L9}G_{L10}G_{L11}T_{D12}T_{D13}G_{L14}G_{L15}$-3'							
	H8/H6	H1'	H2'/H2"	H3'	H4'	H5'/H5"	CH_3
G_{L1}	7.44	6.05	2.93	4.88	4.39	N.D.	-
G_{L2}	7.90	5.94	2.83/2.96	5.04	4.40	N.D.	-
T_{D3}	7.84	6.38	2.35/2.58	4.73	4.50	N.D.	1.95
T_{D4}	7.45	5.94	1.84/2.15	4.73	4.40	4.02	1.59
G_{L5}	7.43	6.04	2.88/3.57	4.83	4.39	4.25/4.13	-
G_{L6}	7.65	5.90	2.59/2.74	5.09	4.23	N.D.	-
T_{L7}	7.86	6.42	2.47/2.59	4.82	4.41	4.25/4.13	1.96
G_{L8}	7.42	5.77	1.97/2.33	4.82	3.99	N.D.	-
T_{L9}	7.27	5.82	1.92/2.38	4.62	3.75	3.56/2.99	1.78
G_{L10}	7.47	6.03	2.87/3.68	4.84	4.23	4.11	-
G_{L11}	7.89	5.92	2.32/2.77	5.03	4.22	4.16/4.01	-
T_{D12}	7.84	6.38	2.35/2.58	4.73	4.51	4.17	1.95
T_{D13}	7.45	5.94	1.84/2.18	4.73	4.40	4.01	1.59
G_{L14}	7.48	6.07	2.94/3.62	4.88	4.51	4.17	-
G_{L15}	7.98	6.10	2.41/2.66	4.78	4.25	N.D.	-

***Table 13**. Proton chemical shifts assignment for G-quadruplex formed by ODN D13 (700 MHz, T = 25°C) in 10 mM KH2PO4/K2HPO4, 70 mM KCl and 0.2 mM EDTA (pH 7.0). N.D. = not determined*

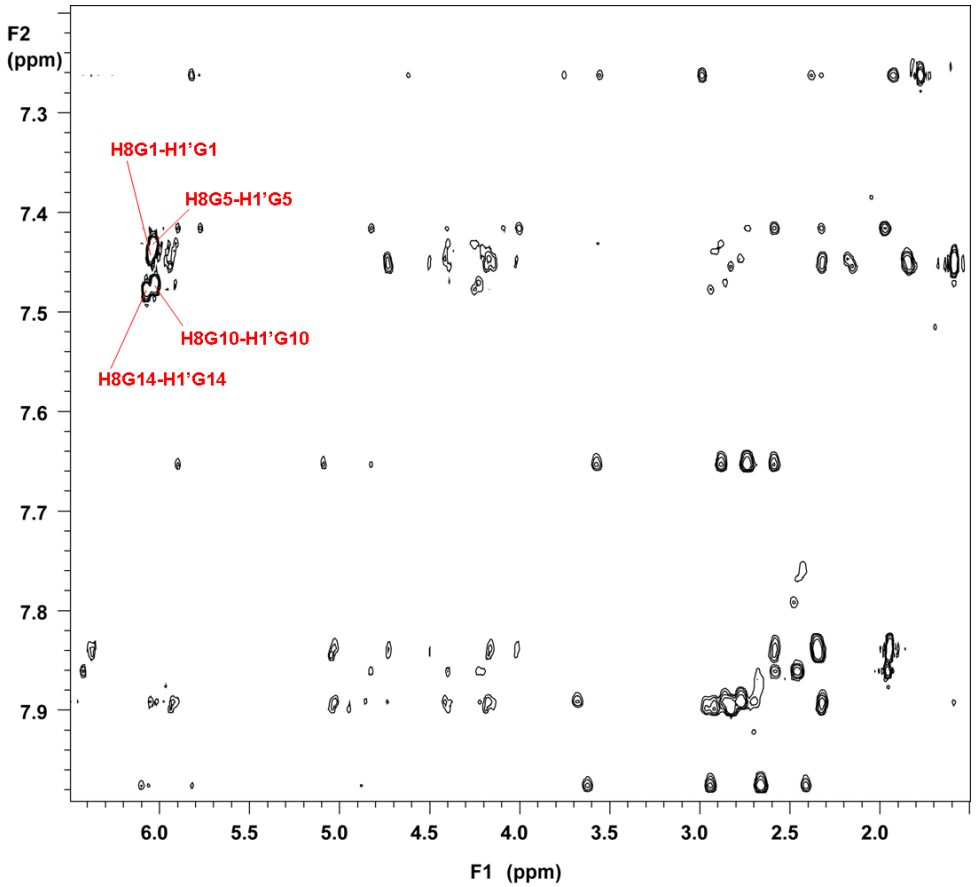

***Figure 43**: Expanded 2D NOESY spectrum of D13 (700 MHz; 25°C; strand concentration 3 mM; 10 mM KH_2PO_4/K_2HPO_4, 70 mM KCl and 0.2 mM EDTA, pH 7.0 in H_2O/D_2O 9:1; total volume 0.6 ml; mixing time 180 ms) correlating aromatic base protons and sugar protons.*

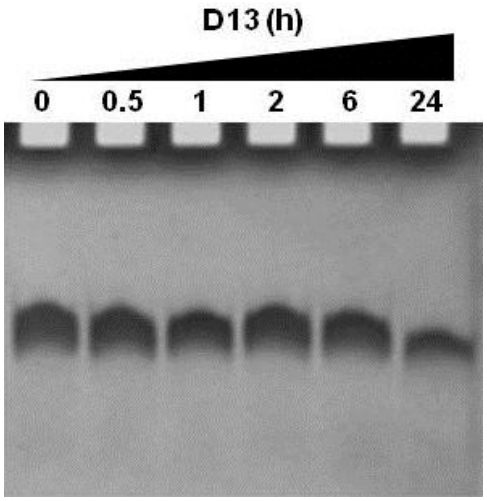

***Figure 44**. Stability of D13 in 10% foetal bovine serum (FBS), as monitored by denaturing PAGE (time points shown in the figure). See the Experimental Section for details.*

6.2 CONCLUSIONS

In summary, we have shown that heterochiral ODNs based on the sequence of TBA are able to fold into G-quadruplex structures. In particular, taken together the data for D13 indicate that, apart from handedness, this ODN folds into the "chair-like" G-quadruplex conformation (typical of TBA), yet it exhibits slightly higher thermal stability. Furthermore, ODN D13 has been shown, by its resistance to both exonucleases and endonucleases, to survive in a biological environment. It should be noted that in the G-quadruplex formed by D13, the two TT loops are composed of natural d-thymines (these residues are mostly responsible for the binding to thrombin).[100, 159]

These properties are particularly important for the potential applications of D13 as an ion sensor in biological fluids and as an anticoagulant agent. Furthermore, from several structural investigations of TBA, it is well known that the central TGT loop makes a remarkable contribution to the thermal stability of the antiparallel quadruplex structure adopted by the aptamer. [100, 159] It is noteworthy that, of the heterochiral ODNs investigated,D13 is the only one in which the guanines involved in G-tetrads formation and the residues of the central TGT loop share the same configuration (l). It is likely that this peculiar feature protects the structure from severe conformationalc hanges that could reduce thermal stability and induce formation of less-stable structures.

Recently, G-quadruplex structures have been used as catalysts for enantioselective Friedel–Crafts[161]and Diels–Alder reactions.[162,163]The discovery that heterochiral ODNs are able to form stable G-quadruplex structures also opens new possibilities in this research area, by adding a further approach to improve stereocontrol and expand substrate variety.

6.3 EXPERIMENTAL SECTION

Oligonucleotides synthesis and purification

All the oligonucleotides were synthesized on a Millipore Cyclone Plus DNA synthesizer using solid phase β-cyanoethyl phosphoramidite chemistry at 15 μmol scale. The synthesis were performed by using normal 3'-phosphoramidites and 5'-dimethoxytrityl-β-L-deoxyguanosine (iBu)-3'-phosphoramidite and 5'-dimethoxytrityl-β-L-deoxythymidine-3'-phosphoramidite. For all ODNs an universal support was used. The oligomers were detached from the support and deprotected by treatment with concentrated aqueous ammonia at 80°C overnight. The combined filtrates and washings were concentrated under reduced pressure, redissolved in H_2O, analyzed and purified by high-performance liquid chromatography on a Nucleogel SAX column (Macherey–Nagel, 1000-8/46), using buffer A: 20mM KH_2PO_4/K_2HPO_4 aqueous solution (pH 7.0) containing 20% (v/v) CH_3CN and buffer B: 1 M KCl, 20mM KH_2PO_4/K_2HPO_4 aqueous solution (pH 7.0) containing 20% (v/v) CH3CN; a linear gradient from 0 to 100% B for 45 min and flow rate 1 ml/min were used. The fractions of the oligomers were collected and successively desalted by Sep-pak cartridges (C-18). The isolated oligomers proved to be >98% pure by NMR.

CD spectroscopy

CD samples were prepared at a concentration of $1x10^{-4}$M by using a buffer solution: 10 mM KH_2PO_4/K_2HPO_4, 70 mM KCl (pH 7.0). CD data of all quadruplexes were registered on a Jasco 715 CD spectrophotometer in a 0.1 cm pathlength cuvette. For the CD spectra, the wavelength was varied from 220 to 320 nm at 100 nm min-1 scan rate,

and the spectra recorded with a response of 16 s, at 2.0 nm bandwidth and normalized by subtraction of the background scan with buffer. The temperature was kept constant at 20°C with a thermoelectrically-controlled cell holder (Jasco PTC-348). CD melting and annealing curves were registered as a function of temperature from 20°C to 80°C at 294 nm for TBA and D13, at 260 nm for all the other quadruplexes with a scan rate of 10°C/h.

Gel electrophoresis

All oligonucleotides were analyzed by non-denaturing PAGE. Samples in the NMR buffer (20 mM KH2PO4, 70 mM KCl and 0.2 mM EDTA, pH=7) were loaded on a 20% polyacrylamide gel containing Tris–Borate-EDTA (TBE) 2.5x and KCl 50 mM. The run buffer was TBE 1x containing 100 mM KCl. For all samples, a solution of glycerol/TBE 1x-100mM KCl 2:1 was added just before loading. Electrophoresis was performed at 9.2 V/cm at a temperature close to 10°C. Bands were visualized by UV shadowing.

Nuclear magnetic resonance experiments

NMR samples were prepared at a concentration of about 3 mM, in 0.6 mL (H_2O/D_2O 9:1 v/v), buffer solution having 10 mM KH_2PO_4/K_2HPO_4, 70 mM KCl and 0.2 mM EDTA (pH 7.0). All the samples were heated for 5-10 min at 80°C and slowly cooled (10-12 h) to room temperature. The solutions were equilibrated for several weeks at 4°C. The annealing process was assumed to be complete when ^{1}H NMR spectra were superimposeable on changing time. NMR spectra were recorded with a Varian Unity INOVA 700 MHz spectrometer. 1D proton spectra of the samples in H2O were recorded using pulsed-field gradient DPFGSE for H_2O suppression. ^{1}H-chemical shifts

were referenced relative to external sodium 2,2-dimethyl-2-silapentane-5-sulfonate (DSS). Pulsed-field gradient DPFGSE sequence was used for NOESY (180 and 80 ms mixing times) and TOCSY (120 ms mixing time) experiments in H_2O (700 MHz, T = 25°C). The experiments were recorded using STATES-TPPI procedure for quadrature detection. In the 2D experiments, the time domain data consisted of 4096 complex points in t2 and 256-512 fids in t1 dimension. A relaxation delay of 1.5 s was used for the experiments.

References

1. Huntington J. A. Molecular recognition mechanisms of thrombin. *J. Thromb. Haemost.* 2005, 3, 1861–1872.

2. Di Cera E. Thrombin interactions. *Chest* 2003, 124, 11S–17S.

3. Davie EW, Fujikawa K, Kisiel W. The coagulation cascade: initiation, maintenance and regulation. *Biochemistry*. 1991, 30, 10363–10370.

4. Kahn ML, Nakanishi-Matsui M, Shapiro MJ, Ishihara H, Coughlin SR.Protease-activated receptors 1 and 4 mediate activation of human platelets by thrombin. J *Clin Invest*. 1999, 103, 879–887.

5. Yun TH, Baglia FA, Myles T, Navaneetham D, Lopez JA, Walsh PN, Leung LL. Thrombin activation of factor XI on activated platelets requires the interaction of factor XI and platelet glycoprotein Ib alpha with thrombin anion-binding exosites I and II, respectively. *J Biol Chem*. 2003, 278, 48112–48119.

6. Monkovic DD, Tracy PB. Activation of human factor V by factor X and thrombin. *Biochemistry.* 1990, 29, 1118 –1128.

7. Fay PJ. Activation of factor VIII and mechanisms of cofactor action. *Blood Rev.* 2004, 18, 1–15.

8. Kanaide H, Shainoff JR. Cross-linking of fibrinogen and fibrin by fibrin-stablizing factor (factor XIIIa). *J Lab Clin Med*. 1975, 85, 574–597.

9. Lenting PJ, DenisCV and Wohner N. Von Willebrand Factor and Thrombosis: Risk Factor, Actor and Pharmacological Target. *Current Vascular Pharmacology* 2013, 11, 4, 448-456.

10. Esmon CT. Molecular events that control the protein C anticoagulant pathway. *ThrombHaemost.* 1993, 70, 29–35.

11. Stubbs MT, Bode W. A player of many parts: the spotlight falls onthrombin's structure. *Thromb Res* 1993, 69, 1–58.

12. Bode W, Mayr I, Baumann U, Huber R, Stone SR, Hofsteenge J. Therefined 1.9 A crystal structure of human alpha-thrombin: interactionwith D-Phe-Pro-Arg chloromethylketone and significance of the Tyr-Pro-Pro-Trp insertion segment. *EMBO J* 1989, 8, 3467–75.

13. Bode W, Turk D, Karshikov A. The refined 1.9-A X-ray crystalstructure of D-Phe-Pro-Arg chloromethylketone-inhibited humanalpha-thrombin: structure analysis, overall structure, electrostaticproperties, detailed active-site geometry, and structure–function relationships.*ProteinSci* 1992, 1, 426–71.

14. Schechter I, Berger A. On the size of the active site in proteases. I. Papain. *BiochemBiophys Res Commun* 1967, 27, 157–62.

15. Di Cera E, Guinto E.R., VindigniA., Dang Q.D., AyalaY.M., WuyiM. and Tulinsky A. The Na^+ binding site of thrombin . *J. Biol. Chem* 1995, 270, 22089–22092.

16.Myles T, Le Bonniec BF, Stone SR. The dual role of thrombin's anion-binding exosite-I in the recognition and cleavage of the protease activated receptor 1. *Eur J Biochem*. 2001, 268, 70–77.

17.Esmon CT, Lollar P. Involvement of thrombin anion-binding exosites 1 and 2 in the activation of factor V and factor VIII. *J Biol Chem.* 1996, 271, 13882–13887.

18. De Candia E, Hall SW, Rutella S, Landolfi R, Andrews RK, De Cristofaro R. Binding of thrombin to glycoprotein Ib accelerates the hydrolysis of Par-1 on intact platelets. *J Biol Chem.* 2001, 276, 4692–4698.

19. Coughlin SR. Thrombin signalling and protease-activated receptors. Nature. 2000, 407, 258–264.

20. Baglia FA, Badellino KO, Li CQ, Lopez JA, Walsh PN. Factor XI binding to the platelet glycoprotein Ib-IX-V complex promotes factor XI activation by thrombin. *J Biol Chem.* 2002, 277, 1662–1668.

21. Ramakrishnan V, DeGuzman F, Bao M, Hall SW, Leung LL, Phillips DR. A thrombin receptor function for platelet glycoprotein Ib-IX unmasked by cleavage of glycoprotein V. *ProcNatlAcadSci USA.* 2001, 98, 1823–1828.

22. Vanhoorelbeke K, Ulrichts H, Romijn RA, Huizinga EG, Deckmyn H. The GPIb alpha-thrombin interaction: far from crystal clear. *TrendsMol Med* 2004, 10, 33–9.

23. Li CQ, Vindigni A, Sadler JE, Wardell MR. Platelet glycoprotein Ib alpha binds to thrombin anion-binding exosite II inducing allostericchanges in the activity of thrombin. *J BiolChem* 2001, 276, 6161–6168.

24. De Cristofaro R, De Candia E, Landolfi R, Rutella S, Hall SW. Structural and functionalmapping of the thrombin domain involved inthe binding to the platelet glycoprotein Ib. *Biochemistry* 2001, 40, 13268–73.

25. Mosesson. M.W. Fibrinogen and Fibrin structure and functions. *Journal of thrombosis and Haemostasis* 2005, 3, 1894-1904.

26. Pechik I, Madrazo J, Mosesson MW, Hernandez I, Gilliland GL, Medved L. Crystal structure of the complex between thrombin and thecentral E region of fibrin. *ProcNatlAcadSci USA* 2004, 101, 2718–23.

27. Weiler H, Isermann BH. Thrombomodulin. *J ThrombHaemost* 2003, 1, 1515–24.

28. Fuentes-Prior P, IwanagaY,HuberR, PagilaR,RumennikG, SetoM,Morser J, Light DR, Bode W. Structural basis for the anticoagulantactivity of the thrombin-thrombomodulin complex. *Nature* 2000, 404, 518–25.

29.Nawa K, Sakano K, Fujiwara H, Sato Y, Sugiyama N, TeruuchiT,Iwamoto M, Marumoto Y. Presence and function of chondroitin-4-sulfate on recombinant human soluble thrombomodulin. *BiochemBiophys Res Commun* 1990, 171, 729–37.

30. Olson ST, Bjork I, Sheffer R, Craig PA, Shore JD, Choay J. Role of the antithrombin-binding pentasaccharide in heparin acceleration of antithrombin-proteinase reactions. Resolution of the antithrombin conformational change contribution to heparin rate enhancement. *J Biol Chem*. 1992, 267, 12528–12538.

31. Olson ST, Bjork I, Shore JD. Kinetic characterization of heparincatalyzed and uncatalyzed inhibition of blood coagulation proteinases by antithrombin. *Methods Enzymol*. 1993, 222, 525–559.

32. Olson ST, Halvorson HR, Bjork I. Quantitative characterization of the thrombin-heparin interaction. Discrimination between specific and nonspecific binding models. *J Biol Chem.* 1991, 266, 6342–6352.

33. Olson ST, Shore JD. Demonstration of a two-step reaction mechanism for inhibition of alpha-thrombin by antithrombin III and identification of the step affected by heparin. *J Biol Chem.* 1982, 257, 14891–14895.

34. Dang OD, Vindigni A, Di Cera E. An allosteric switch controls the procoagulant and anticoagulant activities of thrombin. *ProcNatlAcadSci USA.* 1995, 92, 5977–5981.

35. Di Cera E, Dang QD, Ayala YM. Molecular mechanisms of thrombin function. *Cell Mol Life Sci.* 1997, 53, 701–730.

36. Monod J, Changeux JP, Jacob F. Allosteric proteins and cellular control systems.*J.Mol.Biol*1963, 6, 306–329.

37. Monod J, Wyman J, Changeux JP. On the nature of allosteric transitions: A plausible model. *J. Mol. Biol.*1965, 12, 88–118.

38. Perutz MF. Stereochemistry of cooperative effects in haemoglobin. *Nature*1970, 228, 726–739.

39. Gunasekaran K, Ma B, Nussinov R Is allostery an intrinsic property of all dynamic proteins? *ProtStructFunct Genet*2004, 57, 433–443.

40. Swain JF, Gierasch LM. The changing landscape of protein allostery. *CurrOpinStructBiol* 2006, 16, 102–108.

41. Di Cera E, Page MJ, Bah A, Bush-Pelc LA, Garvey LC Thrombinallostery. PhysChemChemPhys 2007, 9, 1292–1306.

42. Lane, D. A., Philippou, H., and Huntington, J. A. Directing Thrombin. *Blood*. 2005, 106,2605–2612.

43. Gandhi PS, Chen Z, Mathews S, and Di Cera E.Structural identification of the patway of long-range communication in an allosteric enzyme.*PNAS*, 2008, 1832-1837

44. Kamath P, Huntington JA, and Krishnaswamy S. Ligand Binding Shuttles Thrombin along a Continuum of Zymogen and Proteinase-like States *J. Biol. Chem*. 2010, 285, 28651-28658.

45. Pineda AO, Carrell CJ, Bush LA, Prasad S, Caccia S, Chen ZW, Mathews FS, Di Cera E. Molecular dissection of Na^+ binding to thrombin. *J BiolChem*2004, 279, 31842–31853.

46. PrasadS, WrightKJ, RoyDB, BushLA,. Cantwell AM and Di Cera E.Redesigning the monovalent cation specificity of an enzyme.*Proc. Natl. Acad. Sci. USA.* 2003, 100,13785–13790.

47. Guinto ER and Di Cera E. Large heat capacity change in a protein-monovalent cation interaction.*Biochemistry*. 1996, 35, 8800–8804.

48. Griffon N. and Di Stasio E.Thermodynamics of Na+ binding to coagulation serine proteases.*Biophys. Chem*., 2001, 90, 89–96.

49. BahA, GarveyLC, Ge J and Di CeraE.Rapid kinetics of Na+ binding to thrombin.*J. Biol. Chem*. 2006, 281, 40049–40056.

50. Adrogue HJand. Madias NE. Hypernatremia.*N. Engl. J. Med*., 2000, 342,1493–1499.

51. Niu W, Chen Z, Gandhi PS, Vogt AD, Pozzi N, PelcL, ZapataF, Di Cera E. Crystallographic and kinetic evidence ofallostery in a trypsin-like protease. *Biochemistry* 2011, 50, 6301–6307.

52. Gandhi PS, ChenZ, MathewsFS and Di Cera E.Structural identification of the patway of long-range communication in an allosteric enzyme, *PNAS*, 2008, 1832-1837.

53. Bah A, Chen Z, Bush-Pelc LA, Mathews FS, Di Cera E Crystal structures of murine thrombin in complex with the extracellular fragments of murine protease-activated receptors PAR3 and PAR4. *ProcNatlAcadSci USA*2007104:11603–11608.

54. Coughlin SR. Thrombin signalling and protease-activated receptors. *Nature*2000, 407:258–264.

55. Coughlin SR. Protease-activated receptors in hemostasis, thrombosis and vascular biology. *J. ThrombHaemost.* 2005, 3,1800–1814.

56. Nakanishi-Matsui M, Zheng YW, Sulciner DJ, Weiss EJ, Ludeman MJ, Coughlin SR.PAR3 is a cofactor for PAR4 activation by thrombin *Nature*2000, 404:609–613.

57. Esmon CT. Thrombomodulin as amodel of molecular mechanisms that modulate protease specificity and function at the vessel surface. FASEB J 1995, 9, 946–955.

58. Esmon CT The protein C pathway. *Chest*2003, 124, 26S–32S.

59.Xu H, Bush LA, Pineda AO, Caccia S, Di Cera E. Thrombomodulin changes the molecular surface of interaction and the rate of complex formation between thrombin and protein C. *J BiolChem*2005, 280, 7956–7961.

60. Vijayalakshmi J, Padmanabhan KP, Mann KG, Tulinsky A. The isomorphous structures of prethrombin2, hirugen-, and PPACK-thrombin: changes accompanying activation and exosite binding to thrombin. *Protein Sci*.1994, 3, 2254–2271.

61. Krishnaswamy S. The transition of prothrombin to thrombin, *Journal of Thrombosis and Haemostasis.* 2013, 265-276.

62.Kamath P, Krishnaswamy S. Fate of membrane-bound reactantsand products during the activation of human prothrombin byprothrombinase. *J BiolChem* 2008; 283, 30164–73.

63. Kamath P, Huntington JA, Krishnaswamy S. Ligand bindingshuttles thrombin along a continuum of zymogen- and proteinase-like states. *J BiolChem* 2010, 285, 28651–8.

64. Bradford HN, Micucci JA and Krishnaswamy S. Regulated cleavage of prothrombin by prothrombinase: repositioning a cleavage site reveals the unique kinetic behavior of the action of prothrombinase on its compound substrate. *J BiolChem* 2010, 285, 328–338.

65. Higashi S, Matsumoto N, Iwanaga S. Molecular mechanism oftissue factor-mediated acceleration of factor VIIa activity. *J BiolChem* 1996, 271, 26569–74.

66. Kroh HK, Tans G, Nicolaes GA, Rosing J and BockPE.Expression of allosteric linkage between the sodium ion binding site and exosite I of thrombin during prothrombin activation.*J. Biol. Chem*. 2007, 282, 16095–16104

67. VindigniA, White CE, KomivesEA and Di Cera E. Energetics of thrombin-thrombomodulin interaction. *Biochemistry*1997, 36, 6674–6681.

68. Lechtenberg BC, Johnson DJ, Freund SM, Huntington JA.NMR resonance assignments of thrombin reveal the conformationaland dynamic effects of ligation. *ProcNatlAcadSci USA*2010, 107, 14087–92.

69. Bradford HN, Krishnaswamy S. Meizothrombin is an unexpectedlyzymogen-like variant of thrombin. *J BiolChem* 2012, 287, 30414–25.

70. Petrera NS, Stafford AR, Leslie BA, Kretz CA, Fredenburgh JC and Weitz JI. Long Range Communication between Exosites 1 and 2Modulates Thrombin Function*JBiolChem* 2009, 284, 38, 25620–25629.

71. Bjork I, Olson ST. Antithrombin:Abloody important serpin. In: Church FC, Cunningham DD, GinsburgD,Hoffman M, Tollefsen DM, Stone SR, editors. Chemistry and biology of serpins. New York: Plenum Press. 1997, pp 17–33.

72. Craig PA, Olson ST, Shore JD. Transient kinetics of heparin-catalyzed protease inactivation byantithrombin III. Characterization of assembly, product formation, and heparin dissociation steps in thefactor Xa reaction. *J BiolChem* 1989, 264, 5452–5461.

73. ChuangYJ, Swanson R, Raja SM, Olson ST. Heparin enhances the specificity of antithrombin for thrombinand factor Xa independent of the reactive center loop sequence. Evidence for an exosite determinant offactor Xa specificity in heparin-activated antithrombin. *J BiolC*hem. 2001, 276, 14961–14971.

74. Olson ST, Bjork I. Predominant contribution of surface approximation to the mechanism of heparinacceleration of the antithrombin-thrombin reaction. Elucidation from salt concentration effects. *J BiolChem* 1991, 266, 6353–6364.

75. Petitou M, Herault JP, Bernat A, Driguez P-A, Duchaussoy P, Lormeau JC, Herbert JM. Synthesis ofthrombin-inhibiting heparin mimetics without side effects. *Nature* 1999, 398, 417–422.

76. Rezaie AR. Calcium enhances heparin catalysis of the antithrombin-factor Xa reaction by a templatemechanism. *J BiolChem* 1998, 273, 16824–16827.

77. Weitz JI. Low-molecular-weight heparins. *N Engl J Med*1997, 337, 688–698.

78. Bjorn D. Blood coagulation and its regulation by anticoagulant pathways: genetic pathogenesis of bleeding and thrombotic diseases. *Journal of Internal Medicine* 2005, 257, 209–223

79. KeefeAD, PaiS and EllingtonA. Aptamers as therapeutics *Nat Rev Drug Discov*. 2010, 9, 537.

80. Bock LC et al. Selection of single-stranded DNAmolecules that bind and inhibit human thrombin.*Nature* 1992, 355, 564–566.

81. Tasset DM, Kubik MK, Steiner W. Oligonucleotide inhibitors of human thrombin that bind distinctepitopes. *J MolBiol* 1997, 272, 688–698.

82. Müller J, Wulffen B, Potzsch B and Mayer G. Multidomain targeting generates ahigh-affinity thrombin-inhibiting bivalent aptamer.*Chembiochem* 2007, 8, 2223–2226.

83. Müller J, Freitag D, Mayer G and Potzsch B. Anticoagulant characteristics ofHD1–22, a bivalent aptamer that specifically inhibits thrombin and prothrombinase. *J ThrombHaemost* 2008, 6, 2105–2112.

84.SchultzeP, Macaya RF, FeigonJ. Three-dimensionalsolution structure of the thrombin-binding DNA aptamer d-(GGTTGGTGTGGTTGG). *J. MolBiol.* 1994, 235, 1532–1547.

85. Wang, KY, KrawczykSH, BischofbergerN, Swaminathan S, BoltonPH. The tertiary structure of a DNA aptamer which binds toand inhibits thrombin determines activity. *Biochemistry* 1993, 32,11285–11292.

86. MacayaR, SchultzeP, SmithF, RoeJ, FeigonJ. Thrombin-binding DNA aptamer forms a unimolecularquadruplexstructure in solution. *Proc. Natl. Acad. Sci. USA*. 1993, 90, 3745–3749.

87.PadmanabhanK, Padmanabhan KP, Ferrara JD, SadlerJE, TulinskyA. The structure of α-thrombin inhibited by a 15-mersingle-stranded DNA aptamer. *J. Biol. Chem.* 1993, 268, 17651–17654.

88. PadmanabhanK, TulinskyA. An ambiguous structure of a DNA15-mer thrombin complex. *ActaCrystallogr. D: Biol. Crystallogr*. 1996, 52, 272–282.

89. Russo KraussI, MerlinoA, RandazzoA, NovellinoE, MazzarellaL, Sica F. High-resolution structures of two complexes between thrombin and thrombin-binding aptamershedlight on the role of cations in the aptamer inhibitory activity. *NucleicAcids Res*. 2012, 40, 8119-28.

90. KellyJA, FeigonJ, YeatesTO. Reconciliation of the X-rayand NMR structures of the thrombin-binding aptamer d-(GGTTGGTGTGGTTGG). *J. Mol. Biol.* 1996, 256, 417–422.

91. Russo KraussI, MerlinoA, GiancolaC, RandazzoA, MazzarellaL, SicaF. Thrombin-aptamerrecognition: a revealedambiguity. *Nucleic Acids Res*. 2011, 39, 7858–7867.

92. Pagano, B.; Martino, L.; Randazzo, A.; Giancola, C. Stability and binding properties of a modified thrombin binding aptamer. Biophys. J.2008, 94, 562–569.

93. MartinoL, VirnoA, Randazzo A, VirgilioA, EspositoV, Giancola C, BucciM, CirinoG, MayolL. A new modified thrombin binding aptamer containing a 5′-5′ inversion of polarity site.*Nucleic Acids Res*. 2006, 34, 6653–6662.

94. TassetDM, Kubik MF, SteinerW. Oligonucleotideinhibitors of human thrombin that bind distinct epitopes. *J. Mol. Biol*.1997, 272, 688–698.

95. ZhouG, HuangX, QuY. The bindingeffect of aptamers on thrombin. *Biochem. Eng. J.* 2010, 52, 117–122.

96. Nimjee SM, OneyS, VolovykZ, Bompiani KM, Long SB, HoffmanM, SullengerBA. Synergistic effect of aptamers thatinhibit exosites 1 and 2 on thrombin. *RNA* 2009, 15, 2105–2111.

97. KimY, CaoZ, TanW. Molecular assembly for high performance bivalent nucleic acid inhibitor. *Proc. Natl. Acad. Sci. USA*.2008, 105, 5664–5669.

98.SchwienhorstA. Direct thrombin inhibitors a survey of recent developments. *Cell. Mol. Life Sci.* 2006, 63, 2773–2791.

99. He GX, KrawczykSH, SwaminathanS, SheaRG, DoughertyJP, Terhorst T. N2-and C8-substituted oligodeoxynucleotideswith enhanced thrombin inhibitory activity in vitro and invivo. *J. Med. Chem*. 1998, 41, 2234–2242.

100. AviñóA, Fàbrega C, Tintoré, M, Eritja, R.Thrombin binding aptamer, morethan a simple aptamer: Chemically modified derivatives and biomedical applications.*Curr Pharm Des.* 2012, 18, 2036–2047.

101. HeGX, Williams, JP, Postich MJ, SwaminathanS, SheaRG, TerhorstT, LawVS, MaoCT, SueokaC, CoutréS, BischofbergerN. In vitro and in vivo activities of oligodeoxynucleotide-based thrombin inhibitors containing neutral formacetallinkages. *J. Med. Chem.* 1998, 41, 4224–4231.

102. Saccá B, LacroixL, MergnyJL. The effect of chemical modifications on the thermalstability of different G-quadruplex-forming oligonucleotides. *NucleicAcids Res.* 2005, 33, 1182–1192.

103. OlivieroG, BorboneN, GaleoneA, VarraM, PiccialliG, MayolL. Synthesis and characterization of a bunchyoligonucleotide forming a monomolecular parallel quadruplexstructure in solution. *Tetrahedron Lett.* 2004, 45, 4869–4872.

104. OlivieroG, AmatoJ, BorboneN, GaleoneA, PetracconeL, VarraM, PiccialliG, Mayol, L. Synthesis and characterization of monomolecular DNA G-quadruplexes formed by tetra-end-linkedoligonucleotides. *Bioconjugate Chem.* 2006, 17, 889–898.

105. Oliviero G, AmatoJ, BorboneN, D'ErricoS, GaleoneA, Mayol, L, HaiderS, OlubiyiO, HoorelbekeB, BalzariniJ, PiccialliG. Tetraend-linked oligonucleotides forming DNA G-quadruplexes: a new class of aptamers showing anti-HIV activity. *Chem. Commun.* 2010, 46, 8971–8973.

106. SmirnovI, ShaferRH.. Effect of loop sequence and size on DNA aptamer stability.*Biochemistry*2000, 39, 1462–1468.

107. Nagatoishi S, Isono N, Tsumoto K, Sugimoto N. Loop residues ofthrombin-binding DNA aptamer impact G-quadruplex stability and thrombinbinding. *Biochimie*2011, 93, 1231–1238.

108. UeharaS, ShimadaN, TakedaY, KoyamaY, TakeiY, AndoA. 3′Poly(dA)-tailed thrombin DNA aptamer to increase DNase-resistance and clottinginhibitory activity. *Bull ChemSocJpn.*2008, 81, 1485–1491.

109. Buff MCR, Schäfer F, WulffenB, MüllerJ, PötzschB, HeckelA, Mayer G.Dependence of aptamer activity on opposed terminal extensions:improvement of light-regulation efficiency. *Nucleic Acids Res*. 2010, 38,2111–2118.

110. MarathiasVM, SawickiMJ, Bolton PH. 6-Thioguanine alters the structureand stability of duplex DNA and inhibits quadruplex DNA formation. *NucleicAcids Res*199927, 2860–2867.

111. López de la OsaJ, GonzalezC, GargalloR, RuedaM, CuberoE, OrozcoM. Destabilization of quadruplex DNA by 8-aminoguanine. *Chembiochem*. 2006,. 7,46–48.

112. MendelboumRavivS, HorvathA, AradiJ, Bagoly Z, FazakasF, BattaZ. 4-Thio-deoxyuridylate-modified thrombin aptamer and its inhibitory effecton fibrin clot formation, platelet aggregation and thrombus growth onsubendothelial matrix. *J ThrombHaemost*2008, 6, 1764–1771.

113. Nallagatla SR, HeubergerB, Haque A, Switzer C. Combinatorial synthesisof thrombin-binding aptamers containing iso-guanine. *J Comb Chem*2009, 11, 364–369.

114. Goji S, Matsui J. Direct detection of thrombin binding to 8-bromodeoxyguanosine-modified aptamer: Effects of modification on affinityand kinetics*. J Nucleic Acids*, 2011, 316079 (ID).

115. Pozmogova, GE, Zaitseva MA, Smirnov IP, Shvachko AG, Murina MA, Sergeenko VI. Anticoagulant effects of thioanalogs of thrombin-bindingDNA-aptamer and their stability in the plasma. *Bull ExpBiol Med.*2010, 150, 180–184.

116. Peng, CG, Damha MJ. G-quadruplex induced stabilization by 2′-deoxy-2′-fluoro-D-arabinonucleic acids (2′F-ANA). *Nucleic Acids Res*2007, 35, 4977–4988.

117. VirnoA, RandazzoA, GiancolaC, BucciM, Cirino G,MayolL. A novel thrombinbinding aptamer containing a G-LNA residue. *Bioorg Med Chem*2007, 15, 5710–5718.

118. BonifacioL, ChurchFC, Jarstfer, MB. Effect of locked-nucleic acid on abiologically active G-quadruplex. A structure-activity relationship of the thrombinaptamer. *Int J MolSci*.2008, 9, 422–433.

119. Agarwal T, KumarS,Maiti, S. Unlocking G-quadruplex: Effect of unlockednucleic acid on G-quadruplex stability. *Biochimie*2011, 93, 1694–1700.

120. Jensen TB, HenriksenJR, Rasmussen BE, Rasmussen LM, Andresen TL, Wengel J. Thermodynamic and biological evaluation of a thrombinbinding aptamer modified with several unlocked nucleic acid (UNA) monomersand a 2′-C-piperazino-UNA monomer. *Bioorg Med Chem*2011, 19, 4739–4745.

121. Pasternak A, Hernandez FJ, Rasmussen LM, Vester B, Wengel J. Improved thrombin binding aptamer by incorporation of a single unlocked nucleic acid monomer. *Nucleic Acids Res*. 2011, 39, 1155–1164.

122. Coppola T, Varra M, Oliviero G, Galeone A, D'Isa G, Mayol L. (). Synthesis,structural studies and biological properties of new TBA analogues containing an acyclic nucleotide. *Bioorg Med Chem*. 2008, 16, 8244–8253.

123. But TYS, Toy PH. The Mitsunobu reaction: origin, mechanism, improvements, and applications. *Chem. Asian J.* 2007, 2, 1340–1355.

124. Lane AN, Chaire JB, Gray RD, Trent JO. Stability and kinetics of G-quadruplex structures. *Nucleic Acids Res*. 2008, 36, 5482–5515.

125. Neidle S, Balasubramanian S. The role of cations in determining quadruplex structure and stability. In Quadruplex Nucleic Acids; Neidle S, Balasubramanian S, Eds.; *RCS Publishing: London,UK.* 2006, pp 100–130.

126. Chaires, J. B.; Gray, R. D. Kinetics andmechanism of K+- and Na+-induced folding of models of humantelomeric DNA into G-quadruplex structures. Nucleic Acids Res. 2008,36, 4191–4209.

127.Jakubowski HV, Kline MD, Owen WG. The effect of bovine thrombo modulin on the specificity of bovine thrombin. *J. Biol.Chem*. 1986, 261, 3876–3882.

128. Liaw PC, Fredenburgh JC, Stafford AR, Tulinsky A, Austin RC, Weitz JI. Localization of the thrombin-binding domain on prothrombin fragment 2. *J. Biol.Chem.* 1998, 273, 8932–8939.

129. Kretz CA, Stafford AR, Fredenburgh JC, Weitz JI. HD1, a thrombin-directed aptamer, binds exosite 1 on prothrombinwith high affinity and inhibits its activation by prothrombinase. *J. Biol.Chem*. 2006, 281, 37477–37485.

130. Renault J, Laduree D, Robba M. Synthesis and antiviral study of cyclopentano[d]pyrimidine-2,4-diones and octahydroquinazoline-2,4-diones

acyclic nucleosides as potential anti-HIV agents. *Nucleosides,Nucleotides Nucleic Acids*. 1994, 13, 891−901.

131. Kibbe WA. OligoCalc: an online oligonucleotide properties calculator. *Nucleic Acids Res*. 2007, 35 (Suppl. 2), W43−W46.

132. Hwang, TL, Shaka AJ. Water suppression that works.Excitation sculpting using arbitrary wave forms and pulsed field gradients. *J. Magn. Reson. Ser. A* 1995, A112, 275.

133. Dalvit, C. Efficient multiple-solvent suppression for the study of the interactions of organic solvents with biomolecules. *J. Biomol. NMR* 1998, 11, 437.

134. Dauber-Osguthorpe P, Roberts VA, Osguthorpe DJ, Wolff J, Genest M, Hagler AT. Structure and energetics of ligand binding to proteins: E. coli dihydrofolate reductase-trimethoprim, a drug receptor system. *Proteins* 1988, 4, 31−47.

135. Fletcher R. Unconstrained optimization. In Practical Methods of Optimization; *Wiley: New York*, 1980, Vol. 1.

136.Neidle S. Principles of Nucleic Acid Structures; *AcademicPress: London, UK*, 2008.

137. Reichert J, Sühnel J. The IMB JenaImage Library of Biological Macromolecules 2002 Update. *NucleicAcids Res.* 2002, 30, 253−254.

138. Horhota T, Szostak JW and McLaughlin LW. Glycerol nucleoside triphosphates: synthesis and polymerase substrate activities. Org Lett, 2006, 8, 5345.

139. Borbone N, Bucci M, Oliviero G, Morelli E, Amato J, D'Atri V, D'Errico S, Vellecco V, Cirino G, Piccialli G, Fattorusso C, Varra M, Mayol L, Persico M and Scuotto M. Investigating the role of T7 and T12 residues on the biological properties of thrombin-binding aptamer: enhancement of anticoagulant activity by a single nucleobase modification. *J Med Chem*. 2012, 55, 10716.

140. Takaya T, Yoshimoto H and Imoto *E, Bull. Chem: Soc. JPn*. 1967, 40, 2844.

141. De Cristofaro YR and Di Cera E. Phenomenological analysis of the clotting curve. *J. Protein Chem*. 1991, 10, 455.

142. Grove A, Galeone A, Yu E, Mayol L and Geiduschek EP. Affinity, stability and polarity of binding of the TATA binding protein governed by flexure at the TATA box. *J. Mol. Biol*. 1998, 282, 731-739.

143. Marathias VM. and Bolton PH. Determinants of DNA Quadruplex Structural Type: Sequence and Potassium Binding. *Biochemistry* 1999, 38, 4355-4364.

144. MarathiasVM and Bolton PH. Structures of the potassium-saturated, 2:1, and intermediate, 1:1, forms of a quadruplex DNA. *Nucleic Acids Res.*2000. 28,1969-1977.

145. Nagatoishi S and Sugimoto N. Interaction of water with the G-quadruplex loop contributes to the binding energy of G-quadruplex to protein. *Mol. BioSyst*. 2012, 8, 2766-2770.

146. Conte MR, Galeone A, Avizonis D, Hsu VL, Mayol L. and Kearns DR. Solid phase synthesis of 5-hydroxymethyluracil containing DNA. *Bioorg. Med. Chem. Lett.* 1992, 2, 79-82.

147. Jeener J, Meier B, Bachmann HP and Ernst RR. Investigation of exchange processes by two-dimensional NMR spectroscopy. *J. Chem. Phys.* 1979, 71, 4546-4553.

148. Braunschweiler L and Ernst RR. Coherence transfer by isotropic mixing: application to proton correlation spectroscopy. *J. Magn. Reson*. 1983, 53, 521-528.

149. Marion D, Ikura M, Tschudin R and Bax A. () Rapid recording of 2D NMR spectra without phase cycling. Application to the study of hydrogen exchange in proteins*. J. Magn. Reson*. 1989,85, 393-399.

150. Cornell WD, Cieplack P, Bayly CI, Gould IR, Merz KM, Ferguson DM, Spellmeyer DC, Fox T, Caldwell JW. and Kollman PA. A second generation force field for the simulation of proteins, nucleic acids, and organic molecules. *J. Am. Chem.* Soc. 1995, 117, 5179-5197.

151. Weiner SJ, Kollman PA, Case DA, Singh UC, Ghio C, Alagona G, Profeta S. and Weiner PJ. A new force field for molecular mechanical simulation of nucleic acids and proteins*. J. Am. Chem. Soc.* 1984, 106, 765-784.

152. Purschke WG, Radtke F, Kleinjung F, Klussmann S. A DNA Spiegelmer to staphylococcal enterotoxin B. *Nucleic Acids Res*. 2003, 31, 3027 –3032.

153. Kim Y, Yang CJ, Tan W. Superior structure stability and selectivity of hairpin nucleic acid probes with an L-DNA stem. *Nucleic Acids Res.* 2007, 35, 7279 – 7287.

154. Hauser NC, Martinez R, Jacob A, Rupp S, Hoheisel JD, Matysiak S. Utilising the left-helical conformation of L-DNA for analysing different marker types on a single universal microarray platform. *Nucleic Acids Res.* 2006, 34, 5101 –5111.

155. Tran PLT, Moriyama R, Maruyama A, Rayner B, Mergny JL. A mirror-image tetramolecular DNA quadruplex. *Chem.Commun.* 2011, 47, 5437–5439

156. Virgilio A, Esposito V, Citarella G, Mangoni A, Mayol L, Galeone A. Unprecedented right- and left-handed quadruplex structures formed by heterochiral oligodeoxyribonucleotides. *Biochimie* 2011, 93, 1193–1196.

157. Virgilio A, Esposito V, Citarella G, Mangoni A, Mayol L, Galeone A. A novel equilibrium relating to the helix handedness in G-quadruplexes formed by heterochiral oligonucleotides with an inversion of polarity site. *Chem. Commun.* 2013, 49, 7935 –7937.

158. Urata H, Kumashiro T, Kawahata T, Otake T, Akagi M. Anti-HIV-1 activity and mode of action of mirror image oligodeoxynucleotide analogue of Zintevir. *Biochem. Biophys. Res. Commun.* 2004, 313, 55–61.

159. Musumeci D and Montesarchio D. Polyvalent nucleic acid aptamers and modulation of their activity: a focus on the thrombin binding aptamer. *Pharmacol. Ther.* 2012, 136, 202–215.

160. Chung CH, Kim JH, Jung J, Chung BH. Nuclease-resistant DNA aptamer on gold nanoparticles for the simultaneous detection of Pb^{2+} and Hg^{2+} in human serum. *Biosens. Bioelectron.* 2013, 41, 827– 832.

161. Wang C, Li Y, Jia G, Liu Y, Lu S, Li C. Enantioselective Friedel-Crafts reactions in water catalyzed by a human telomeric G-quadruplex DNA metalloenzyme. *Chem. Commun.* 2012, 48, 6232–6234.

162. Wang C, Jia G, Zhou J, Li Y, Liu Y, Lu S, Li C. Enantioselective Diels-Alder reactions with G-quadruplex DNA-based catalysts. *Angew. Chem. Int. Ed.* 2012, 51, 9352–9355.

163.Wang C, Jia G, Li Y, Zhang S, Li C. Na^+/K^+ switch of enantioselectivity in G-quadruplex DNA-based catalysis. Chem. Commun. 2013, 49, 11161 –11163.